DEM SIMULATION AND ANALYSIS OF OPERATING PARAMETERS ON GRINDING PERFORMANCE OF A VERTICAL STIRRED MILL

by

Yu Hou

B.A., University of Science and Technology Beijing, 2011

A THESIS SUBMITTED IN PARTIAL FULFILLMENT OF

THE REQUIREMENTS FOR THE DEGREE OF

MASTER OF APPLIED SCIENCE

in

THE FACULTY OF GRADUATE AND POSTDOCTORAL STUDIES

(Mining Engineering)

THE UNIVERSITY OF BRITISH COLUMBIA

(Vancouver)

April 2014

Abstract

Stirred media mills have been increasingly used in ultra-fine grinding. The VXPmill is a vertical high speed stirred media mill for grinding mineral ores with high efficiency. Since it is a new technology in the industry, there is little understanding on the breakage kinetics of the mill. In order to gain more knowledge about the VXPmill, computer modelling of the mill was performed. Laboratory grinding trials were also conducted on a pilot scale mill to provide more information about the mill's capability, as well as verify simulation results.

DEM (Discrete Element Method) is a powerful tool in predicting particle behaviour, which is ideal for the study of stirred media milling. The CFD (Computational Fluid Dynamics) is used to model the motion of slurry by numerically solving the Navier–Stokes equations facilitated with the Volume of Fluid (VOF) and multiphase flow models. Simulation results suggested that a velocity gradient exists in the fluid field and grinding media in the mill. The highest grinding media velocity was reached near the disc edge in the horizontal direction and near the bottom of the mill in vertical direction. Those are the most active grinding zones in a vertical stirred mill. Different operating parameters such as stirrer rotational speed, slurry solid content and slurry viscosity have an influence on mill performance. Simulation results show that operating the mill at a high impeller speed helps to improve mineral liberation, while at too high impeller speed leads to a waste of electric energy without much improvement in mineral liberation. As well, a mid-level slurry solid content (15% v/v to 30% v/v) was found to achieve the best energy utilization during grinding. The slurry viscosity should be kept low to minimize the effect of high shear stress in the slurry. The influence of various operating parameters can be combined into the 'stress intensity' which describes the capability of a stirred media mill. Operating parameters also have an influence on the magnitude of force magnitude between grinding media which will

result in different breakage mechanism. Fracture breakage mechanism plays a more important role than attrition in VXPmill.

Preface

The research project was conducted at UBC's Mineral Processing Laboratory from 2011 to 2013. Test work consisted of two parts: one is computer modeling using a combined approach of DEM and CFD conducted by the author. The other is real grinding tests performed on laboratory scale VXPmill in collaboration with Master's student Baker Francis.

During the modeling work, all the geometry parameters are based on the design drawing of VXP—10 mill provided by CFD engineer Zhi Huang from FLSmidth, Salt Lake City, USA. The simulation programs were run on a Dell T3600 work station.

During the grinding test works, specific gravity and hardness of the ore sample were measured by the author together with Baker Francis. X-Ray diffraction was performed by Dr. Elisabetta Pani from the UBC Department of Earth and Ocean Sciences to determine the composition of the ore. The samples used for the tests were crushed and screened by Baker Francis in August, 2012. Measurement of particle size distribution and slurry rheological properties were done by the author and Baker Francis.

Table of Contents

List of Tables

List of Figures

List of Symbols

P80	80% passing (product)
F80	80% passing (feed)
ρ	density
ρ_m	Density of grinding media
V_t	tip speed
ω	rotational speed
R	radius
D	diameter
η	apparent viscosity
m	solid concentration
wt.%	weight %
% v/v	% volume by volume
τ	shear stress
γ	shear rate
η	plastic viscosity
κ	consistency coefficient
SI_m	media stress intensity
δ_n	normal overlap
R*	equivalent radius
E	Young's Modulus
ν	Poisson ratio
R	particle radius

e	coefficient of restitution
δ_t	tangential overlap
S_t	tangential stiffness
G*	equivalent shear modulus
μ_s	coefficient of static friction
F_n	normal force
F_t	tangential force
rpm	revolution per minute
AG	autogenous grinding
SAG	Semi-autogenous grinding
CAD	computer aided design
CFD	computational fluid dynamics
DEM	discrete element method
HPGR	high pressure grinding roll
HIG	high intensity grinding
HMI	human machine interface
PLC	programmable logic controller
PEPT	positron emission particles tomography
PSD	particle size distribution
XRD	X-ray diffraction
VXP	vertical extra performance
SG	specific gravity
SC	solid content

SMD	stirred media detritor
API	application programming interface

Acknowledgements

First, I would like to express my gratefulness to my supervisor Dr. Robert Hall. His guidance and kind support helped me finished my graduate study. I would also like to thank Dr. Bern Klein who is my co-supervisor in this project. His technical advice and tutoring was a great momentum for me to finish my research project. Thanks to Mr. James Yue from Fluor Canada Ltd. for his professional input to this project. It helped me improve myself in the field of comminution and mineral processing. I would like to say thanks to my colleague Mr. Baker Francis. His cooperation in this project is a great contribution to my work.

The financial support from National Science and Engineering Research Council as well as FLSmidth Co. is much appreciated. Their sponsorship is very important to this research and my graduate study. I would like to thank the equipment supplier FLSmidth Co. and UBC mining engineering department.

Last but not least, I would like to thank my dear family. Their love and encourage helped me get through my life as a graduate student in UBC Vancouver.

Chapter 1: Introduction

1.1 Background

Mining is an energy intensive industry. In 2014, it was reported that energy used in mining operations account for 3.3 percent of total industrial energy in the U.S. and energy accounted for 21 percent of all costs in mining. Among all equipment used in the mining industry, grinding and crushing equipment used 40 percent of total energy consumption (DOE, 2007). It is reasonable to say that grinding is the single greatest energy cost in the mining industry. However, it is reported that only 5% of the input energy is used for particle breakage during the milling process (Cleary, 2001). Meanwhile, the increasing complexity of ore bodies and lower ore grade make grinding more sophisticated than before (Yang et al. 2006). Some particles need to be grind to fine grains or even sub-micron level to achieve better mineral liberation.

In the mineral processing industry, it is generally accepted that grinding ore particles to a P_{80} of 75 μm is considered as the "conventional grinding" range (Jankovic, 2003). It is the area where existing conventional tumbling mills are typically applied to (as shown in Figure 1-1). When the targeted product size goes finer to between 75 μm and 30 μm, the stage is defined as "regrinding". Fine grinding is usually considered as grinding below 30 μm, whereas below 10 μm the term "very fine" or "ultra-fine" grinding is usually used. Research shows that during fine and ultra-fine grinding stages, "conventional" tumbling mills no longer provide enough liberation at an economical cost since the energy consumption rises sharply (Jankovic et al., 2008). Instead, stirred media mills can achieve size reduction in fine and ultra-fine grinding stage more efficiently (Gao & Forssberg, 1994). The appearance of stirred media mills provided an alternative for fine and ultra-fine grinding because of its high energy intensity (Kwade, 1999).

As the rotational motion is imparted by high speed stirrer and smaller grinding media are used, stirred media mills are able to treat particles in sub-micron level 50% more efficiently than conventional ball mills (Jankovic, 2003).

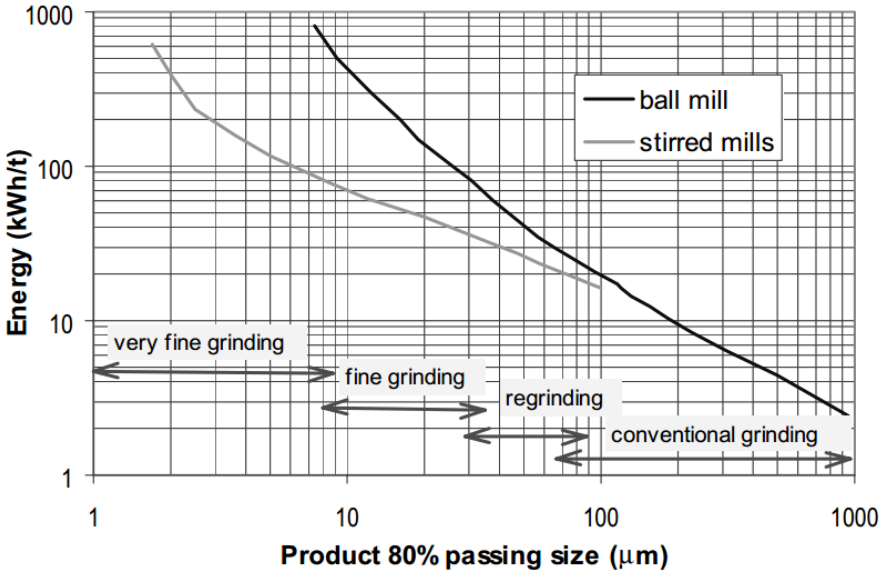

Figure 1-1 Application ranges of different grinding technologies (Jankovic, 2003).

1.2 Research Objectives

This research project attempts to bridge the gap between existing theories in ultra-fine grinding and vertical stirred milling technology. The primary objective of this research is to develop an understanding on how different variables affect the performance of a vertical stirred media mill during wet- fine grinding. The influence of mill geometry parameters will also be examined.

The secondary objective is to investigate breakage mechanism in a vertical stirred media mill and its influence on product particle size distribution.

Some specific objectives of this research are to:

- Use DEM simulation to gain a fundamental understanding on the slurry and grinding media behavior inside the mill chamber under various operating conditions and their potential effect on grinding performance and energy utilization.
- Investigate the influence of stirrer speed, slurry solid content and slurry viscosity on normal and tangential forces between grinding media and its resulting breakage mechanism.
- Analyze mill stirrer speed, slurry solid content and slurry viscosity's influence on media kinetic energy and media collision frequency.
- Investigate three different mill geometries and evaluate how they affect mill performance.

The results will give a better understanding of vertical stirred milling technology and that information will be useful in the selection of mill operating parameters during production, mill design and mill scale up.

1.3 Thesis Outline

This thesis is divided into five chapters.

Chapter 1 gives a general introduction to this research and presents the objective of this study.

Chapter 2 presents a literature review of stirred media milling technology. The concept of the discrete element method is introduced and its mathematical model is explained. This chapter also introduced previous studies and findings on the effect of operating parameters on mill

performance, some classic theories on slurry rheology, and information on slurry and particle behaviour as well as geometry issues.

In Chapter 3, the experimental plan of this research is presented. Methods of material characterization, sample preparation and product sample analysis are discussed in details. Test procedures for both laboratory grinding tests and computer simulations are outlined.

In Chapter 4, results and discussions of this research are presented. The simulation results are first confirmed by comparing it with test data. Slurry fluid patterns and grinding media velocity magnitude are studied. The mill chamber is divided into three zones and the grinding media distribution in these zones is investigated. The prediction of breakage mechanism in vertical stirred media mill is made by analyzing force type in the mill under various operating conditions. Stirrer speed and slurry properties effect on media kinetic energy and media collision frequency is also studied. In the end, the effect of different mill geometries on grinding behaviors is also compared.

Chapter 5 presents research results and important findings of this research. Recommendations on how to select mill operating parameters and mill optimization are demonstrated. Some aspects of future work are suggested.

Chapter 2: Literature Review

2.1 Introduction

The VXPmill is a new vertical oriented high-speed stirred mill. It operates at a high stress intensity that is able to bring the P_{80} down to 20 µm with high energy efficiency. In comparison to other existing stirred milling technologies, it has a number of potential advantages: the mill can operate at high to low speed using a broader range of grinding media sizes, different impeller designs can be used and no bearing or mechanical seals are in contact with the slurry.(Rahal et al., 2011). Although the mill has already been applied in a wide range of industrial metal mining applications, there have been no systematic studies to understand its characteristics in operation and to determine the optimal operating conditions.

Grinding is a process were electrical energy is converted into mechanical energy and results in size reduction of ore particles (Roufail, 2011). The comminution energy is determined by the properties of the mill, the size of the feed particles, and the grinding conditions. The relationship between grinding energy requirement and particle size by Hukki (1961) is shown in Figure 2-1. From this figure, it is seen that conventional energy-size relationship is only valid for particles that are bigger than 100 µm. This is also the size range where crushers and tumbling mills are applicable. When it comes to below 100 µm area or even sub-micron levels where stirred mills are utilized, there is little knowledge applicable to this work (Hukki, 1961).

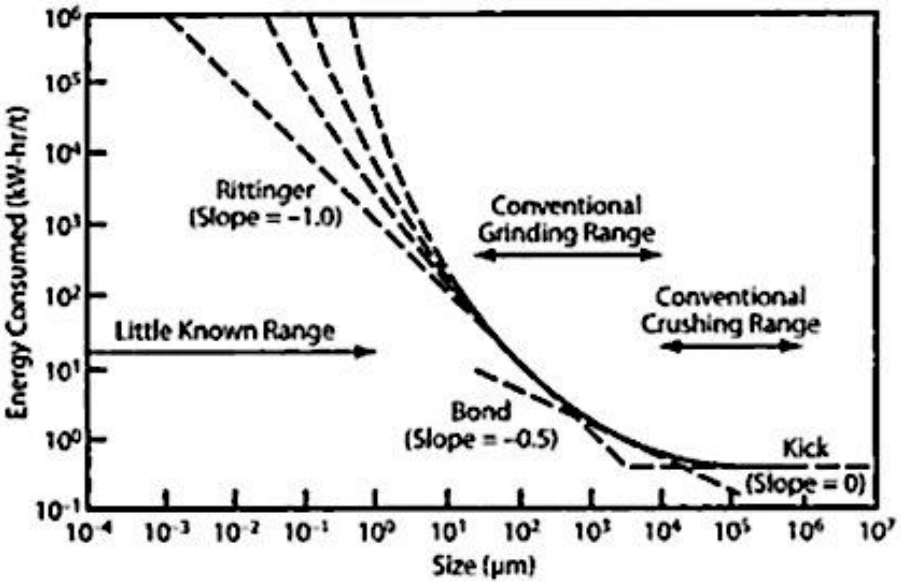

Figure 2-1 Net energy input versus particle size (Hukki, 1961)

2.2 Stirred Milling Technologies

Stirred milling technology was brought into the mineral processing due to the demand for finer grinding. This technology was originally employed in the size reduction process in the pigment industry and it has a wide range of application examples in other field such as pharmaceuticals, ceramic and chemical industries (Mio et al., 2004; Mannheim, 2011; Jayasundara et al., 2011). Large-scale production application in the mineral processing industry was first introduced by Xtrata Technology in the late 1980s at Mount Isa Mine in Australia (Rule, 2011). Four mills were installed in parallel in lead/zinc flotation concentrate circuit to provide regrinding treatment.

Stirred mills function in a way that a high speed rotating shaft mounted with discs (or pins, or skews), known as the stirrer, transmits kinetic energy to grinding media (beads). The central

shaft is coupled and driven by a high torque motor installed outside of the mill chamber (Blecher et al., 1996). Following this, the collision and attrition between beads causes breakage of ore particles trapped in between, bringing the feed material to a smaller particle size (Hogg, 1999; Kwade, 1999). Ceramic compound ball shaped beads with small diameter (usually 1 to 6 mm) are selected as the grinding media since they have higher intrinsic density and they are durable in the process of grinding.

The stirred media mill is preferred over conventional ball mills in fine grinding and regrinding circuits because they have a higher energy intensity and the ability to achieve smaller particle sizes and a smaller footprint (Wang & Frossberg, 2007). The use of large size grinding media has become a major barrier for improving grinding efficiency. In stirred media milling, a smaller grinding media size compared to a conventional ball mill makes high-speed movement possible, thus the force applied on the grains trapped in media increases. This is important because as the particle sizes become smaller, the force needed to break them apart increases (Shi et al., 2009). Additionally, smaller media size eliminates void spaces, thus increasing the probability of contact between beads. A higher collision frequency enables sufficient breakage of ore grains within a certain period of time. Using ceramic beads instead of steel beads can also minimize contamination released into the solution due to media wear.

There is a wide variety of stirred media mill equipment commercially built for the mineral processing industry. According to the shaft orientation, they can be categorized into horizontal and vertical mills. Based on their shaft rotation speed, they can be categorized into high speed and low speed mills.. Based on the shape of stirrer, they can be divided into three categories disc

shaped, pin shaped and skew shaped mill. In the following section some of the most popular stirred milling technologies are introduced.

IsaMill

The IsaMill is shown in Figure 2-2. It is a horizontal high speed stirred media mill with a maximum tip speed of 19—22 m/s. The high operating tip speed makes it possible to provide a high stress intensity ranges from 300—1000 kW/m^3. It is typically installed and operated in an open circuit configuration. The mill is driven by a motor coupled to a cantilevered shaft mounted with rubber lined circular discs (Figure 2-2 down). The feed slurry comes into the mill from the inlet at one end of the cylindrical chamber and passes through all the discs in the chamber. The mill is typically operated with 70%—80% full of 1.5—6 mm small grinding media. The high stress intensity allows the product size to reach sub-micron level. Before being discharged from the product outlet at the opposite side to the inlet, the slurry passes through a product classifier that separates product and grinding media, then it goes to downstream processing. Excessive heat is generated due to high rotational speed of the stirrer. Therefore water is circulated through the water-cooled jacket surrounding the outside of shell to maintain the mill temperature. To keep the slurry flow fluidized in the mill, a certain pressure inside the chamber should be maintained while the mill is running. As a consequence, the mill chamber is sealed to prevent air leakage (Xstrata, 2013).

(a)

(b)

Figure 2-2 Schematic of IsaMill (a) and its stirrer system (b) (Xstrata, 2014)

HIGmill

HIG (High Intensity Grinding) mill is a relatively new fine grinding technology; it is shown in Figure 2-3 (a). Before it was applied in the mineral processing industry, this technology was used in paper filler and carbonate grinding for over 30 years. It is a vertical stirred media mill with high stress intensity. The operating tip speed of the stirrer ranges from 4—12m/s. In a typical application, the mill is operated with a 70% media charge ratio. The feed is pumped into a scalping cyclone upstream of the mill to remove fines and modify slurry density to a targeted

mill requirement. Then the slurry is fed into the grinding chamber from bottom of the mill. The slurry is pumped upward through a mill chamber consisting of rotating discs which provides momentum to stir the charge against a series of static discs lining on the inner surface of the wall (Figure 2-3, b). The high stress intensity of HIGmill can bring the feed size from 200 µm to less than 40 µm. The product slurry is discharged by over flowing from the top of the mill. The HIGmill is usually operated in an open circuit configuration and there is no need for an external classifier (Outotec, 2013).

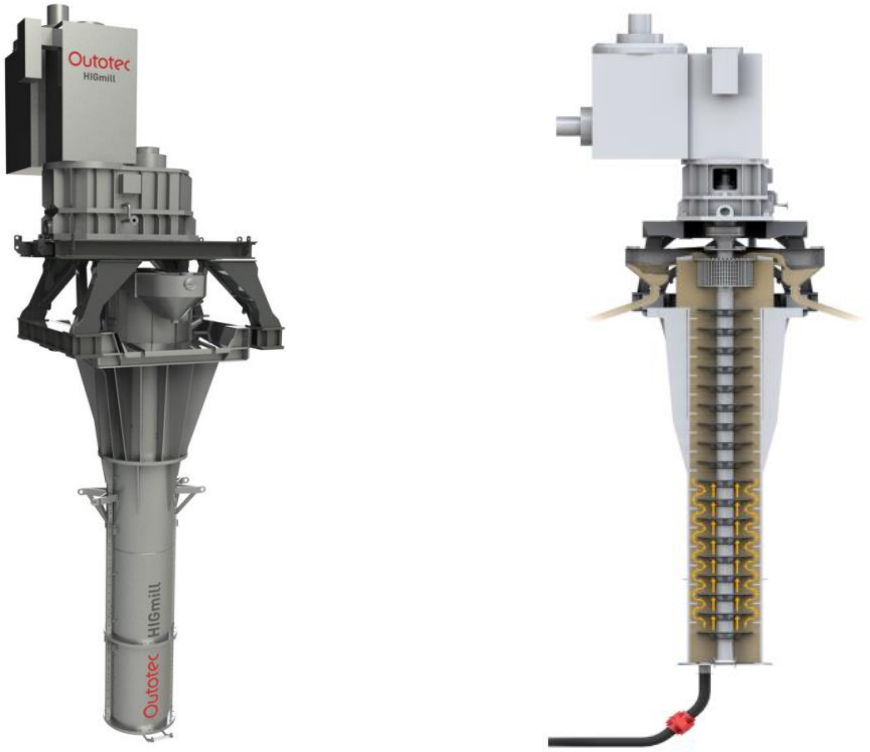

(a) **(b)**

Figure 2-3 Schematic of Hig mill (a) and its stirrer system (b) (Outotec, 2013)

Tower mill

The Tower mill shown in (Figure 2-4 a) is a low speed stirred media mill usually operated at a tip speed below 3 m/s. The power intensity it is able to provides from 20—40 kW/m^3. Tower mill technology was developed in 1950's and was first applied in grinding of metalliferous ore in 1980's. The standard arrangement of a tower mill is vertically oriented with an agitating screw (Figure 2-4 b) suspended into the grinding chamber, supported by spherical roller bearings and driven by a fixed speed motor through a planetary gearbox. It is typically operated in a closed circuit and fed by cyclone under flow. Grinding media and slurry in the chamber are stirred by the screw which is driven by a motor running at constant speed. After the particles are ground, they are lifted to the top portion of the mill by the screw shaped stirrer and overflow into the separating tank. Turbulences induced by the agitator help coarse particles to settle down preventing them from escaping into the next level of processing. The coarse particles are recycled back into the bottom of the mill through a pipe attached to the separating tank. The size of media used in a tower mill is typically 9—20 mm. It is capable of grinding feed particles as coarse as 6mm to product size as fine as 20 μm (Metso, 2013).

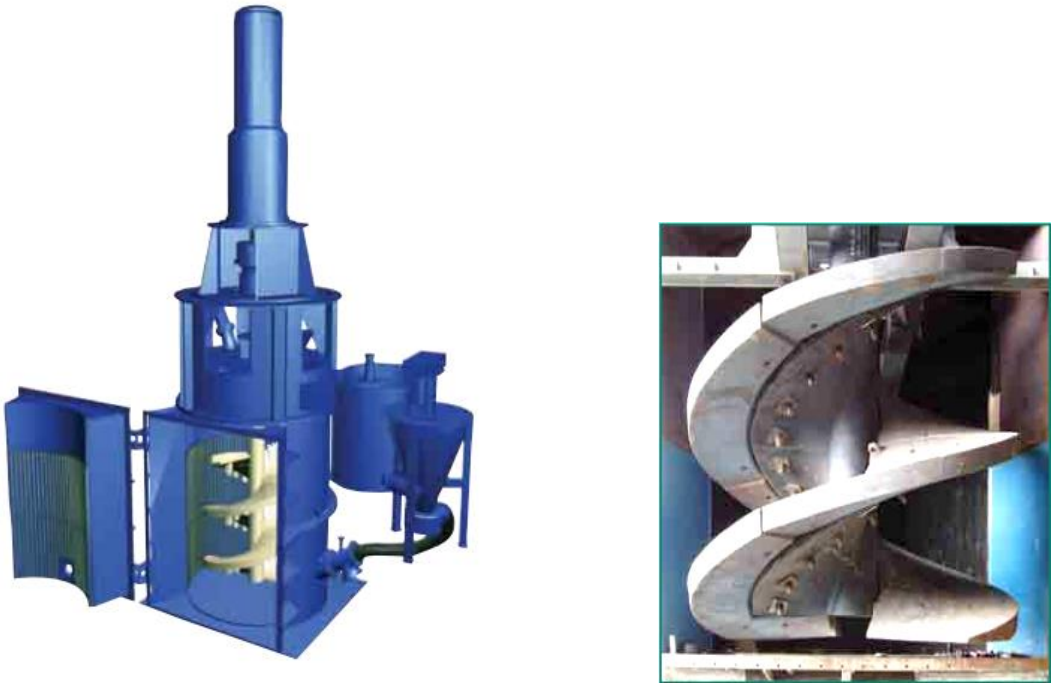

(a) **(b)**

Figure 2-4 Schematic of tower mill (a) and its stirrer system (b) (Metso, 2014)

Stirred Media Detritor

The Stirred Media Detritor (SMD) is a vertical low speed stirred media mill used in fine grinding (Figure 2-5 a). It was developed by English China Clays (ECC) in 1960's and its first industrial application was in a kaolin grinding plant. The mill has an octagonal body and pin shaped multi-armed impeller (Figure 2-5 b). Feed slurry is introduced into the grinding chamber from the port on top of the mill. The milled product is allowed to discharge into a launder passing through a media retention screen. The feed particle size to SMD is around 250 µm and the product size can reach sub 5 µm.

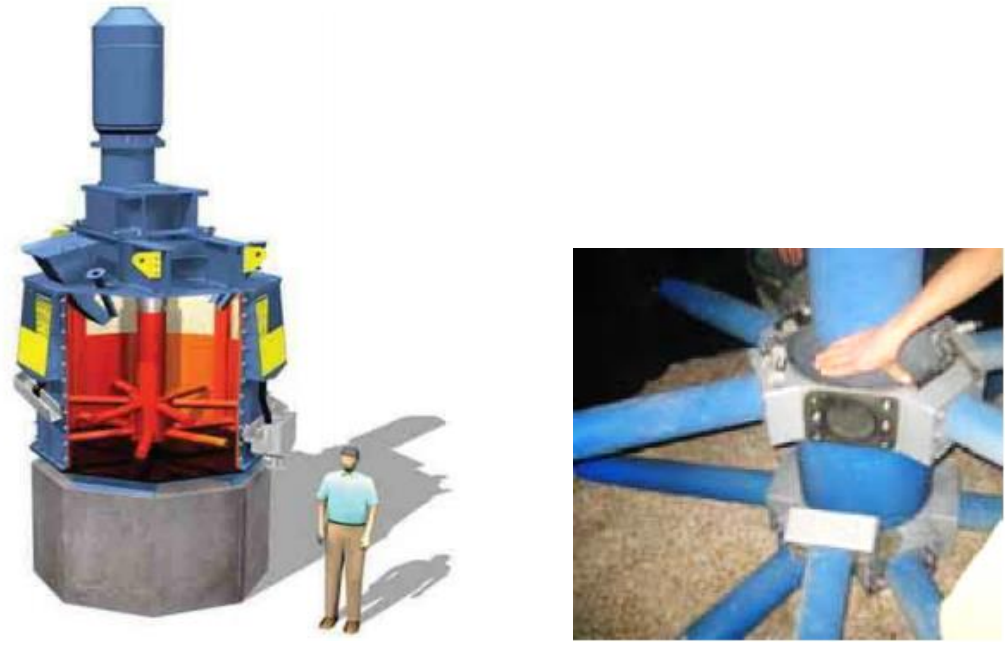

(a) **(b)**

Figure 2-5 Schematic of SMD (a) and its impeller system (b) (Metso, 2014)

VXPmill

The VXPmill as shown in Figure 2-6 (a) has recently gained acceptance for use in the mining industry. It was first used in the mineral industry in 1990's; it was originally built for the pigment industry for the purpose of processing magnetite-based pigments with less than 1 μm mean particle size. The VXP mill was named the Deswik mill when it is first built. This was after its designer—Des Erasmus and his son Wikus Erasmus. The mill was originally horizontal and was applied for a large variety of different materials apart from magnetite. It is able to grind the material from a feed size of 75 μm down to a mean size of 0.15 μm. Experiments on optimization of the Deswik mill were performed and the mill was changed to a vertical design

(Rahal, 2011). The vertical design eliminated some shortcomings of a horizontal orientation. Compared to conventional stirred mills, the Deswik mill has a number of potential advantages; a wide range of stir speeds and grinding media sizes; mechanical seals that prevent bearings from contact with slurry; different impeller configuration can be employed to provide various mechanical performances. The wide operating speed range of the VXPmill also narrows the gap between low speed vertical mills and high speed horizontal mills (Rahal et al., 2011)

(a) **(b)**

Figure 2-6 Pictures of VXP mill (a) and its impeller system (b)

The laboratory scale mill that is used in this research project is the FLSmidth VXP10—10 liters mill (Figure 2-7). Some of the operation parameters are listed in Table 2-1. All of them come from FLSmidth-Knelson VXP—10 Test Procedure manual.

Figure 2-7 VXP10 pilot scale mill (FLSmidth, 2012)

Table 2-1 Operating Parameters of FLSmidth VXP—10 (FLSmidth-Knelson, 2011)

FLSmidth VXP—10	Value
Net Volume (L)	10.2
Disc Diameter (mm)	130
Mill Inner Diameter (mm)	166
Mill Outer Diameter (mm)	186
Stir Speed (rpm)	0—1736
Tip Speed (m/s)	0—12
Slurry Density (kg/m^3)	1.25—1.5
Media Load (%)	50%—80%
Media Volume (L)	5.1—8.2
Shaft Diameter (mm)	30
Mill Chamber Height (mm)	650
Number of Discs	12

2.3 Effect of Operating Conditions on Mill Performance

The performance of a stirred media mill is affected by a number of associated variables (Jankovic et al., 2002; Jayasundara et al., 2010). “There are up to 44 parameters of influence as identified by Molls and Hornle in 1972” (Jankovic, 2003). However, researches are focused

mainly on some of the most important influencing factors such as media size, stirrer speed, slurry density and rheological effects. Rahal (2011) suggests that operating variables of a vertical stirred media mill that can be optimized to improve performance can be best described as two categories, namely process stage and mill configuration. Influencing parameters during the process stage includes feed particle characteristics (particle size, hardness, etc.), slurry density, slurry rheology and flow rate. Mill configuration factors can include mill speed, grinding media size and density as well as impeller design. Those parameters in the process stage and mill configuration stage are influencing parameters that can be optimized to reduce energy consumption and improve particle size and particle size distribution in grinding.

In the process stage, although the characteristics of feed material, particle size and particle size distribution are hard to control since they are pre-determined and dependent on what is available, they can be manipulated to get a normalized particle size and size distribution using screens and hydro cyclones (Rahal et al., 2011). The same thing happens to solid density of mineral. Gao and Forssberg (1993) studied pure dolomite in a horizontal stirred ball mill. Their results showed that a downward tendency of energy utilization at higher slurry density, and an obvious drop in energy utilization appears when slurry density gets above 70 wt. %. Jankovic (2003) concluded that an increase in slurry density would benefit mill performance up to a certain point, but after that point a decrease in mill efficiency would be expected. This is because of the increased slurry density caused a raise in the viscosity of slurry flow. He et al. (2005) also showed that the best grinding results are obtained at 70 wt. % with 0.2 wt. % dispersant. Chen et al. (2007) pointed out that the viscosity could be described by

$$\eta = ae^{bm}$$ Equation 2-1

Where $\eta -$ apparent viscosity

$m -$ solid concentration

$a, b -$ coefficient related to shear rate

This relationship showed that the apparent viscosity increases exponentially over a certain slurry solid content and the critical value was 75 wt.% and the aggressive raise in slurry viscosity might be the reason why energy utilization increases after the solid concentration gets over 70 wt. %

The effect of slurry density on the product size distribution was also studied. For coal slurry, a change from 20 to 50 wt% solids has no significant effect on the energy efficiency. However, at higher values (over 60%), adverse viscosity conditions inhibit grinding resulting in a coarser particle size distribution (Mankosa et al., 1989)

The feed characteristics and solid density also have an effect on the flow rate which influences the intensity of grinding required to achieve a target product size distribution (Rahal, 2011). Flow rate also decides the grinding time needed to get a favorable mill discharge density. The grinding time will further affects the rheological behavior of slurry in that the viscosity of slurry increases with grinding time as the reduction of particle size (Ding et al., 2007).

The slurry rheological properties strongly influence the surface properties of minerals causing the slurry to exhibit non-Newtonian flow properties (Yue & Klein, 2004). Viscosity is the dominant parameter affecting the rheological property of given slurry (Yue & Klein, 2004; He et al., 2004). For fluid, the viscosity is defined as

$$\eta = \frac{\text{Shear stress}}{\text{Shear rate}} = \frac{\tau}{\gamma}$$ Equation 2-2

For the case of Newtonian fluids (such as water and oil), η is a constant. The viscosity is the slope of the straight line passing through the origin (as shown in Figure 2-8). However, most semisolids in nature, such as mineral slurries exhibit non-Newtonian characteristics (Wang & Forssberg, 1995). The viscosity of this type of fluid varies with shear stress and shear rate. In this case, apparent viscosity can be used to determine the rheology property of the slurry. For a given shear tress-rate of shear curve of a non-Newtonian fluid, the apparent viscosity is the slope of a line that passes through the origin and intersects the flow curve at a specific rate of shear (Yue & Klein, 2004). The relationship curves between shear stress η and rate of shear strain for different types of fluid are shown in Figure 2-8.

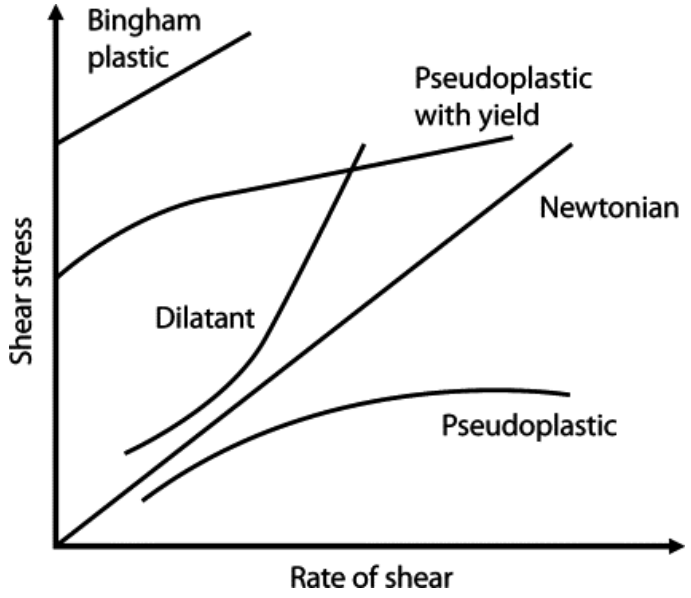

Figure 2-8 Shear stress versus shear rate curves for different type of fluid (He et al., 2004)

According to rheological behaviour, test data of shear stress can be fitted to a Bingham model, a Herschel—Bulkey model and a Casson model (Yang & Chen, 1995) which are expressed as follows

Bingham model	$\tau = \tau_y + \eta_0 \gamma$	Equation 2-3
Herschel-Bulkey model	$\tau = \tau_y + K\gamma^n$	Equation 2-4
Casson model	$\sqrt{\tau} = \sqrt{\tau_y} + \sqrt{\eta_0 \gamma}$	Equation 2-5

Where τ_y is defined as yield stress, h_0 and K are plastic viscosity and consistency coefficients respectively and n is flow exponent.

Yue and Klein (2004) showed that the relationship between sheer stress and sheer rate is better fitted into the Casson equation than the Bingham equation by performing grinding test on a suspension of quartz particles. The research also showed how yield stress, solid content and particle size interact with each other. Yield stress strongly influences power consumption in that the mill power draw is proportional to the yield stress of the slurry. The interaction between yield stress and breakage rate is that breakage rate decreases as the yield stress increases; By plotting a Rosin—Rammler size distribution against slurry yield stress, it is shown that when yield stress is higher, the distribution coefficient increases which means that the size distribution becomes narrower. The same result can also be found in He et al. (2005).

Mill speed is considered one of the most important operating parameters for a stirred media mill (Mankosa et al., 1989; Gao & Forssberg, 1993; Jankovic, 2002; Toraman & Katırcıoglu, 2011; Jayasundara et al., 2010). The stirrer speed determines breakage mechanism of the ore particles and distribution of energy in a grinding chamber (Kwade, 1999). It is obvious that the kinetic

energy of grinding media is high when the stirrers are running at high speeds. However, the selection of mill stirrer speed is not the higher the better. A very high stirrer speed could reduce energy efficiency. Therefore, the selection of mill rotation speed is a condition—based problem (Jayasundara et al., 2010). A lower mill speed is efficient in energy utilization but can only handle a small quantity of ore mineral while a higher mill speed can process a large capacity of mineral but will cause energy waste. The influence of mill stir speed on coal product particle size distribution in a stirred ball mill was studied by Mankosa et al. (1989). Results show that, at a specific input energy value, a lower stirrer speed is preferred because the mean particle size decreased as the speed goes down. The shifting of particle size distribution to the finer value reflects this phenomenon. It was also observed that this effect was more pronounced at higher energy input. Gao and Forssberg (1993) indicate that higher energy input at high speed grinding causes lower energy utilization because more energy is consumed by collision between grinding media and generation of heat to overcome mechanical difficulties rather than improve particle breakage rate. Jankovic (2003) also found that a higher stirrer tip speed has a negative effect on energy utilization. The coarser the particle size is, the bigger the influence is. The research was carried out on pilot scale Netzch mill, Tower mill and SAM mill. Their results from three types of stirred mills shows identical stir speed-energy utilization interactions. All the previous research results demonstrated that an optimum mill operating speed exist when performing high speed ultra-fine grinding in stirred media mills. However, research on understanding the optimal operating speed of the VXP mill has not been done to the author's knowledge.

Grinding media size is another important operating parameter that affects ultra-fine grinding in that it has a large impact on grinding efficiency (Lichter et al., 2002; He & Forssberg, 2006).

Grinding media size also affects grinding kinetics in the mill significantly (Mankosa et al., 1986). A decrease in media size results in an increase in number of media at a given volume. In this way, the probability that a particle is captured by a bead is increased resulting in a raise in breakage rate and energy utilization (Yue & Klein, 2006). Jankovic (2002) performed a series of test on three different types of stirred ball mills. The result indicated that finer media should be utilized because they are more efficient in getting fine particles. It also reveals that there is an optimum media size between 4.8 mm to 6.8 mm for a particular stirrer speed. This result is in accordance with Jayasundara (2010) whose work indicated that there is an optimum media size between 2 mm and 6 mm when using glass bead in grinding aluminum hydroxide powder.

In conventional ball grinding, heavier media is always preferred since it provides higher kinetic energy in collision with mineral particles. Mankosa et al. (1986) found that a steel bead is slightly more efficient than a glass bead which indicates that the density of individual grinding media is important to grinding efficiency because the attrition force is stronger. However, Gao and Forssberg (1993) revealed that for a stirred ball mill, media density has an optimum value of 3.7 kg/m^3 that gives the highest energy utilization. If the density continues to go up after the optimum point, the energy utilization goes down and the heaviest beads turn out to be the most inefficient ones.

Besides the force factors previously discussed, there are more parameters considered to have an impact on grinding performance such as the addition of dispersant (Gao & Forssberg, 1993), the pH value of the slurry (Muster & Prestidge, 1995), particle size (Yuan & Murray, 1997) and temperature (Yang et al., 2001) etc.

Since the comminution process in a stirred media mill is influenced by a number of parameters, it is hard to assess the performance of a stirred media mill based on one single variable (Kwade & Schwedes, 2002). Mixed reactions were observed when change was made on one variable when looking into different types of stirred mills (Jankovic, 2003). For example, the selection of a high density grinding media may produce a finer product but it will consume more energy to be stirred. Work done by Schwedes et al. (1996) suggested that in a high speed stirred mill media size, tip speed, slurry and media density can be evaluated simultaneously to indicate grinding efficiency. The concept of "stress intensity" was introduced. It is defined in Equation 2-6.

$$SI_m = D_m^3(\rho_m - \rho)v_t^2 \qquad \text{Equation 2-6}$$

where $D_m -$ grinding media size (m)

$\rho_m -$ grinding media density (kg/m^3)

$\rho -$ slurry density (kg/m^3)

$v_t -$ stirer tip speed (m/s)

It is suggested that stress intensity is the most important indicator of mill capability in stirred ball mill grinding (Becker et al., 2001; Jankovic, 2001). The "stress intensity" of a stirred mill is important in the selection of operating parameters as well as optimization of existing grinding conditions (Kwade, 1999). The value of stress intensity should not be too high or too low. A very high stress intensity value results in excessive energy consumption, whereas a low value is inefficient since more stress is required to break the particles. There is an optimum stress intensity for a particular stirred media mill application where the finest grinding size is achieved with minimum energy input (Kwade et al., 1996). Jankovic (2001) indicated that at a fixed energy input, to get the finest particle size, the optimum stress intensity for tower mill should be

maintained around 0.02×10^{-3} Nm to 0.1×10^{-3} Nm. The conception of optimum stress intensity point could also be used in scale-up of stirred media mills.

2.4 Breakage Mechanism in Stirred Media Mills

Hogg (1999) suggested that massive fracture and attrition are two most important breakage mechanisms in stirred milling process. By using numerical simulation based on approximate solutions to the size-mass balance relationship formula, Hogg concluded that the contribution from attrition breakage results in the appearance of non-first order breakage and the product size distribution tends to show an increasingly bimodal character. Kwade (1999) concluded the breakage mechanism in stirred media mill into three categories: the compression between two media moving at high velocity; the pressing force between media and mill chamber wall and the abrasion between two media moving in tangential direction. By calculating the stress intensity and number of stress event in each zone of the mill, he identified that the breakage caused by the collision between two media moving along tangential direction is the most important breakage mechanism. Yue and Klein (2004) conducted research on breakage mechanism of quartz suspension in a horizontal stirred media mill. Based on their size distribution result in Figure 2-9, they found that fracture breakage is the primary breakage mechanism in horizontal stirred media mill. However, when approaching the grinding limit of the mill, attrition is dominant and the particle size distribution curve shows a bimodal shape.

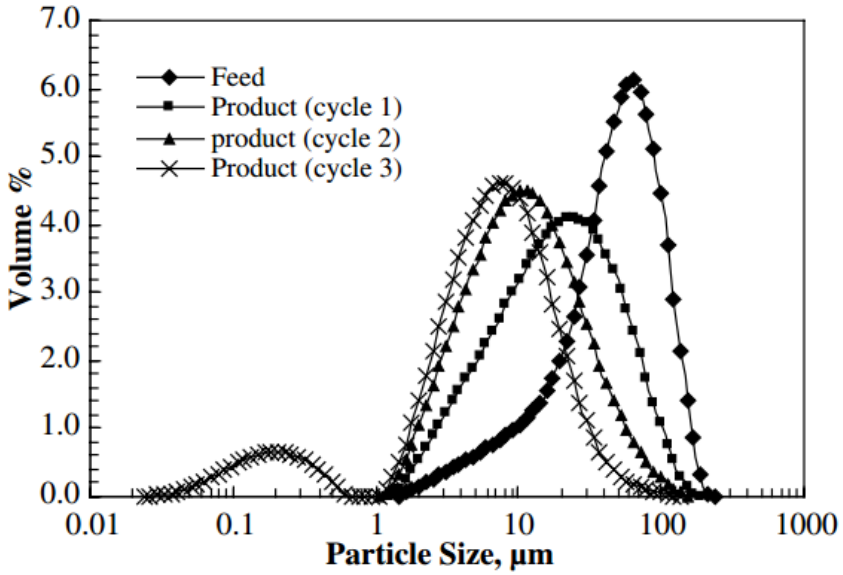

Figure 2-9 Particle size distribution of product from a horizontal stirred media mill (Yue & Klein. 2004)

2.5 Discrete Element Method

The Discrete Element Method consists of a group of computational modeling techniques suitable for describing the mechanical behavior of a group of rigid or deformable bodies (Stein et al., 2004). The multi-body contact event is calculated based on Newton's Second Law that gives the motion of a particle based on the result of forces applied on it. The force-displacement law is applied to calculate contact forces from particle displacement (Cundall & Strack, 1979). In this scenario, the collision between two particles can be illustrated in a linear spring-dashpot model (Figure 2-10), which represents elastic and non-elastic behavior respectively. The default contact model used in EDEM is Hertz-Mindlin model. It is named after Hertzian contact theory (Hertz, 1882) and Mindlin-Deresiewicz who developed the tangential force model (Mindlin, 1949). In this model, the force between particle A and particle B is divided into two components: normal

forces and tangential force. Both normal and tangential forces have damping and a spring component; however, the friction component only exists in the tangential direction. The damping coefficient is related to the coefficient of restitution (Tsuji et al., 1992) and the tangential friction force follows the rule of Coulomb law of friction model.

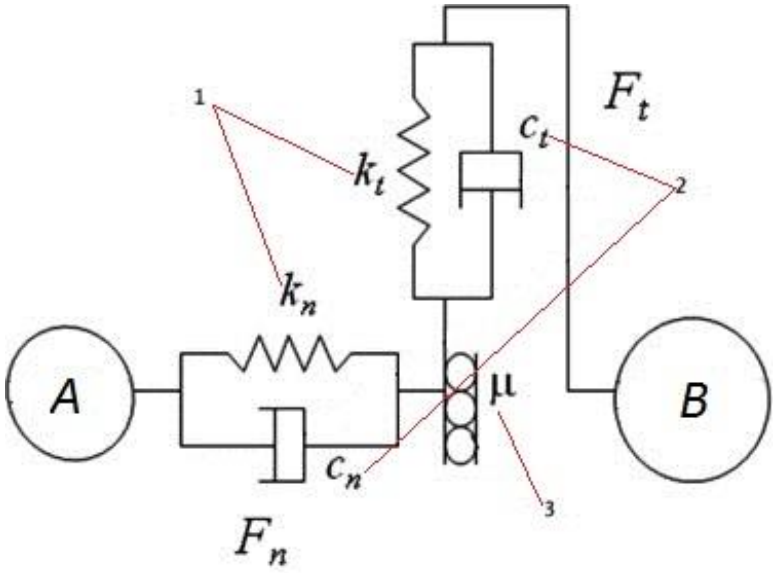

1-Spring 2-Damping 3-Tangential friction

Figure 2-10 Hertz-Mindlin contact model between two spheres (EDEM, 2012)

Particularly, the normal force is calculated by

$$F_n = \frac{4}{3} E^* \sqrt{R^*} C \qquad \text{Equation 2-7}$$

Where C is the normal overlap captured when two particles collide with each other, E^* is Young's Modulus and R^* is equivalent radius defined as

$$\frac{1}{E^*} = \frac{(1-v_A^2)}{E_A} + \frac{(1-v_B^2)}{E_B} \quad \text{Equation 2-8}$$

$$\frac{1}{R^*} = \frac{1}{R_A} + \frac{1}{R_B} \quad \text{Equation 2-9}$$

where E^A, v^A, R^A and E^B, v^B, R^B represent Young's Modulus, Poisson ratio and radius of particle A and B. There is also a damping force in the normal force component given by

$$F_n^d = -2\sqrt{\frac{5}{6}}\beta\sqrt{S_n m^*}\,v_n^{\overrightarrow{rev}} \quad \text{Equation 2-10}$$

in which $m^* = \left(\frac{1}{m_1} + \frac{1}{m_A}\right)^{-1}$ is the equivalent mass, $v_n^{\overrightarrow{rev}}$ is the normal component of relative velocity, β and S_n are defined by the following equations

$$\beta = \frac{\ln e}{\sqrt{\ln^2 e + \pi^3}} \quad \text{Equation 2-11}$$

$$S_n = 2E^*\sqrt{R^*\delta_n} \quad \text{Equation 2-12}$$

in which e is the coefficient of restitution. The tangential force is calculated by

$$F_t = -S_t\delta_t \quad \text{Equation 2-13}$$

with δ_t and S_t stand for tangential overlap and tangential stiffness respectively. S_t can be obtained from the following equation with G^* stands for equivalent shear modulus

$$S_t = 8G^*\sqrt{R^*\delta_n} \quad \text{Equation 2-14}$$

Similar to the normal force component, there is a tangential damping force and it is given by

$$F_t^d = -2\sqrt{\frac{5}{6}}\beta\sqrt{S_t m^*}\overrightarrow{v_t^{rev}} \qquad \text{Equation 2-15}$$

where $\overrightarrow{v_t^{rev}}$ is the relative tangential velocity and the tangential force is limited by Coulomb friction $\mu_s F_n$ with μ_s to be the coefficient of static friction.

2.6 DEM Simulation Merits and Limits

Due to the fast development of simulation technology and computer techniques in recent years, numerical modeling methods have been increasingly used in solving engineering problems. DEM is one of those modeling techniques. It has been widely applied in modeling systems consisting of discrete particles because of its advantages over traditional numerical modeling methods. DEM simulation is able to provide dynamic information such as grinding media trajectories, transient forces acting on individual particles and tracking collisions at a given period of time. All of that information is extremely complicated to get by applying conventional physical experiment (Deen, 2007). Meanwhile, the dynamic coupling of DEM and CFD makes the application of this method more versatile. Modeling on a particle-fluid, two-phase system (such as wet grinding in ball mill and stirred) is possible.

The main limitation of applying DEM modeling on a stirred media mill is the number of beads that can be simulated in a reasonable period of time (Cleary, 2001; Roufail, 2011). The number of particles in a stirred milling system is often exceptionally large. Calculating the force and displacement of tens of millions of particles needs the support of a powerful computer with intensive computing ability. Another issue with respect to DEM simulation on stirred milling is

that the high rotational speed of discs makes the system less stable. To catch the movement of every bead in the mill, the simulation step time has to be shortened to 10^{-6} seconds which makes the overall simulation time considerably long (EDEM, 2011). For example, it takes nearly 100 hours of simulation time to model the movement of 45,000 grinding media in a stirred media mill in 2 seconds in real time.

It is essential to examine the validity of computer simulation results by comparing them with experimental tests; otherwise the ability of DEM to predict micro field fluid and particle motions cannot be determined (Jayasundara, 2011). Although DEM simulation provides an approximation to real conditions, it is not enough to predict microscopic behavior very accurately. Therefore, verification and testing of predictions by modeling results is essential for the application of DEM simulation (Powell & Morrison, 2007).

Because of the power of DEM in modeling discrete phases, it is suitable for describing the mechanical behavior of a group of rigid or deformable bodies, such as the ore breakage in ball milling in the mineral industry (Cleary, 1998; Cleary, 2003; Morrison & Cleary, 2004; Mishra & Rajamani, 1994). A number of papers on DEM modeling of comminution equipment can be found. The first application was by Mishra (1991) which was a research study on media charge motion in a ball mill. Cleary (1998) studied charge motion in a full-scale ball mill through 2D DEM modeling and analyzed the sensitivity of mill power draw to particle properties and operating parameters. Cleary and Hoyer (2000) compared their 2D DEM simulation result of ball motion in a centrifugal mill to pictures taken by high-speed photographs, and their results were consistent. Cleary (2003) predicted the SAG mill power draw by comparing DEM simulation

results with experimental data. Hoyer (1999) studied the influence of mill operating conditions and design parameters to mill performance of a stirred media mill. A scale-up method is also presented which can be applied to other types of ball mills. Bwalya et al. (2001) performed DEM on a SAG mill and obtained mill breakage rate and other parameters under different mill loading. Mio et al. (2004) investigated a method to scale-up a pilot-scale ball mill using DEM. Powell et al. (2011) studied the linear wear evolution in a ball mill using DEM modeling and found that the wear model could be used with an initial liner profile and fitted wear constant.

The DEM was used to simulate an IsaMill by Yang et al. (2006). It was the first time that DEM was applied on the study of a high speed stirred mill. Particle flow was studied under different operational conditions. Jayasundara et al. (2010) investigated the influence of rotation speed and mill loading on impact energy of grinding beads. Non-linear breakage energy with time was confirmed. Jayasyndara et al. (2011) successfully modeled particle and flow behaviour in an IsaMill model and compared their results with Positron Emission Particle Tracking technology. In this research the CFD (Computational Fluid Dynamics)-DEM two way coupling method was introduced. It works in a way that the CFD software simulates the continuous slurry flow phase while the DEM software models the discrete particle flow phase. The coupled software exchanges information at each time step. Sinnott et al. (2011) studied how different grinding media shape influence energy utilization in a tower mill with DEM. Sinnott et al. (2011) carried out a research on slurry flow in a tower mill with one-way coupled DEM-SPH (Smoothed Particle Hydrodynamics) method. In this case, the discrete phase-grinding beads are modeled using DEM and the resulting media motion is transferred to SPH to predict slurry flow behavior through the porous charge. Morrison et al. (2012) compared a pilot scale tower mill with a ball

mill in terms of energy efficiency using DEM simulation. They found that even though the tower mill is more energy efficient, the ball mill has more tolerance to variations of feed ore hardness and size distribution. Jayasundara et al. (2011) studied disc wear in an IsaMill and its effect on grinding performance by incorporating a wear model into the DEM model. Jayasyndara, Yang and Yu (2012) investigated the effect of grinding media size on breakage performance in stirred mills using coupled CFD and DEM. Yamada and Sakai (2013) applied a combined DEM and Lagrangian method to the study of a horizontal stirred media mill. The velocity distributions of grinding media in the mill under different stirrer speeds were computed. Their results were then validated by experimental data.

2.7 Particle and Slurry Motion in Stirred Mills

In wet grinding in a vertical stirred media mill, the grinding system inside the mill chamber is a combination of stirrer discs, grinding media and pulp slurry. Kinetic energy is imparted into the inner atmosphere by disc shaped stirrers rotating at a very high speed. Then the energy is transferred to both grinding media in contact with the stirrers and slurry around them. Apart from this, the interaction between grinding media and slurry exert forces on each other. The fluid drag force produced by the slurry around particles gives the bead a momentum to move forward and the buoyant force keeps the particles moving upward. In return, the inertia of grinding media prevents the slurry from rotating fast in the mill. The interaction among these three items in the mill chamber makes the particle and slurry movement in the grinding chamber difficult to predict.

Research on flow patterns in stirred media mills has been conducted. The pioneering study of Blecher et al. (1996) on the motion and stress intensity of grinding media in a horizontal stirred media mill found that fluid velocity gradients of tangential direction exist in the area surrounding the stirrer discs. Those zones with high velocity gradients happened to be the areas with highest stress intensity where the majority of particle breakage took place. Theuerkauf and Schwedes (1999) investigated the fluid and particle flow pattern in a pin—stirrer stirred media mill by using numerical modeling and then compared their result with experiment result. They plotted the velocity profile around the stirrer discs and between stirrer tip and mill chamber wall. They found that the maximum velocity between stirrer tip and chamber wall can only reach 35% of stirrer tip speed.

Barley et al. (2004) measured the grinding media motion in a vertical stirred media mill with only one impeller using Positron Emission Particle Tracking (PEPT) technology. The result showed that although various operating conditions can affect the fluid motion, they have similarities. The streamlines originated from the impeller surface and were split into two categories, namely upstream and downstream. The upstream fluid forced the grinding media up and it eventually fell back because of the gravitational force. The down stream fluid drove the media against the mill wall and it circulated back to the impeller band. Thus, the media flow field in a vertical stirred media mill is divided into three zones: upper circuit, lower circuit and impeller band as shown in Figure 2-11 (Barley et al., 2004).

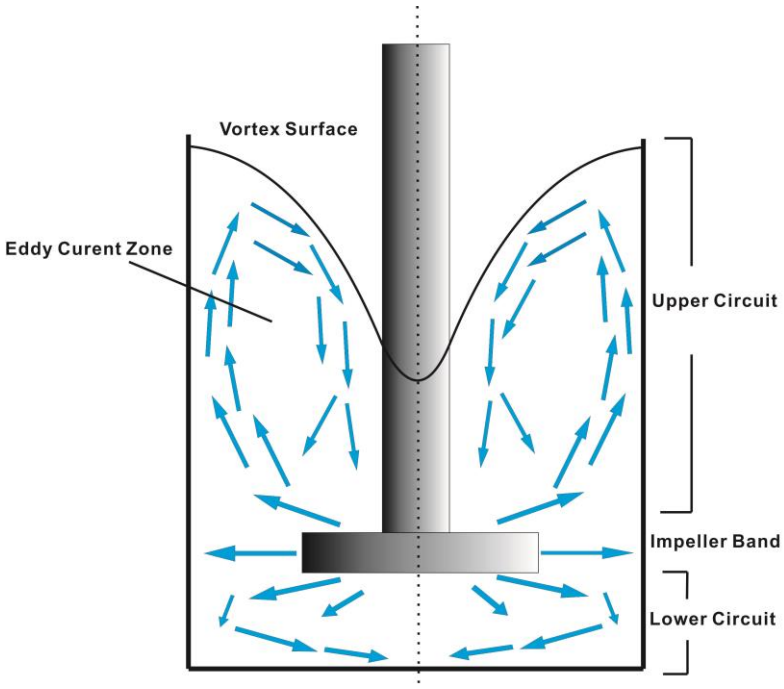

Figure 2-11 Fluid flow circuits in a vertical stirred media mill (Barley et al., 2004)

Jayasundara et al. (2009) investigated slurry properties effect on flow motion in an IsaMill using DEM modeling. They concluded that changing both slurry density and slurry viscosity could induce changes in flow motion. Increasing slurry density could cause a more rigorous grinding media motion due to the increase in fluid drag force. As a result, impact energy and collision frequency increased dramatically. Increasing slurry viscosity limited the movement of grinding media and made them more dispersed in the suspension. Jayasundara et al. (2011) did a numerical modeling study on particle flow behavior in an IsaMill and compared the result with PEPT study. They found that the flow property is influenced by a number of factors such as mill loading, stirrer speed and grinding media properties. The comparison between the two techniques showed agreement

2.8 Effect of Mill Geometry on Mill Performance

Although all stirred media mills are similar in their basic principle- a rotary stirrer shaft mounted in the center of a stationary shell, a large number of different stirrer designs exist in the field. Kwade (1999) divided stirred mills into three categories according to their stirrer design: disc shaped stirrer, pin—counter—pin stirrer and drum shaped stirrer. Those designs are different in energy transfer efficiency. At a given rotational speed, the pin—counter—pin stirrer has a higher energy density than the disc stirrer because the former design moves the grinding media mainly by displacement force while the latter one moves media by adhesion. The annular gap stirrer provides the highest power density among the three since it has a larger contacting surface with slurry and media providing a more uniform force distribution.

Radziszewski (2013) evaluated mill power density of different stirred mill geometry designs. In this study, a new parameter used to examine mill power between different design configurations was defined. He mentioned that "shear volume" could be used to assess the power consumption of a given stirred media mill. The definition of shear volume is given in Equation 2-16

$$V_\tau = A\frac{r^2}{y}(m^3) \qquad \text{Equation 2-16}$$

Where V_τ is shear volume, A is the total area where the shear is acting, r is the radius at which the shear is acting and y is the gap distance over which the shear is acting. The power consumption at a given shear volume is in Equation 2-17

$$P_\tau = \mu\omega^2 V_\tau\,(W) \qquad \text{Equation 2-17}$$

Where μ the viscosity of slurry being processed is, ω is the angular rotational speed of the stirrer.

It is assumed that the higher the shear volume of a given mill design, the more surface area will be in contact with grinding media and slurry. Therefore the machine will consume more energy.

2.9 Conclusion

Stirred media mill has been widely applied in the mineral processing industry. They are an alternative to conventional tumbling mills since they are able to provide much higher stress intensities. A lot of research has been done in evaluation these types of mills. However, their acceptance by the industry has been slow and thus requires more research to demonstrate their applicability. This is particularly true of the vertical stirred media mills as research on their behaviors is somewhat limited. The key areas that need further study are: the slurry and grinding media movement in a vertical stirred media mill; the effect of operating conditions such as mill speed, slurry density and viscosity on mill performances and the influence of mill geometry configuration on mill performances.

Discrete element method is a powerful tool when studying a system that consists of individual particles. It has been widely applied in studying comminution equipment such as ball mill, tower mill and IsaMill and the results are accepted as reasonable for mill design and optimization. However, a similar study on vertical disc-shaped stirred mill has not been conducted. Since their is similarity between vertical and horizontal mills, applying DEM modeling to the study of vertical mills should provide useful knowledge for their application.

Shear volume is a newly proposed parameter used to assess geometry configuration of stirred media mills, yet it has not been applied to any mill model in practice. The verification of this concept could be helpful to better understand energy consumption of a mill.

Chapter 3: Experimental Program

3.1 Introduction

The experimental component of this research consisted of two parts. The first was a closed circuit pendulum test carried out on the lab scale VXPmill in the UBC mineral processing laboratory. The other was modeling grinding activities of the mill using DEM simulation. The pendulum test results were used to validate the DEM method. Then DEM was used to investigate various operating scenarios.

The objective of the pendulum grinding test work is to evaluate the grinding performance of the vertical stirred media mill under different operating conditions. To meet this objective, a total amount of twelve pendulum tests were performed using the VXP-10 mill at UBC. The variable parameters being changed in this test were stirrer speed, slurry solid content and residence time. Results are analyzed based on particle size distribution, slurry rheological properties and energy consumption. The grinding test results will further be compared with and explained by computer simulation results.

3.2 Grinding Test

3.2.1 Material Characterization

The ore sample used in this test is from Barrick's Veladero mine located in San Juan, Argentina. The primary mineral contained is copper and gold in low grade with other minerals in the ore. A quantitative mineralogy composition analysis is performed using X-Ray Diffraction (XRD) analyzer. This was done by the mineralogy analysis laboratory in the Department of Earth and

Ocean Science in UBC and the result is listed in Table 3-1. The specific gravity of ore sample is determined by using the "volumetric flask method" proposed by Klein (1992). The average measured SG of the material is 2.63.

Table 3-1 Quantitative analysis result of experiment sample

Name of Mineral	***Weight %***
Quartz	23.6
Clinochlore	2.0
Kaolinite	2.4
Muscovite 2M1 - Illite	13.2
Biotite	6.8
Plagioclase	13.1
K-feldspar	30.1
Gypsum	0.7
Siderite	1.1
Pyrite	5.7
Chalcopyrite	0.6
Rutile	0.8
Total	100.0

3.2.2 Sample Preparation

Since the VXP mill is typically applied in fine and ultrafine stage of grinding, there is a limitation on the maximum particle size of feed material. To ensure optimal performance of the mill and to keep the grinding discs from wearing out too fast, it is recommended that the F_{80} of material entering the VXPmill is not more than 500 µm (FLSmidth, 2012). To eliminate variations in particle size distribution and top size particles in ore feed sample, the raw material was crushed and ground prior to VXPmill tests.

The grinding circuit used to prepare feed material is shown in Figure 3-1. A total amount of 600kg of raw sample with F_{80} ranges from 20 mm to 30 mm is fed into the lab scale High Pressure Grinding Rolls (HPGR), generating a P_{80} of 6 mm. Then the product is dry screened and the undersize went to a lab scale cone crusher, the oversize was brought back to the HPGR. After passing through the cone crusher, the material reached a P_{80} of 2 mm. Before going into the VXP mill, the material is ground in a lab scale rod mill downstream of the cone crusher and dry screened using a 300 µm sieve. Eventually, the undersize was fed into the VXPmill while the oversize was reground by rod mill until it was brought to the desired size.

After passing all the material through the grinding circuit, the whole sample achieved a top size of -300 µm which is eligible for VXP mill treatment. According to FLSmidth (2012), the close circuit grinding test requires 25.0 kg of solid to recycle through the mill. Therefore, the sample was then split into 12 buckets with 25.0 kg in each by rotary splitter for testing.

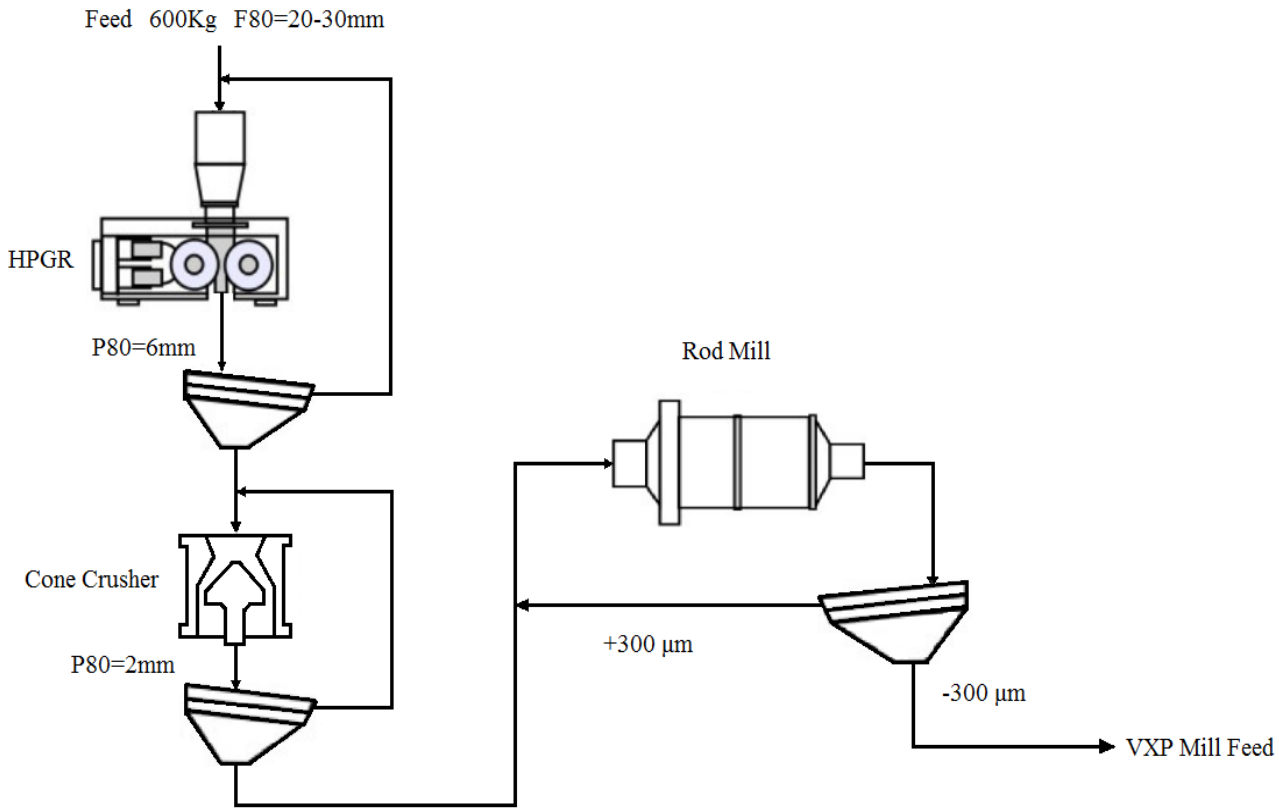

Figure 3-1 Diagram of sample preparation flow sheet

3.2.3 Experimental Plan

Based on the recommendation of Rahal (2011) presented in section 2.3 and the objectives of this research presented in section 1.2, the main operating variables studied in this research are: slurry solid content, stirrer speed and slurry viscosity. They are considered to be the most influential parameters in mill process stage (Jankovic, 2003). The VXPmill operates at its highest efficiency when the slurry density ranges from 1.35 kg/L to1.45 kg/L, which gives a slurry solid content between 20% v/v to 30% v/v (FLSmidth, 2012). In this case, 30% v/v is selected to represent the

medium solid content value for test, 15% v/v is selected as the low solid content value and 40% as the high solid content.

For stirrer speed selection, the VXP—10 mill can operate at any speed between 300 rpm and 1700 rpm (FLSmidth, 2012). Therefore, a speed of 1350 rpm is set for this study as a medium level while 1100 rpm as the lowest and 1600 rpm as the highest speed.

Grinding test number and their corresponding operating parameters are listed in Table 3-2. Detailed experiment results of each test are shown in **Error! Reference source not found.**

Table 3-2 Grinding variables for each grinding test

Test #	Operating parameters			
	Feed size F_{80} (μm)	Mill speed (rpm)	Slurry solid content (v/v)	Grinding media
1	200	1100	15%	CZS, 3mm diameter, 50% filling ratio
2	200	1350	15%	
3	200	1600	15%	
4	200	1100	30%	
5	200	1350	30%	
6	200	1600	30%	
7	200	1100	40%	
8	200	1350	40%	
9	200	1600	40%	
10	200	600	30%	

3.2.4 Test Procedures

The mill used in the test is a 10 liters pilot scale VXPmill. The schematic of the pilot test circuit set up is shown in Figure 3-2. Test procedures are developed based on Laboratory Testing Procedures by FLSmidth (2012).

1) Turn on the power and log into the system through the control panel. Plug in flash drive for data logging.
2) Turn on the agitator in both mixing tank 1 and 2. Set the mill stirrer speed to 300 rpm. Mix solids with a certain amount of water in a bucket using a handhold stirrer and then transfer them into the mixing tank 1.
3) Adjust the speed of pump 1 to get a desired flow rate. Circulate material through the circuit to make sure slurry is well mixed and homogenized. After running slurry through the circuit for 3 minutes, take feed sample from sampling point 1.
4) Change valve settings to allow slurry to go through grinding chamber and discharge to product tank. At the same time, increase the stirrer speed to a test rpm and fill the chamber with 3 mm beads to a 50% filling ratio.
5) At the time point when 2/3 of the slurry has come out to product tank, take 200ml sample from sampling point 1(2) for analysis.
6) When the mixing tank 1(2) is empty, switch valve 1 and 2 to direct pulp slurry flow from mixing tank 2 to mixing tank 1.
7) Repeat the above procedures for 9 cycles and collect samples for analysis.

Drain waste material and collect grinding beads. Clean the circuit with clear water and shut down the system.

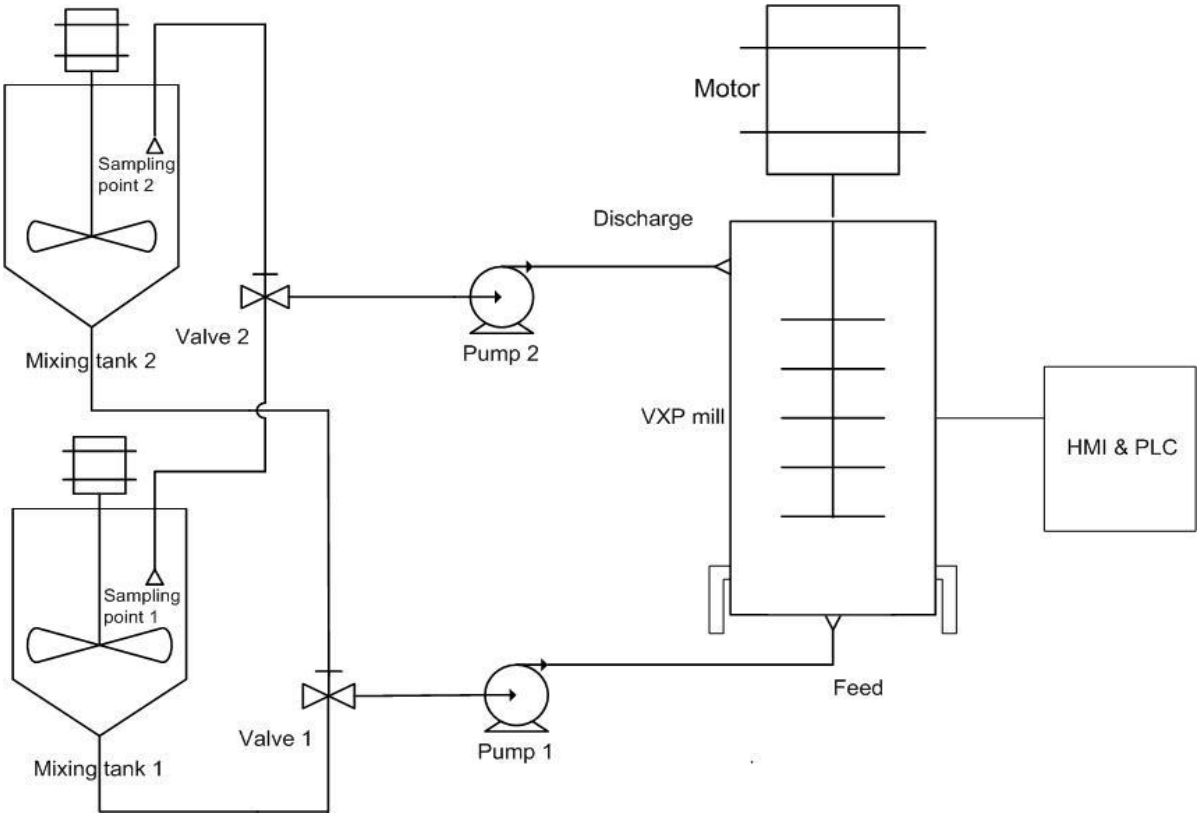

Figure 3-2 Diagram of VXP10 mill lab grinding test circuit

3.2.5 Product Characterization

Measurement of product particle size distributions was performed on a Malvern Mastersizer 2000 laser diffraction size analyzer. There is an ultrasound dispersion unit installed prior to the laser analyzer in order to keep the sample suspended and homogenized. Wet samples are added into the dispersion unit and then circulated through the measurement zone. The tested results are recorded on a PC.

The rheological properties of slurry were determined using a HAAKE Viscotester 550 Rotational Viscometer. A cylindrical cup filled up with slurry sample was agitated by a bob connected to a

sensor. A rotational speed program is pre-set and the resistance against the flow is measured. The final information on viscosity, shear stress and yield stress were given digitally on a controlling computer. To minimize the effect of particle settling and wall slip on measuring results, an elongated cylinder fixture developed by Klein (1992) was used in this test. This design can significantly reduce the error induced by particle settling.

3.3 Computer Modeling Test

3.3.1 Software

EDEM software is one of the most popular commercialized DEM software in the world. It was introduced by DEM solutions in 2005 and it recently released version 2.5. This software is designed to fulfill the simulation tasks of particle handling and processing operations. It has been successfully applied throughout the production chain in the mining industry-from mine to mill to bulk terminal (EDEM, 2012).

The EDEM software is made up of three parts: the Creator, the Simulator and the Analyst. In EDEM creator, one can create physical geometry, particles and define mathematical models to be used on a particular engineering case. With EDEM Simulator, the solver engine can do iterations and find the optimal solution for each time step. With EDEM Analyst, managing and tracking information about each individual particle such as mass, velocity and forces acting on it can be done. It also provides powerful analysis tools, 3D visualization of particles and video creation.

ANSYS Fluent is a powerful software in computational fluid dynamic modeling. It has been applied to simulation of a wide of fluid flow in mineral processing engineering field. It is integrated into the ANSYS Workbench platform where users can build geometry, mesh parts and run a simulation.

3.3.2 Model Set-up

3.3.2.1 Mill Geometry

The model is pre-drafted in CAD software based on the actual dimensions of VXP10 pilot scale machine. It is then imported into the EDEM software for simulation. The simulation is only focused on the grinding media activities in the mill chamber (Roufail, 2011).

There are two types of simulations in this study. In the first type, a simplified mill geometry with reduced number of beads is used to model grinding under various operating parameters and their results are going to be used in the discussion and analysis in Chapter 4: section 4.2—4.6; In the second type, a 1:1 mill model with the same amount of beads as the actual grinding test is used to validate the grinding test result by comparing their torque values. The discussion of this is given in Chapter 4: section 4.2.

As mentioned in Chapter 2: section 2.6, one problem for DEM modeling is the long simulation time when using a large number of media particles in the model. In this case, the number of grinding media used in the grinding tests is around 140,000 and to perform a DEM modeling on this amount of media in a full scale VXPmill took around 2 weeks to finish a 2 seconds simulation. Therefore, after validating the model, instead of modeling a full size mill with 12

discs, the geometry is scaled down to a mill with 4 discs for this work as has been done in most other published work. Meanwhile, some unnecessary and complex parts that will not affect the function of the mill, such as bearing and screw bolts are also removed. In this way, the number of beads simulated is reduced and the same level of media filling ratio is maintained. With the number of grinding media becomes almost 1/3 of real grinding tests, the time to finish one simulation program is shortened to 5—7 days.

The components in the simplified mill are: a stirrer with its polyurethane discs rigidly connected to the shaft; an enclosed steel mill chamber; grinding media made of CZS (ceramic zirconium silicate) and slurry being ground. The simplified mill geometry is illustrated in Figure 3-3. Some size parameters of the pilot scale mill are given in Table 3-3.

Table 3-3 Parameters of simplified VXP10 model

FLSmidth—Knelson VXP 10	Value
Net Volume (L)	3.4
Disc Diameter (mm)	130
Stir Speed (rpm)	0—1736
Tip Speed (m/s)	0—12
Mill Inner Diameter (mm)	166
Mill Outer Diameter (mm)	186
Shaft Diameter (mm)	30
Mill Chamber Height (mm)	230
Number of Discs	4

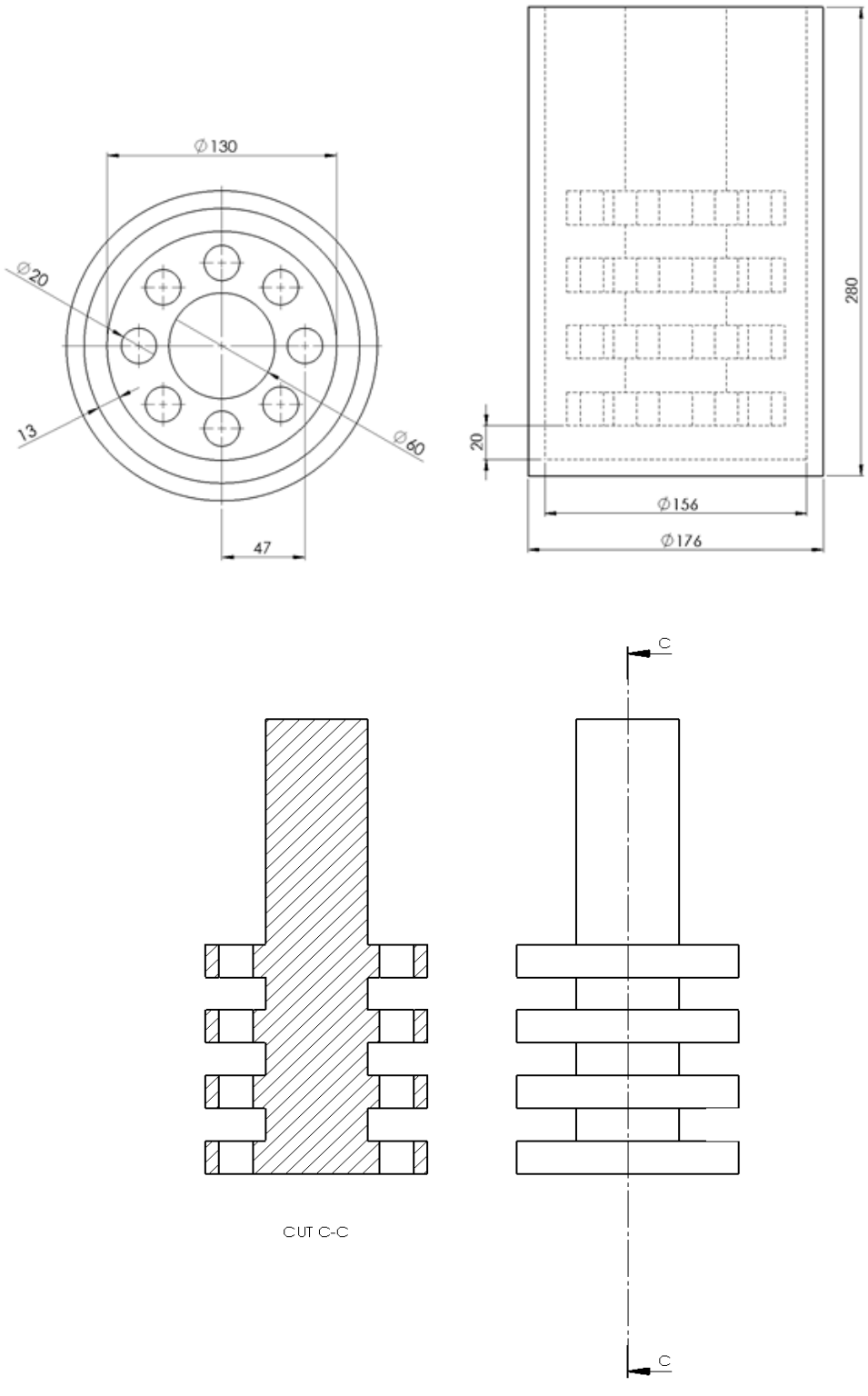

Figure 3-3 Schematic of simplified VXP10 mill geometry

3.3.2.2 Input Parameters to EDEM

The EDEM software requires users to assign parameters to each item modeled in the simulation. The coefficient parameters between items also needed to be defined by users. Those parameters are important to defining intrinsic physical properties of objects in the system. They are fixed for all the tests and through the entire duration of the simulation. Some input parameters are listed in Table 3-4 and Table 3-5.

Table 3-4 Component interaction parameters[1]

Items	Coe. of Restitution	Coe. of Static Friction	Coe. of Rolling Friction
Media-Media	0.5	0.5	0.01
Media-Mill Wall	0.5	0.2	0.01
Media-Stirrer	0.4	0.3	0.01

Table 3-5 Input material property parameters[2]

Items	Material	Shear Modules ($GPa=10^9Pa$)	Poisson Ratio	Density(kg/m^3)
Grinding Beads	CZS (65% ZrO_2; 35% SiO_2)	100	0.285	4000(Intrinsic)
Chamber Wall	Steel	78	0.28	7850
Stirrer Discs	Engineering Plastic	0.86	0.38	1300

[1] Interaction parameters between components are from www.roymech.co.uk and www.accuratus.com.

[2] Physical properties of grinding media in are from Bannikov et al. (2012) and SolidWorks Help Document (2010).

3.3.2.3 Experimental Plan

Besides the physical properties of materials listed in section 3.3.2.2, there are some dynamic parameters that need to be defined by users in EDEM. They are stirrer speed, slurry solid content, slurry viscosity and grinding media size. For the purpose of duplicating real grinding results and reflecting the grinding media behavior in the mill, the dynamic parameters listed in Table 3-6 are used and are based on the grinding test plan presented in section 3.2.3, except test No. 13 and No. 14. They are conducted to demonstrate the influence of bead size on its moving trajectory in the mill. The slurry viscosity presented in Table 3-6 is based on the measured values as discussed in section 3.2.5.

Table 3-6 Variables for each simulation test

Test #	Operating parameters			
	Stirrer speed (rpm)	Slurry solid content (v/v)	Slurry viscosity (Pas)	Grinding media
1	600	15%	0.005	CZS, 3 mm diameter
2	1100	15%	0.005	
3	1350	15%	0.005	
4	1600	15%	0.005	
5	600	30%	0.025	
6	1100	30%	0.025	
7	1350	30%	0.025	
8	1600	30%	0.025	
9	600	40%	0.125	
10	1100	40%	0.125	
11	1350	40%	0.125	
12	1600	40%	0.125	
13	1100	15%	0.025	
14	1100	15%	0.125	
15	1100	15%	0.025	CZS, 2 mm diameter
16	600	15%	0.025	CZS, 4 mm diameter

3.3.2.4 Fluid Flow Modeling

The flow in the VXPmill consists of a discrete particle flow phase and a continuous fluid flow phase. Since the DEM was developed to only simulate particle behaviour in dry conditions, it is necessary to introduce the fluid flow effect into the system. To model the slurry in the VXPmill, the computational fluid dynamic (CFD) is applied.

In numerical modeling, the continuous fluid flow field is solved using the Navier-Stokes equation which is given by

$$\frac{\partial \rho}{\partial t} + \nabla \cdot (\rho \vec{v}) = 0$$ Equation 3-1

$$\frac{\partial}{\partial t}(\rho \vec{v}) + \nabla \cdot (\rho \vec{v} \vec{v}) = -\nabla p + \nabla \cdot \left(\mu(\nabla \vec{v} + \nabla^t \vec{v})\right) + \rho \vec{g}$$ Equation 3-2

where ρ is the fluid density, $\vec{v}$ is fluid velocity, p is pressure, μ is fluid dynamic viscosity.

In EDEM, the fluid is introduced into the system by coupling the software with the CFD software—ANSYS-Fluent. The fluid domain model was built in WORKBENCH environment (Figure 3-4). Similar to DEM modeling, a 4-discs model is used to ensure simplicity of the model. The fluid near the stirrer discs was modeled using MRF (multi-reference frame) model. It is a popular method used to simulate the fluid flow motion stirred by impellers in a cylindrical container because it requires less input and gives satisfactory results (Santos-Moreau et al., 2012). In this case, the fluid domain geometry is divided into two parts — the rotating domain

which simulates the rotation of stirrer discs at a given speed and a static domain which represents the fluid between impellers and the mill inner wall.

The boundary conditions of the model are also shown in Figure 3-4. Velocity-inlet and velocity-outlet are used to define the movement path of slurry flow. A mesh interface which corresponds to pressure and flow continuity between the two domains is set up. The geometry is then meshed with “structured mesh” type in ICEM meshing software. The total element number is around 1.3 million. Calculation is achieved by commercial computational fluid dynamics software ANSYS-FLUENT. Before running a simulation, FLUENT requires some input parameters to define the problem. Some of the parameters used in this study can be found in Appendix C

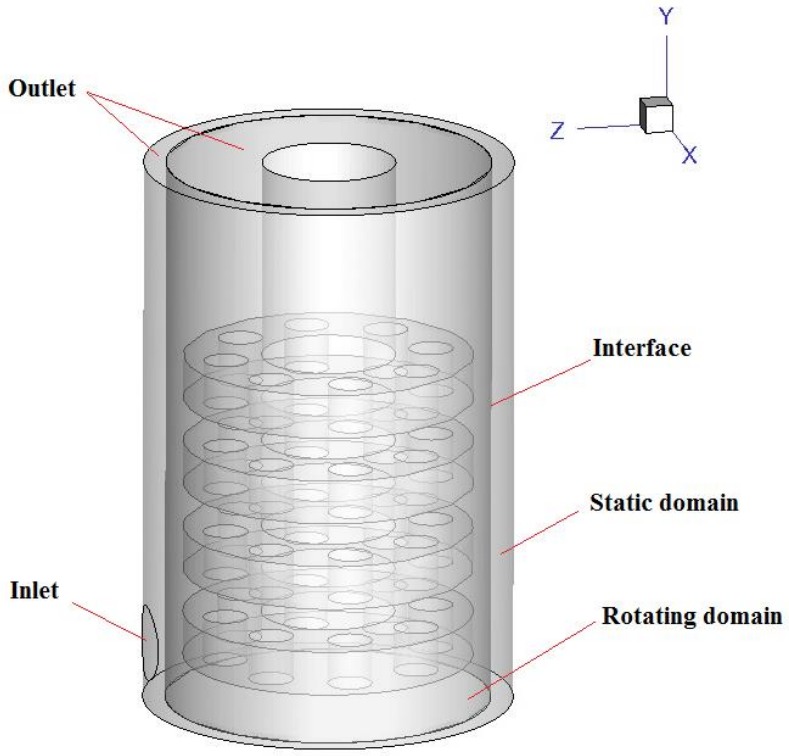

Figure 3-4 Simulated fluid domain in ANSYS using MRF model

There is an Application Programmable Interface (API) provided that enables communication between EDEM and the CFD software. The fluid information is calculated in CFD software and the particle-particle interaction is calculated by EDEM. The effect of slurry flow on grinding media is calculated by applying a fluid drag force and buoyant force and in return the grinding media react a counter force on the slurry flow stream.

$$F_B = gV\rho_s \quad \text{Equation 3-3}$$

$$F_d = \frac{1}{2}\rho_s C_d A v|v| \quad \text{Equation 3-4}$$

where F_B is buoyant force governed by gravity acceleration$g$, volume of grinding media$V$, and slurry densityρ_s; fluid drag force F_d is calculated with drag coefficient C_d, intersection area of grinding media A and the slurry velocity v of that point.

The fluid drag coefficient C_d is a function of Reynolds number of the slurry Re and is calculated by the following equations (Theuerkauf & Schwedes, 1999)

$$C_d = \frac{23.5}{Re} + \frac{4.6}{\sqrt{Re}} + 0.3 \quad \text{Equation 3-5}$$

$$Re = \frac{D|u_r|\rho_s}{\gamma_s} \quad \text{Equation 3-6}$$

where D is the bead diameter which the slurry stream passes by, u_r is the relative velocity between fluid velocity and bead velocity and ρ_s is the density of slurry. The relationship between drag coefficient C_d and Reynolds number is obtained from laboratory experiment and is shown in Figure 3-5. The solid line is for a sphere with a smooth surface and the dash line is for the case of a sphere with a rough surface.

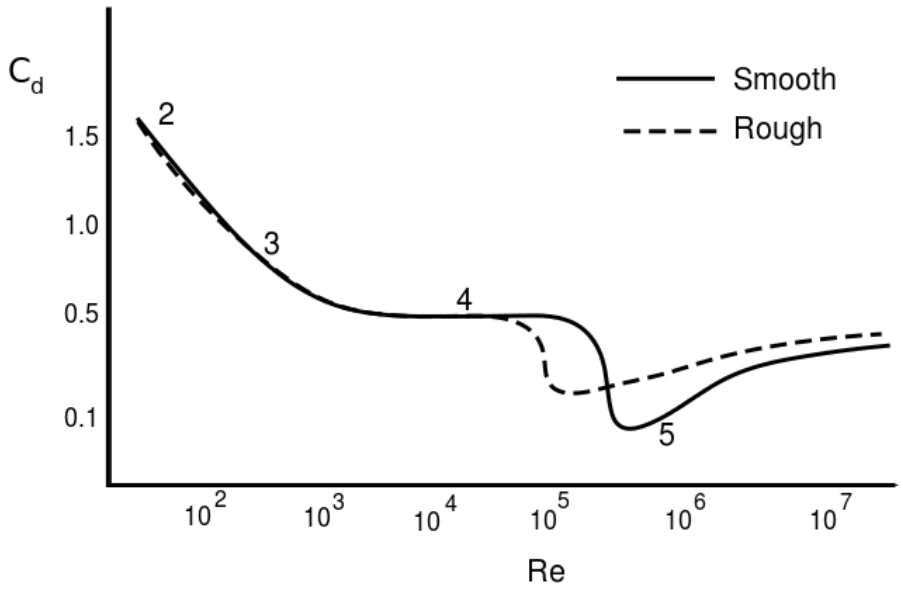

Figure 3-5 Drag coefficient as a function of Reynolds number (Munson et al., 1990)

Once all the parameters needed are set, the simulation is started. The mill is first filled with a pre-determined number of grinding media, 45,000 in this case. The method used to determine the number of grinding media used in the simulation program is stated in section 3.3.2.1. Then the stirrer starts to rotate at a given speed. The logic block diagram of the simulations in this study is shown in Figure 3-6. Results are exported after the simulation is finished.

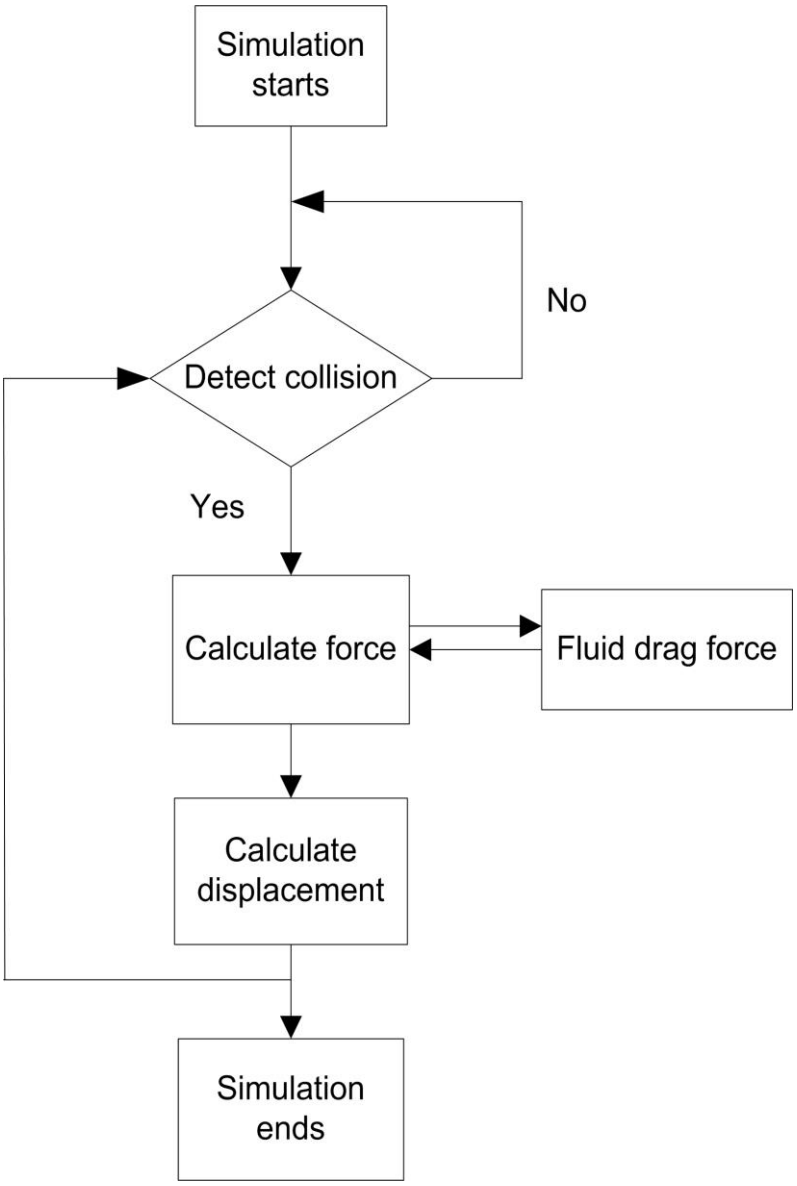

Figure 3-6 Simulation process block diagram

Chapter 4: Results and Analysis

4.1 Introduction

In this chapter, simulation and grinding test data will be analyzed. The results from the computer modeling are first validated by comparing them with the measured torque from the real grinding tests. Discussions on simulation and grinding results will focus on four parts:

- Slurry flow and grinding media movement in the mill.
- Effect of operating parameters (mill speed, slurry solid content and viscosity) on the breakage mechanism in the mill.
- Effect of operating parameters on media kinetic energy and collision frequency.
- Effect of different mill geometry configuration on mill performance.

4.2 Simulation Result Validation

The validation of simulated results is usually done by comparing the power draw (or power consumption) of the motor in experiments with that completed by simulation (Yang, 2006; Jayasundara, 2009). Since the power draw is a product of the stirrer rotational speed and the torque of the mill stirrer shaft and in this scenario, stirrer shafts in both grinding tests and simulations have uniform speeds, the torque values are used as the criteria for comparison. Another reason for using torque as a standard of comparison is because the torque values of the grinding tests can be easily read from the HMI control panel shown in Figure 3-2, and it can be calculated and exported by the EDEM software during simulation.

The test data used are from test No. 1, No. 2 and No. 3 in Table 3-2 and simulation conditions are the same as test No. 1, No. 2, and No. 3 in Table 3-6. Test torque was measured by a built-in sensor mounted on the center shaft connected to the drive motor, and simulated torque values of simulation were calculated by and exported from the EDEM software.

In Figure 4-1, the torque values of the shaft under different stirrer speeds are shown. It is seen that the torque of the main shaft increases as the stirrer speed increases. The figure shows a discrepancy between the simulated value and the measured value exists. Torque from the simulation is smaller than the torque from actual tests. Note the difference is more pronounced at high stirrer speed than at low speed. At a tip speed of 7m/s, the difference is 15.1%; at a tip speed of 10m/s, the difference is 14.3%; at a tip speed of 12m/s, the difference is 21.9%.

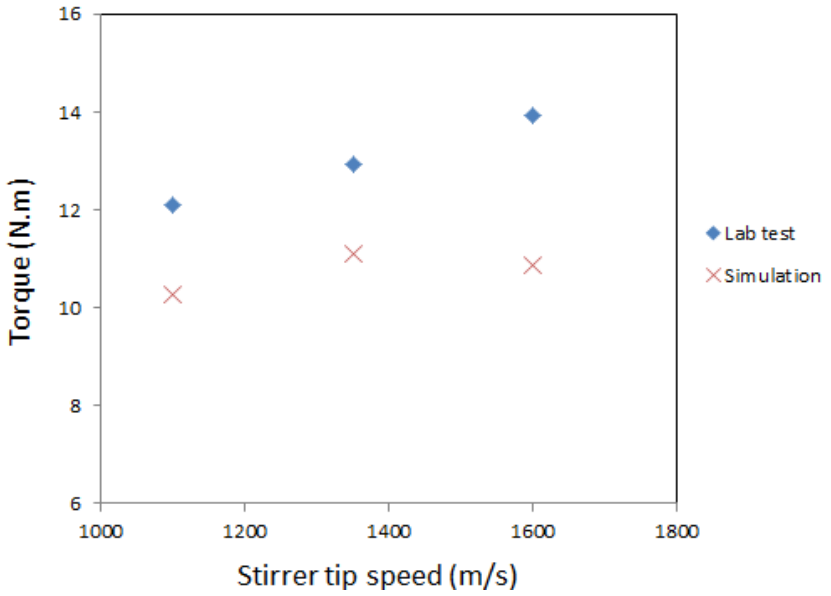

Figure 4-1 Simulated and tested torque data for different stirrer speeds

A similar level of discrepancy between experiment data and simulation data was reported by Jayasundara (2006) when studying the grinding performance in a pilot scale IsaMill using DEM simulation. By comparing the energy consumption data of physical and numerical tests in his research, it was found that the difference was around 10% at lower stirrer speed and went up to 18% when the speed was higher than 1300 rpm. This is because in the real grinding test, the input energy cannot be fully transferred to the grinding media due to energy losses in the form of heat and sound. However, these losses are not considered in modeling work (Yang et al., 2006). The results from the EDEM model in this research are consistent with this and hence can be used for investigating other aspects of mill performance.

4.3 Fluid and Grinding Media Motion in Vertical Stirred Mill

4.3.1 Grinding Media Distribution

Each simulation starts with a packed grinding media bed. Then the central shaft starts to rotate at a given speed and the particles are driven by stirrer discs to move towards the mill chamber wall. After running a certain period of time, the system will eventually reach a steady state. The number of particles distributed in each area of the mill is an apparent indicator of the stability of grinding system (Roufail, 2011). Although the period of time varies with different operating conditions, it is generally considered 0.5 seconds is long enough to let the system reach equilibrium (Yang et al., 2006). Sinnott et al. (2006) mentioned in their research on modeling of a Vertimill that there is a sudden surge in beads kinetic energy due to the start-up of stirrer. After that, the beads will redistribute in the mill and form a steady state in less than 0.5 second.

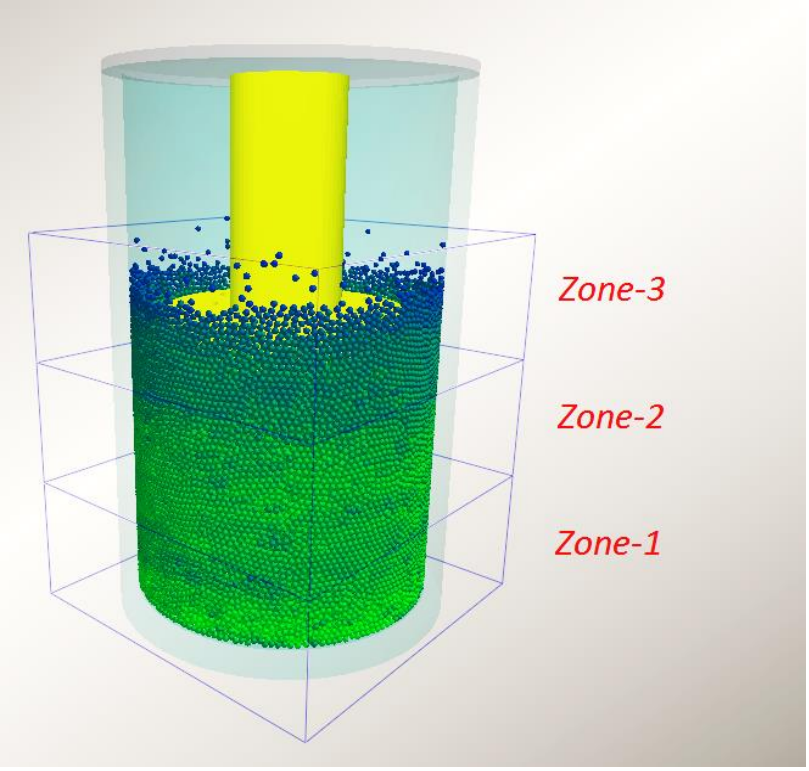

Figure 4-2 Zone division of VXP10 mill model

For the sake of better understanding the bead distribution in each area inside the mill as well as the time it needs to reach a steady state, the model is divided into three different zones. They are Zone-1, Zone-2 and Zone-3 from bottom to top as the sections showed in Figure 4-2. They have the same height of 70 mm. The three blocks only cover the spaces where beads will reach.

Although there is no standard on how long the simulation time should be, a longer running time is always preferable since it is closer to a real grinding test and more information can be acquired. However, a too long simulation time is impractical in this study because there are a number of simulations to be finished in a limited time and the capability of the computer is not able to perform that work.

To decide how long the simulation time for each model would be in this study, a group of preliminary simulations are done. One of the results is shown in Figure 4-3 while other results under different operating conditions can be found in Appendix A . The number of beads in each zone is plotted versus simulation time to assess at which time point the distribution of beads reaches equilibrium. From the curves below, it is observed that particles in the bottom zone are moving to middle and top zones of the mill due to the stirring motion of discs. Within the first 0.5 seconds, a balance of beads has been reached and the number of media particles in each zone does not change with simulation time. Therefore the simulation time is selected as 2 seconds and it is enough to get the system to an "equilibrium state".

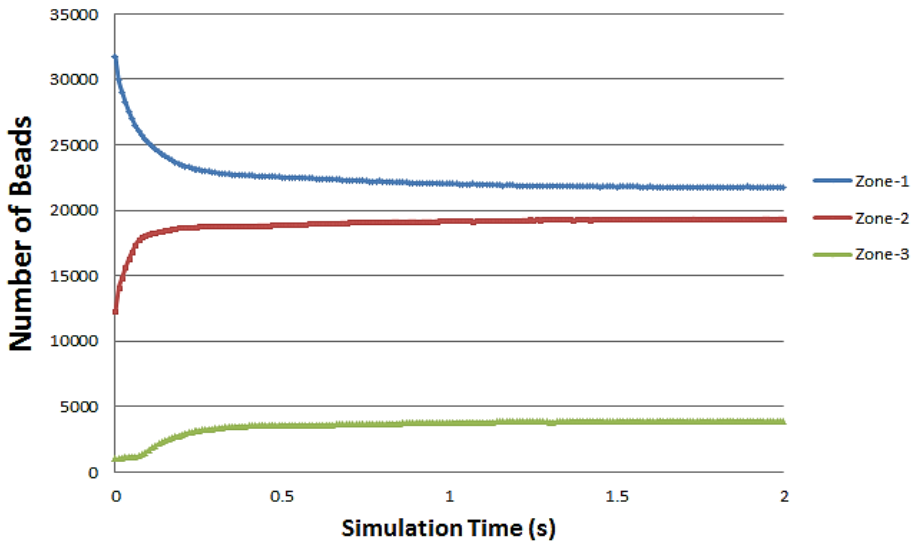

Figure 4-3 Grinding media distribution in 3 zones over time

(15% v/v, 0.005 Pas, 1100 rpm The number of beads in each zone is plotted against stirrer rotational speed in Figure 4-4. It is shown that stirrer speed affects beads distribution in that as

the speed increases, media tend to distribute more evenly across the mill. Among the three zones, the beads number in Zone 1 decreased by 16.6% from 600 rpm to 1100 rpm. From 1100 rpm 1600 rpm, the beads number decreases by 16.8%. This is because most of the beads reside in the bottom zone (Zone 1) due to gravitational force and compressive force from beads in Zone 2 and Zone 3. Bead numbers in Zone 2 tends to be constant across the three speeds. It means that the beads lost in Zone 1 are mostly transported to the top area causing an increase in beads in Zone 3. It is observed that the number of beads in Zone 3 increases 2226.5% when the speed is increased from 600 rpm to 1100 rpm. From 1100 rpm to 1600 rpm, the number of beads increases 114.9%. After increasing the stirrer speed from initial speed to top speed, the bead number in Zone 1 and Zone 2 becomes the same and both of them are greater than the beads number in Zone 3. This indicates that most of the grinding activities happen in the bottom and middle area of the mill.

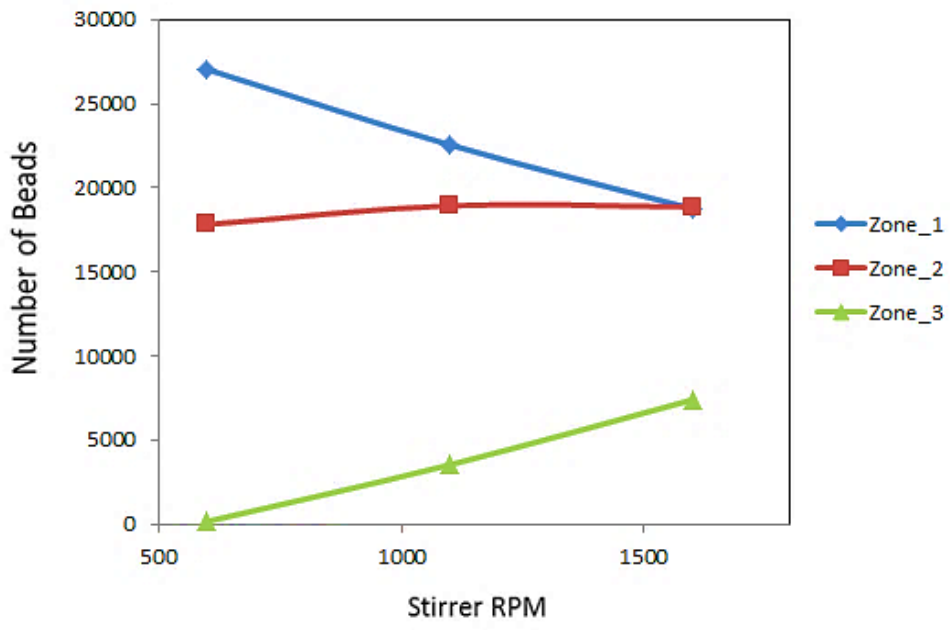

Figure 4-4 Grinding media distribution in 3 zones under different stirrer speed

Figure 4-5 shows how solid content of slurry affects bead distribution in the mill. Three different slurry solid content 15% v/v, 30% v/v and 40% v/v are tested and their influences on beads existing in different zones are plotted. It is shown that the effect of slurry solid content is minimal. The amount of beads in the bottom zone increase slightly as solid content goes up, while the number of beads in top zone and middle zone drops a bit. Across all solid contents assessed, Zone 1 and Zone 2 hold the majority of beads, namely 92.2% 93.6 and 92.6%. This means that most of the grinding activities between beads and ore particles take place in the bottom and middle area of the grinding chamber. From Figure 4-5, it is concluded that the solid content of feed slurry is not a major influence on bead distribution through the mill.

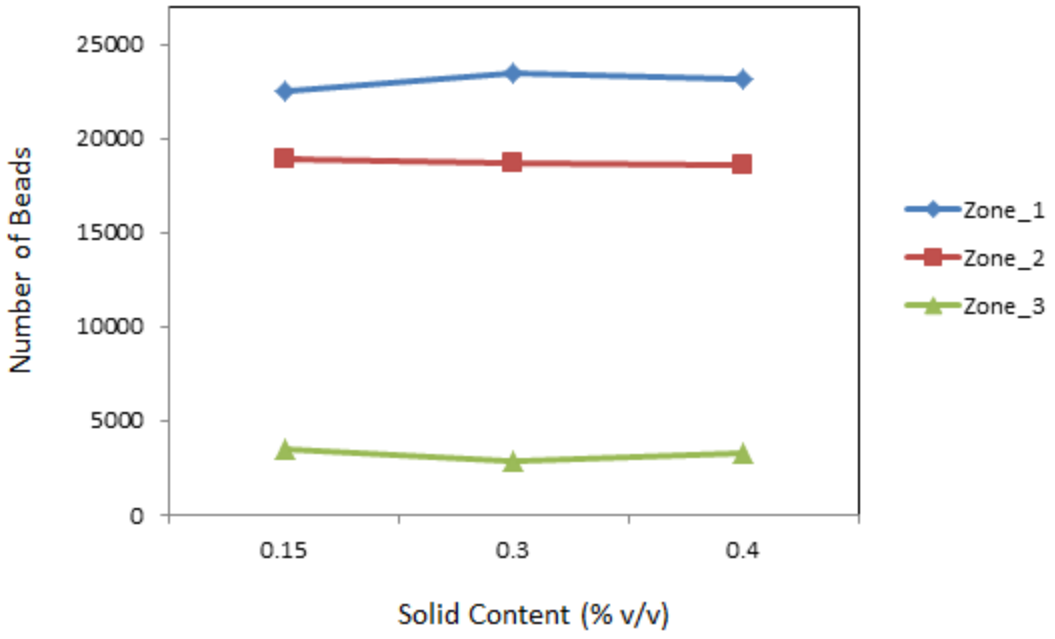

Figure 4-5 Grinding media distribution in 3 zones under different solid content

The influence of slurry viscosity on bead distribution was also studied (Figure 4-6). Three tests were conducted using slurry viscosity values of 0.005 Pas, 0.025 Pas and 0.125 Pas and the number of beads in each zone is counted. The number of beads is plotted against slurry viscosity in Figure 4-6. The change of bead numbers in different zones is quite significant. When the slurry viscosity is increased from 0.005 Pas to 0.025 Pas, the number of beads moving in zone 1 increased by 81%. From a slurry viscosity of 0.025 Pas to 0.125 Pas, the numbers of beads in zone 1 increase by 21.8%. Adding additional solids resulted in a drop in number of beads in Zone 2 and Zone 3. When the viscosity of slurry changes from 0.005 Pas to 0.025 Pas, the number of beads in zone 2 decreases by 4.7% and the number of beads in zone 3 decreases by 29.6%. When the viscosity increases from 0.025 Pas to 0.125 Pas, the number of beads in zone 2 drops by 16.6% and the number of beads in Zone 3 drops by 94.9%. It is clear that the viscosity of feed slurry has a major influence on bead distribution in the mill.

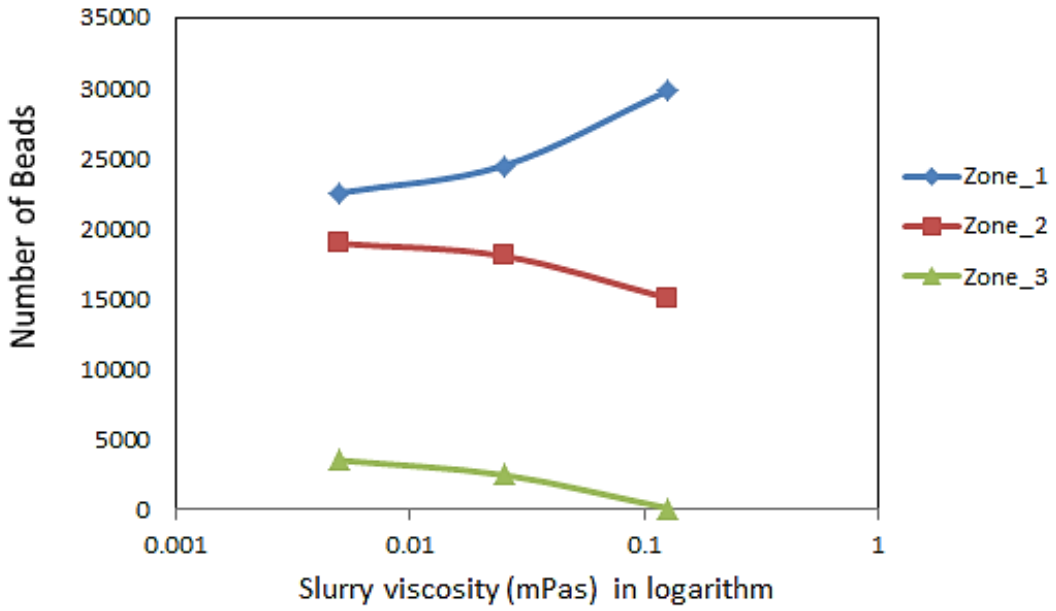

Figure 4-6 Grinding media distribution in 3 zones under different slurry viscosities

4.3.2 Grinding Media Trajectory

Grinding media movement pattern is considered to be a combined effect of the movement of viscous fluid and the rotation of disc impellers. To better understand the media motion in a vertical stirred media mill, a set of snapshots of beads trajectory over 2 seconds of simulation time is shown in Figure 4-7. Three beads diameters were chosen to show the influence of media size to bead trajectory. The beads being tracked were randomly selected among the 45,000 beads simulated. The point where the blue line starts (the positions where the points suggest in Figure 4-7) stands for the initial position of the beads selected, they are from top, middle and bottom zones of the mill chamber.

It is shown in Figure 4-7 A. that the beads are stirred in the beginning and get an initial speed to move along the annular gap between stirrer discs and mill inner wall. Due to the high rotational

speed of the stirrer, the beads gain a high velocity in the axial direction and are being forced to move outward. They move upward in a helical pattern until they reach a certain height. Then those beads will just keep revolving at the same level although there are fluctuations in their tracks. This is because of the packing effect of media beads. It enables the bottom media layer to support the upper layer, thus the beads will move at a constant height. The observations show that at a high stirrer rotational speed the beads are more influenced by the rotation of the impeller rather than the slurry streams moving upward. Although there is a complicated slurry flow pattern in a high speed stirred mill, the bead motion seems to be independent from the slurry streams and is more influenced by the dynamic motion of disc impeller. There is no migration of beads from one zone of the chamber to another, instead they all stay in a constant zone. The results are in agreement with Gers et al. (2010) who investigated the hydrodynamics and collision characteristics in vertical stirred media mill using numerical modelling. They found that tangential flow in a mill is the dominant driving force of grinding activity compared to axial flow, but the axial flow is helpful in mixing the suspension.

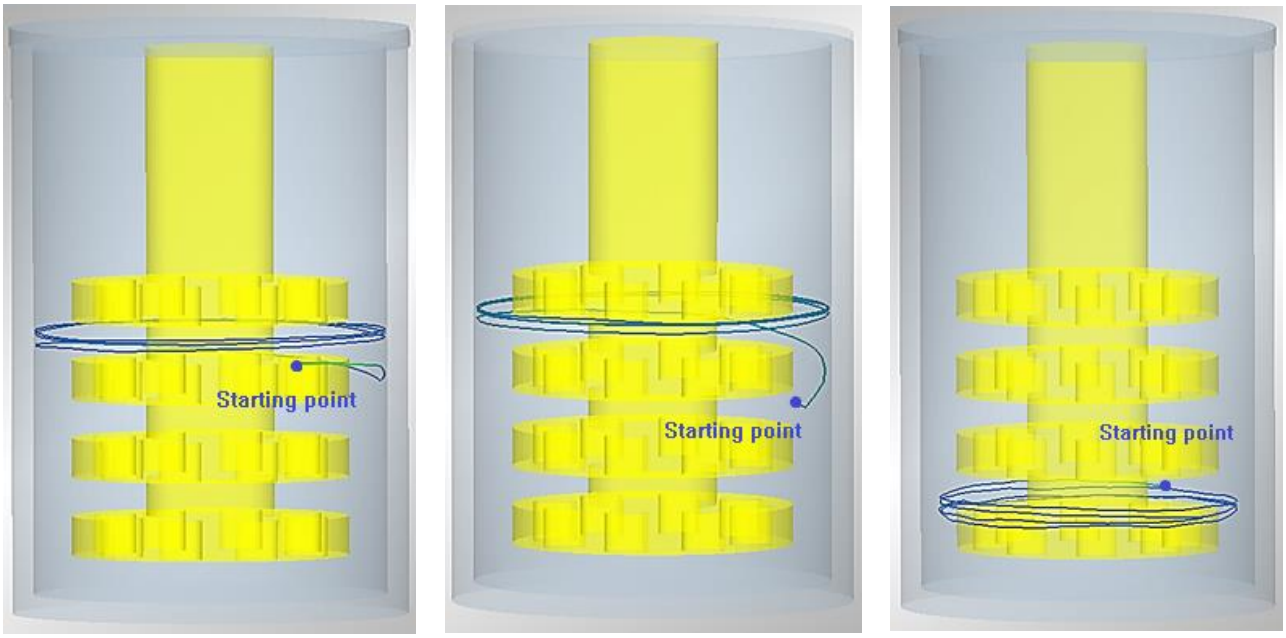

A. 2 mm bead, 15% v/v **B. 3 mm bead, 15% v/v** **C. 4 mm bead, 15% v/v**

Figure 4-7 Grinding media trajectory under different operating conditions

4.3.3 Study on Slurry Motion

The slurry motion is tested under different stirrer speed, slurry solid content (slurry density) and slurry viscosity.

The effect of impeller rotation speed on slurry motion was investigated. Results of simulation test No.1, No.2 and No.4 in Table 3-6 are shown in Figure 4-9. A middle plane (shown in Figure 4-8) was extracted from the mill model and slurry volume fraction information is shown in colored contours where blue area stands for air, red area stands for slurry and green stands for the transition part in between. The density and viscosity of slurry in this case is 1350 kg/m^3 and 5 mPas respectively which is the same as the feed material with 15% solid content V/V. The shape

of slurry is assessed under three different stirrer rotational speed: 600 rpm, 1100 rpm and 1600 rpm. The corresponding grinding conditions are test No. 1, No. 2 and No.4 in Table 3-6.

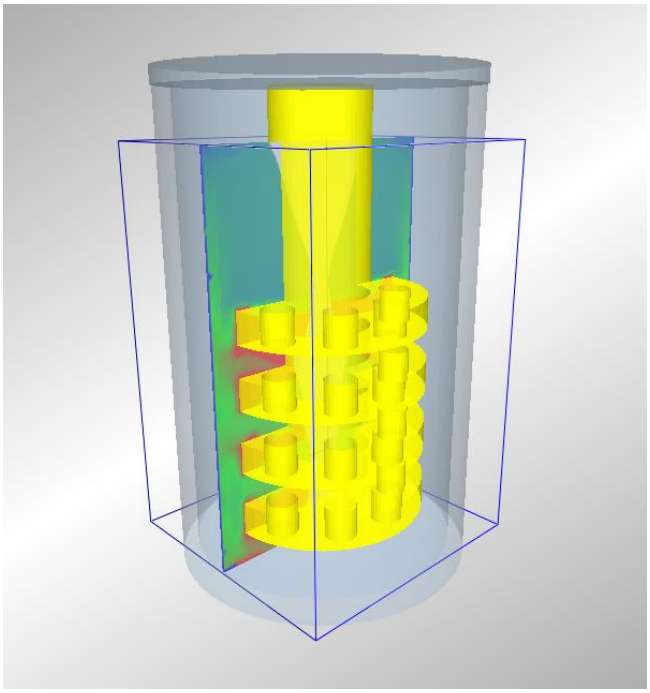

Figure 4-8 Illustration of a plane taken from the center of the VXPmill model

Figure 4-9 A shows that at a low operating speed (600 rpm), a large air vortex exists in the center. The vortex is conical which is narrower at the bottom and grows wider up the axial direction. This is because the gravity force is greater than centrifugal force generated by disc rotation so that it pulls the slurry down to the bottom. The fluid in the vicinity of stirrer discs is being pushed to the wall due to the strong shear stress generated by disc rotation and when they

go up beyond the discs region, the fluid flows back and resides on the top surface of the first disc.

When the stirrer speed increases to 1100 rpm (Figure 4-9 B.), the volume of the air vortex grows. More void space is being generated which means less ore particles are being ground by media. The shape of the air vortex becomes more cylindrical rather than conical. The bottom wall of mill chamber is exposed to air and becomes a void zone with a diameter of 60mm. More air bubbles in the slurry are trapped in the slurry compared to the low speed.

When the disc rotates at the highest speed (Figure 4-9 C.), slurry is squeezed to the wall and the shape of the air cone becomes uniform from top to bottom. The back flow on top of the first disc is minimized. More air bubbles are observed in disc tip area.

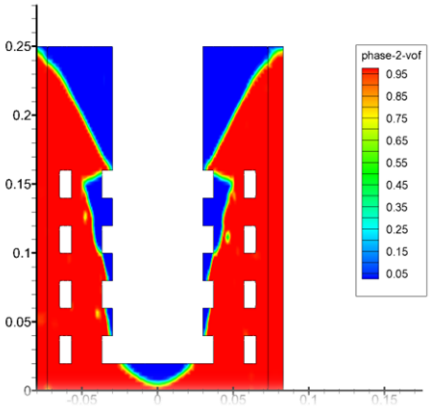

A. Low speed (600 rpm)

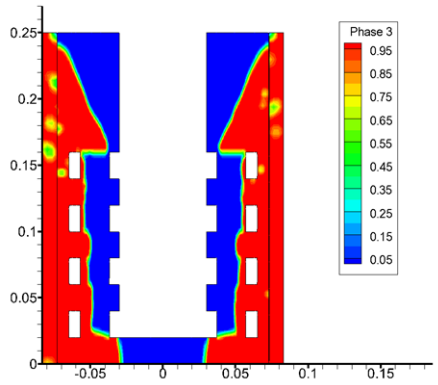

B. Mid speed (1100rpm)

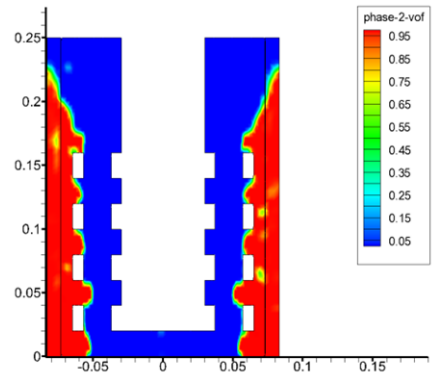

C. High speed (1600 rpm)

Figure 4-9 Slurry profile under different stirrer speed

Figure 4-10 shows the influence of slurry viscosity on slurry shape in the mill. Results are from simulation No.1, No. 5 and No.9 in Table 3-6. It is observed that the air vortex in the center of the mill enlarges with the increase of viscosity. The vortex remains a conical shape from 0.005 Pas to 0.025 Pas and changes to cylindrical at high viscosity value. Compare to the slurry moving at low viscosity, the outline of slurry body is rather unstable and a large chunk of slurry rises at the top part of the mill.

Results shown in Figure 4-10 confirm the findings by Sinnott et al. (2011). They presented a computational fluid model on slurry characteristics in a stirred media mill and found that slurry viscosity is the most influential factor to fluid behavior. At low viscosity, pressure distribution is more static and fluid is more mobile. When the viscosity increases, the fluid tends to be pulled around by beads and a much wider band is observed.

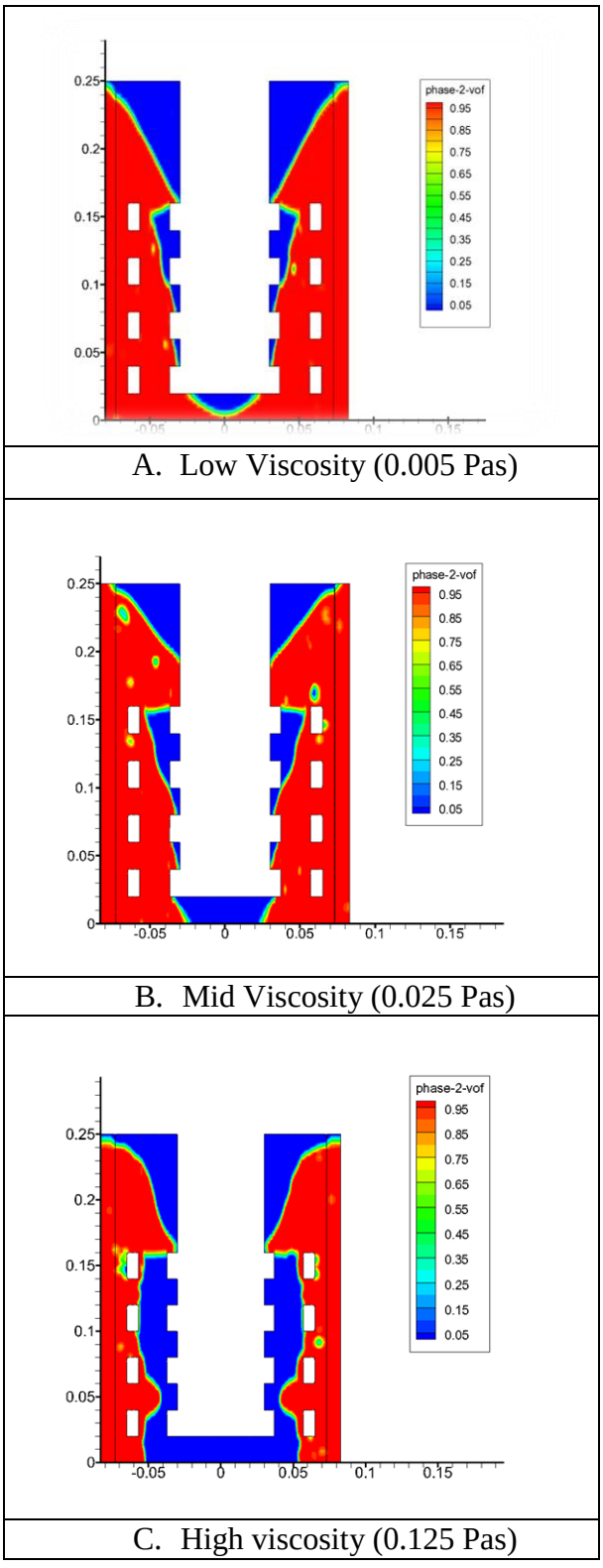

A. Low Viscosity (0.005 Pas)

B. Mid Viscosity (0.025 Pas)

C. High viscosity (0.125 Pas)

Figure 4-10 Slurry profile under different slurry viscosity

To investigate the influence of vortex to grinding volume in the mill, the concept of "effective grinding volume" is introduced. It is defined as the ratio between total slurry volume and the overall empty volume in the mill. The effective grinding volume reflects the utilization of the space inside of the mill chamber. The higher the percentage number is, the smaller the air vortex will be and more space will be used in grinding ore particles.

Simulation data from test No. 1, No. 13 and No. 14 in Table 3-6 are demonstrated in Figure 4-11. When looking at one curve under a given slurry viscosity, the effective grinding volume is higher at low speed and decreases as the stirrer rotates faster. It confirms that the size of the air vortex in the center of the mill grows as the stirrer speed increases. By comparing three curves under different slurry viscosity, it is observed that the effective grinding volume drops as the slurry viscosity decreases for all stirrer speeds tested.

Figure 4-11 also shows that the slurry viscosity affects the stability of slurry being stirred. When the slurry viscosity is low (0.005 Pas), the effective volume of grinding drops smoothly with the increasing stirrer speed, indicating that the movement of slurry in the mill is steady. When the slurry viscosity is increased to 0.025 Pas, the curve shows some fluctuations compared to lower viscosity, especially when the stirrer speed is below 1000 rpm. When the slurry viscosity is very high (0.125 Pas), the curve shows an obvious wave motion which means the ratio of slurry volume to the air vortex volume is changing all the time. This curve shape suggests a very unstable slurry flow in the mill.

Jayasundara et al. (2009) studied the influence of slurry viscosity to media and slurry motion in an IsaMill by using DEM modeling. They reported that at lower viscosity, slurry and grinding media tend to move to the mill wall, creating an empty space in the center of the mill. At higher

viscosity, slurry and media move more vigorously due to the stronger viscous force and distribute more evenly in the mill. The empty space minimizes under high slurry viscosity. Their findings attested results shown in Figure 4-11.

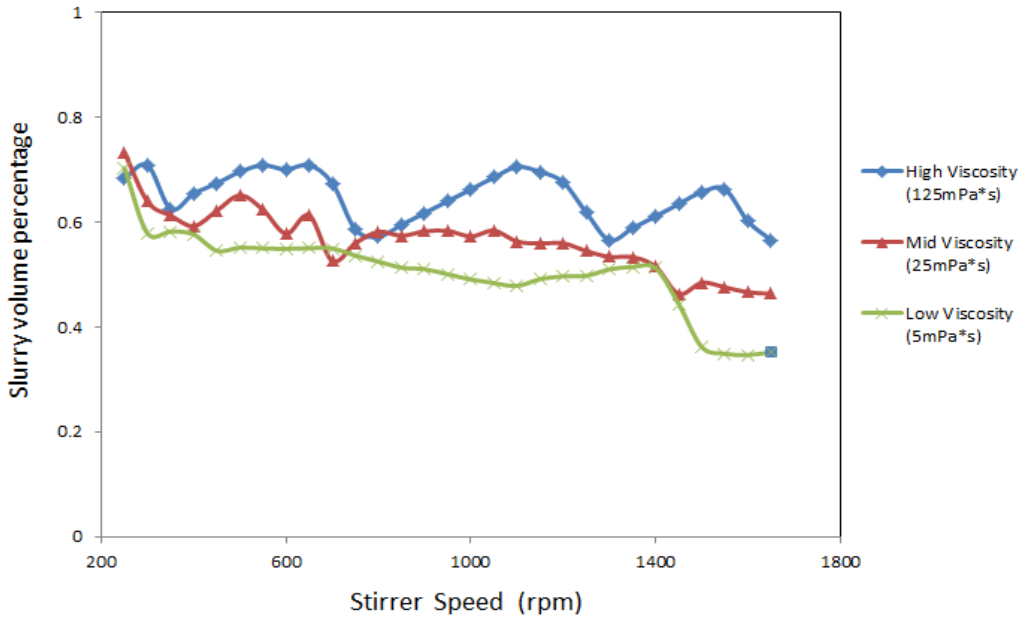

Figure 4-11 Slurry effective grinding volume under different stirrer speed

4.3.4 Study on Grinding Media Motion

To investigate the bead velocity and movement within the same level, a cross-sectional plane from different height levels was used to demonstrate grinding media motion (Figure 4-12). The figures were taken after an "equilibrium state" (as described in section 4.3.1) was reached. Their corresponding velocity profiles along the radial direction are attached on the left column. Particles are coloured according to their velocity magnitude.

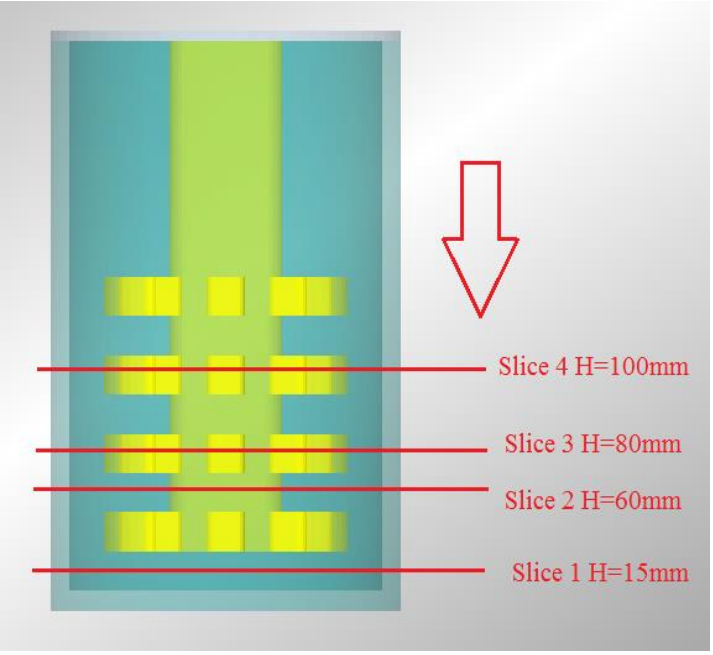

Figure 4-12 Illustration of position of slices taken from different height levels

Within the same plane, it is shown that the highest particle velocities (which are coloured by green and red in Figure 4-13) in a vertical stirred mill are observed in the vicinity of the circular disc edges. There is a low particle velocity zone adjacent to the inner chamber wall, and the particles in this area are dark blue. Therefore, a velocity gradient exists between the disc edge and the chamber wall. It is believed that the velocity difference between each layer of beads results in a stress event that eventually causes ore breakage. Since the high rotational speed of the discs disperses beads in the radial direction creating a space void of beads in the center of the mill, there is no interaction between beads and ore particles in this zone. The diameter of the space with no beads increases as stirrer speed increases. There is a 'stagnant zone' close to the chamber wall and it has little stress energy so that the grinding stress in that area is negligible. The most active zone is considered to be the circumferential space around disc surfaces, where

beads have the highest kinetic energy. Therefore, it is concluded that the beads which are close to the disc edges and surfaces have the highest energy to break ore particles. This result agrees with Stender et al. (2001, 2004). In their research, the space in the mill was divided into 4 active grinding zones and the one near the disc edge had the most number of collisions.

When putting the 4 slices together and examining them along the mill longitude direction, it is observed that the number of beads in each slice decreases as height increases. This conclusion is also verified in Chapter 4:. This is due to the gravitational forces that hold most of the beads in the bottom zone of the chamber. The highest average velocity is reached in the position of slice 2, which is about 1/3 from the bottom. This indicates that although the bottom zone of the mill holds the most number of grinding beads, it does not necessarily mean that it is also the only area with the highest density of breakage energy. The spaces around the vicinity of impellers are also high breakage energy areas.

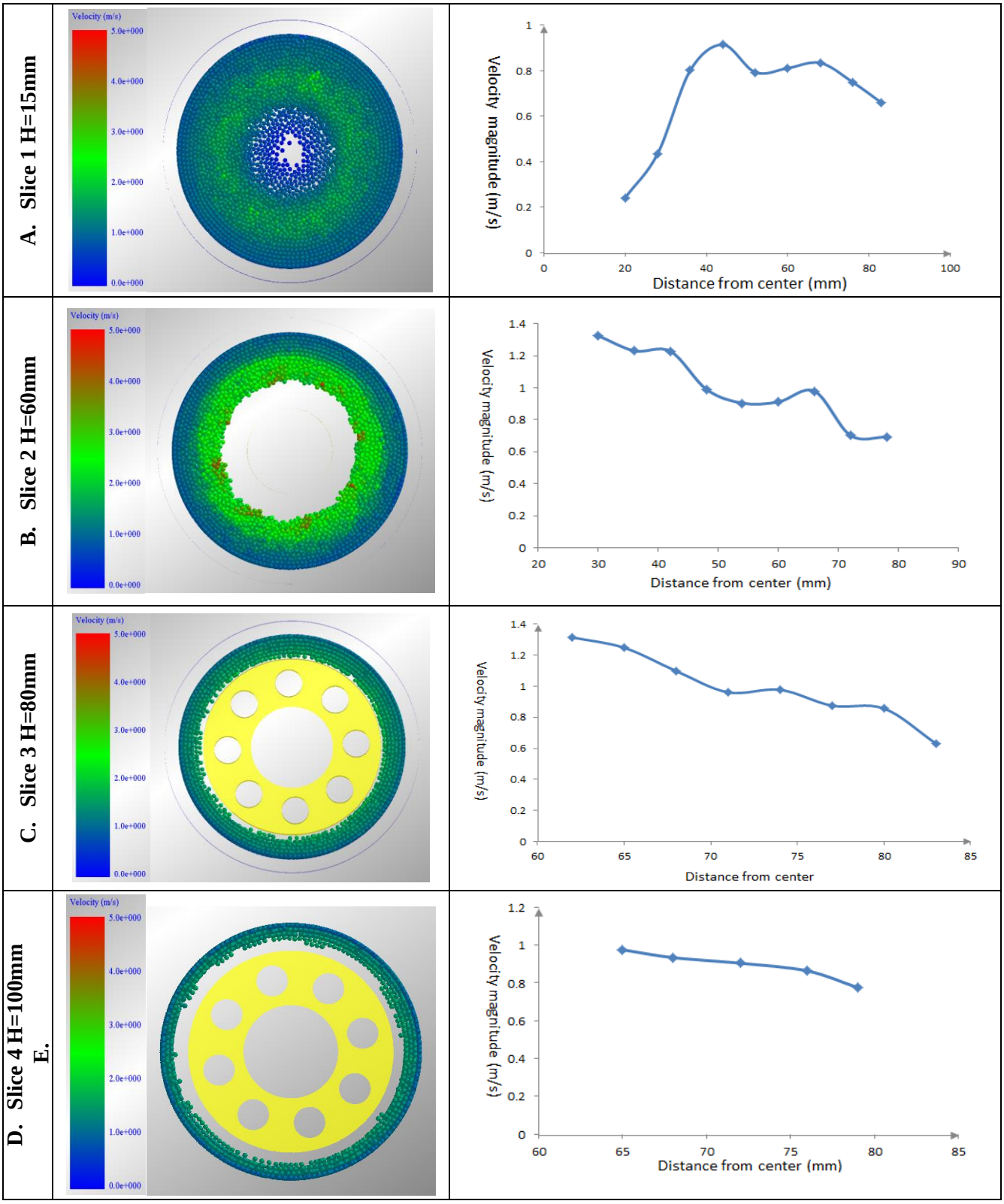

Figure 4-13 Grinding media velocity gradient along radial direction at 600 rpm

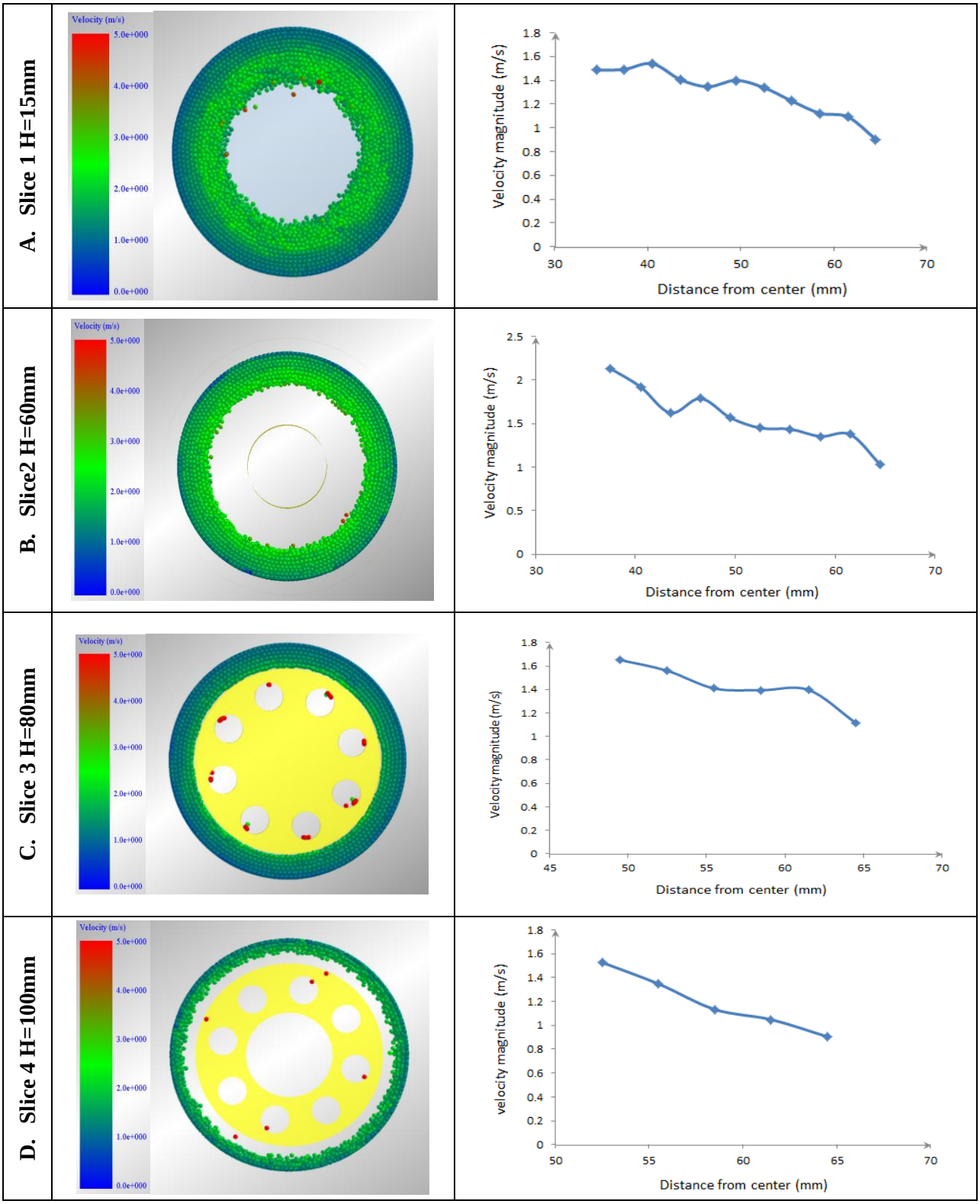

Figure 4-14 Grinding media velocity gradient along radial direction at 1100 rpm

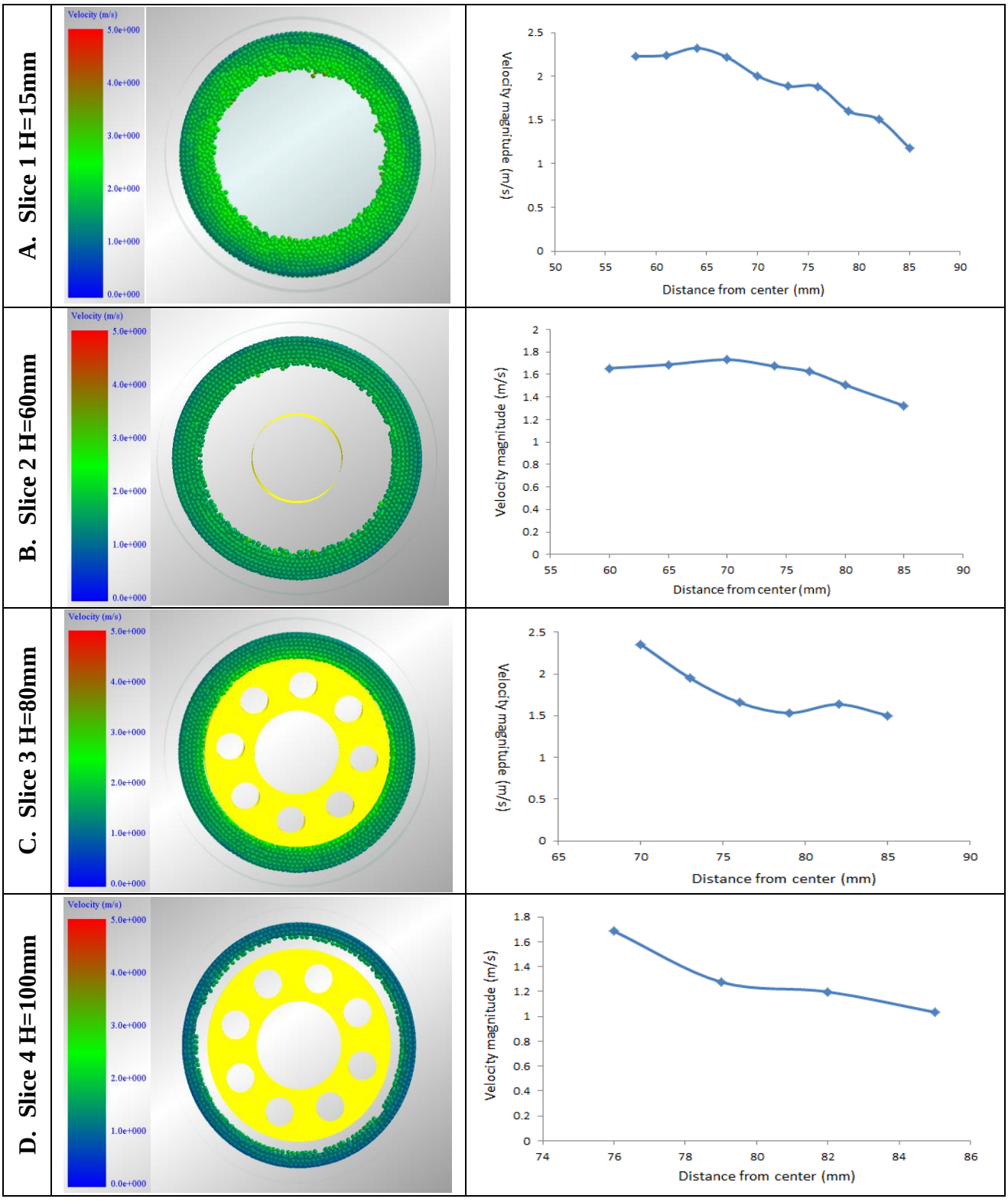

Figure 4-15 Grinding media velocity gradient along radial direction at 1600 rpm

To investigate the influence of slurry solid content on grinding media velocity, slices were cut from the same height of three different simulations (Figure 4-16). They have different slurry solid content values: 15% v/v, 30% v/v and 40% v/v respectively. The three simulations were performed at the same stirrer rotational speed which was 600 rpm. The velocity information of grinding media in slice 2 is analyzed as an example because the media in this level have a higher average velocity compared to media in other levels and there are a large number of grinding media in this level. This gives the advantage to plot a curve with enough points. The images of grinding media colored by their velocity magnitude and the relationship between their position and velocities are shown in Figure 4-16.

The figures show that the shape of velocity gradient of grinding media changes with slurry solid content. When the mill is operated at 15% v/v solid content, the maximum media velocity is observed near the disc edge and it drops fast in the disc radial direction. There are significant fluctuations in bead velocity along the disc radial direction. When increasing the slurry solids content to 30% v/v, the shape of media velocity gradient in the same level becomes smoother and media near chamber wall travel faster than those with 15% v/v. The velocity magnitude is more uniformed compared to 15% v/v. This causes an increase in average media velocity. When the solid content is further increased to 40% v/v, the trend of media velocity gradient changes. Instead of decreasing along stirrer radial direction, it goes up slightly when approaching the mill inner wall and a smaller average velocity is observed.

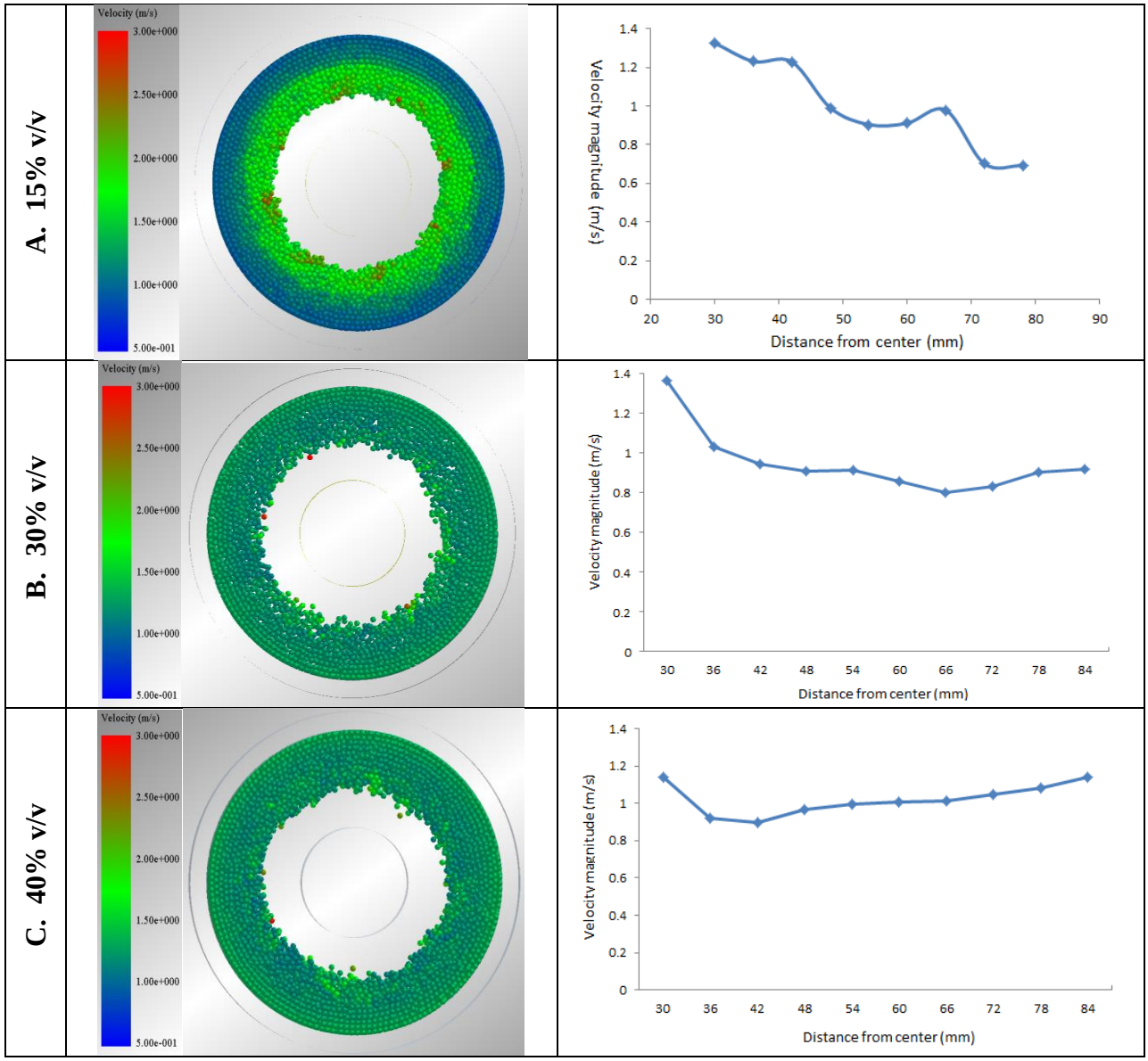

Figure 4-16 Grinding media velocity gradient of slice 2 under different solid contents

To study the effect of slurry viscosity on grinding media velocity, bead slices are cut from the same height under three different slurry viscosities: 0.005 mPas, 0.025 mPas and 0.125 mPas (Figure 4-17). The three simulations are run under the same stirrer rotational speed.

The influence of slurry viscosity on media velocity is similar to that of slurry solid content. With the increase in viscosity, media velocity magnitude tends to be more uniform. The magnitude of fluctuation also decreases. Meanwhile, the velocity of media that are away from the disc edge is much higher at high viscosity than at low viscosity. At the highest slurry viscosity, an increasing media speed along disc radial direction is observed. This result can be explained using models done by Jayasundara et al. (2009). In their study on DEM modeling of an IsaMill, the effect of slurry viscosity on grinding media velocity was studied. They found that due to stronger viscous forces at higher viscosity, the energy was transferred more effectively from the stirrer to the slurry and beads gained a high velocity along radial direction.

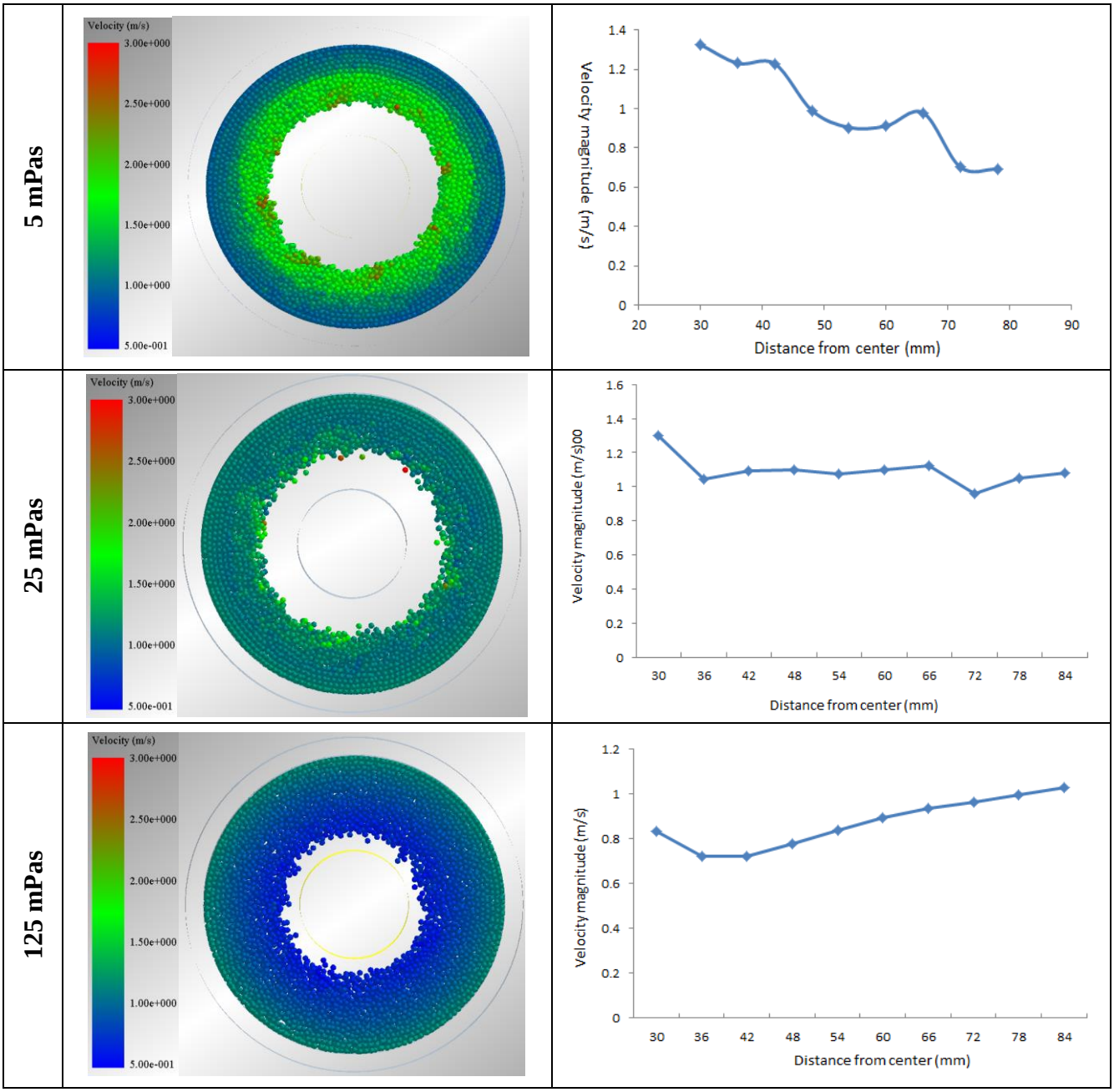

Figure 4-17 Grinding media velocity gradient of Slice 2 under different slurry viscosity

A group of cross-sectional views (Figure 4-18) of the vertical stirred mill under different stirrer speed is shown to demonstrate the characteristic of media velocity gradient along the mill axial

direction. The position of the planes is the same as in Figure 4-8. Beads are colored according to their velocity magnitude with the highest velocity in red and lowest in dark blue. This demonstrates how stirrer rotational speed affects the distribution of beads across the mill chamber, especially along its vertical extension. At the same time, a 2D velocity profile as a function of mill height is plotted and attached on the right. By connecting the median value of velocity at each level, a velocity profile along the mill longitude direction is generated.

It is observed that when the mill is running at 15% v/v slurry solid content 600 rpm, beads are poorly suspended as compared to 1100 rpm and 1600 rpm. The majority of beads reside in the vicinity of the first and second disc from the bottom, leaving the third and fourth disc exposed to air without touching with beads. There is a stagnant zone of beads at the bottom center of the mill resulting from insufficient kinetic energy to move beads. High breakage energy exists in the circumferential area at the disc surface where grinding beads have the highest speed. Then the speeds drop along the radial direction between the disc edge and the mill inner wall creating a less active grinding zone. Near the bottom corner of the mill, there are two low particle velocity zones colored by dark blue. It is also observed from the velocity profile that the average velocity at the bottom zone is smaller than the area above it. This is because of the high compressive pressure generated by beads piled on top of the bottom layers; as well the backflow of pulp slurry is not able to provide enough energy to fluidize beads. As height increases, the low velocity zones fade away as there are fewer beads and slurry falling on top. It is noticed that on the top part of the mill, there is a heap of beads with a certain angel and the angle is rather sharp compared to those at higher stirrer speed. This is also an indication that demonstrates the beads

under this operating condition are less stirred and not enough energy is provided to drive the particles upward.

From the 2D curve between beads velocity and mill height, it is observed that beads in the vicinity of impeller discs have a higher velocity than beads in the bottom and top area. This means that stirrer discs are important in providing energy to the grinding system and the number of discs will influence grinding efficiency of the mill.

Some beads with extremely high speed are observed in the holes in the stirrer discs, they are trapped inside and moving at the same tip speed as the disc tip speed at that point. It should be noticed that those beads are not contributing as much to ore breakage as their velocity indicates because there is no velocity gradient and relative velocity that is able to trigger breakage of ore particles.

From Figure 4-18, it is observed that stirrer speed influences beads distribution and velocity in that a lower speed will generate a more smooth profile while high speed will generate a velocity profile with a distinct boundary between high and low particle speed.

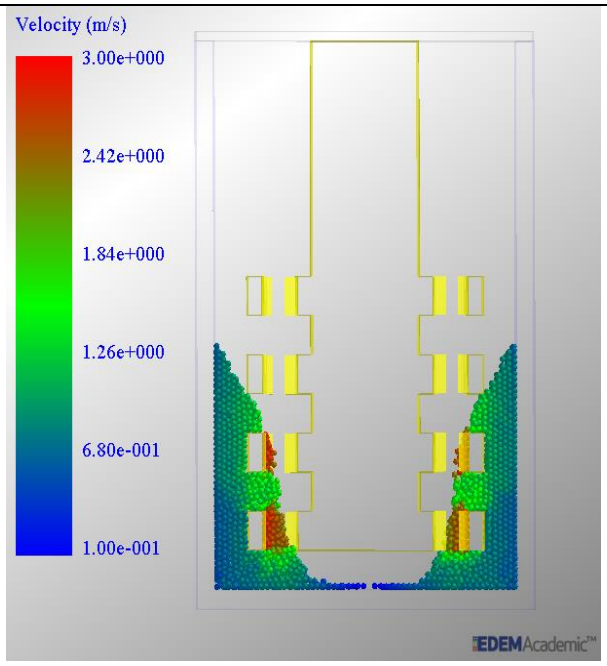

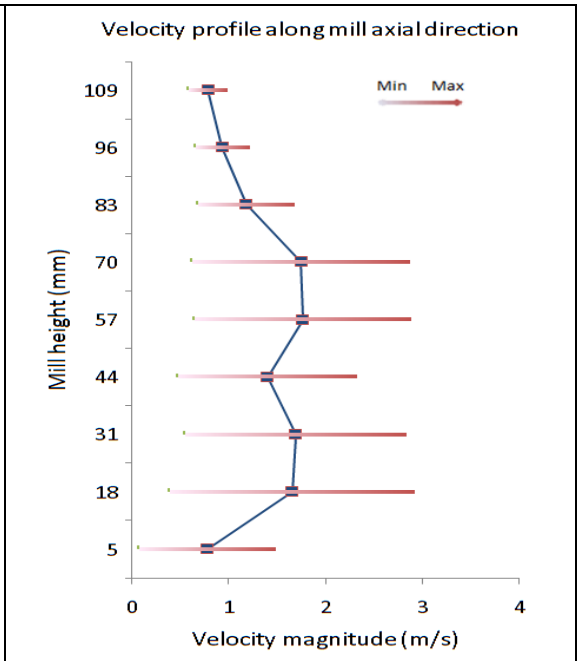

A. 15% v/v at 600 rpm

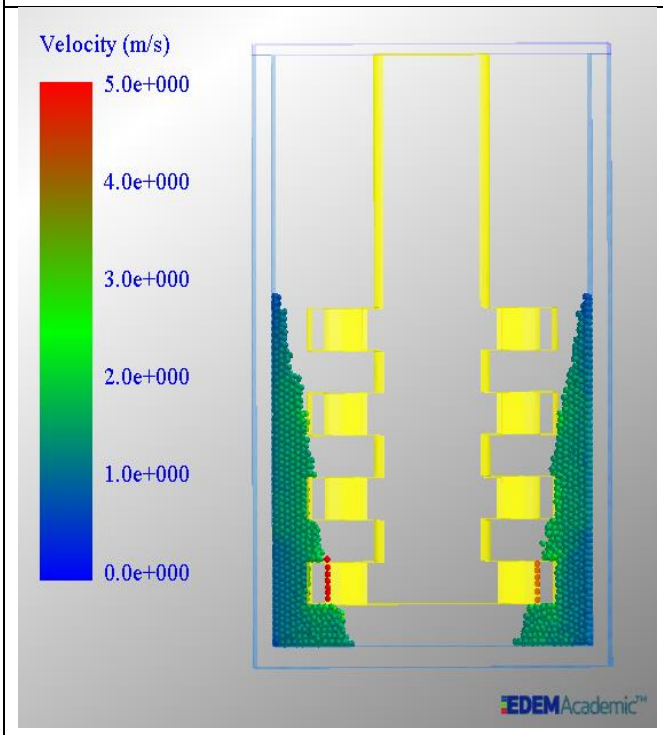

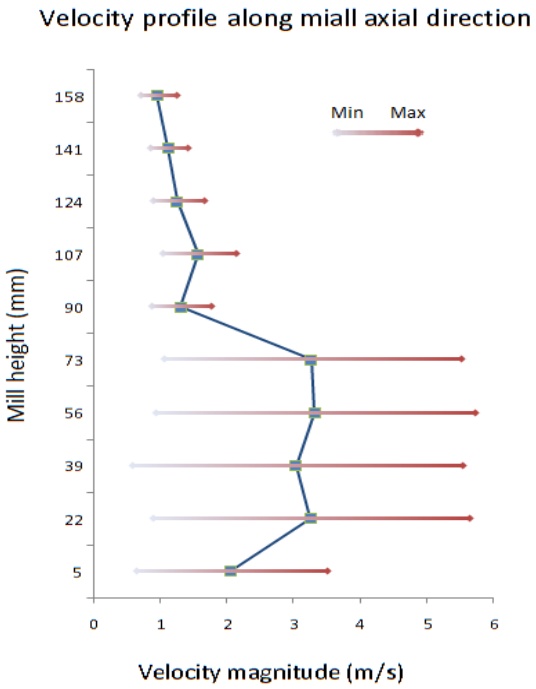

B. 15% v/v at 1100 rpm

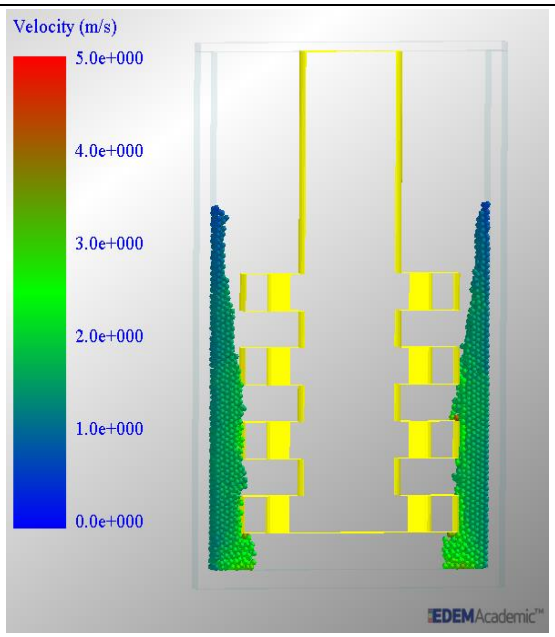

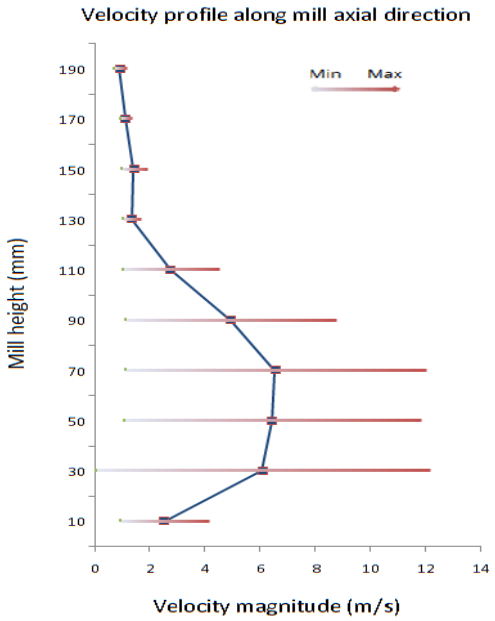

C. 15% v/v at 1600 rpm

Figure 4-18 Cross-sectional view of bead velocity in mill under different stirrer speed

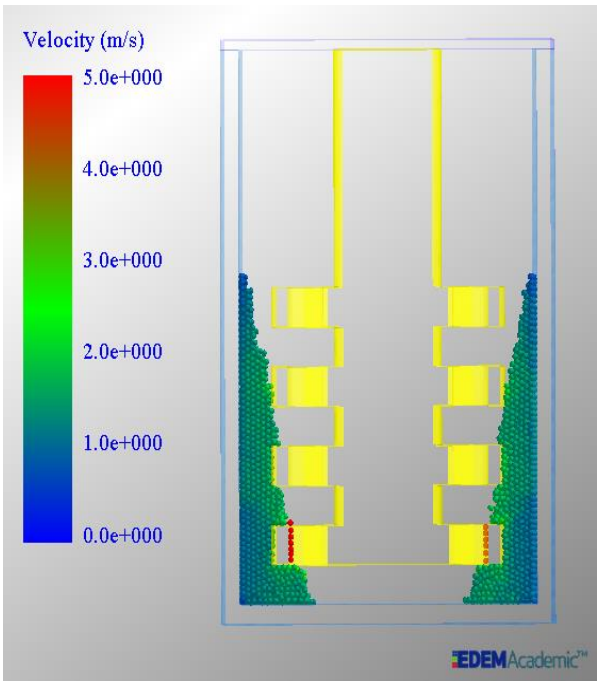

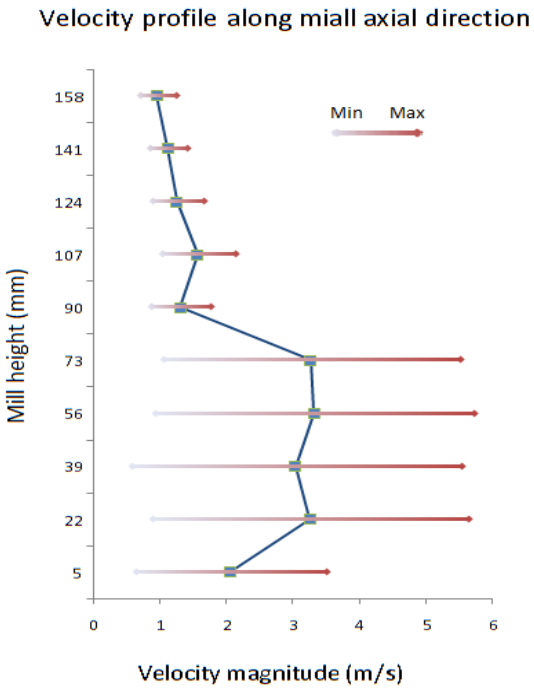

15% v/v at 1100 rpm

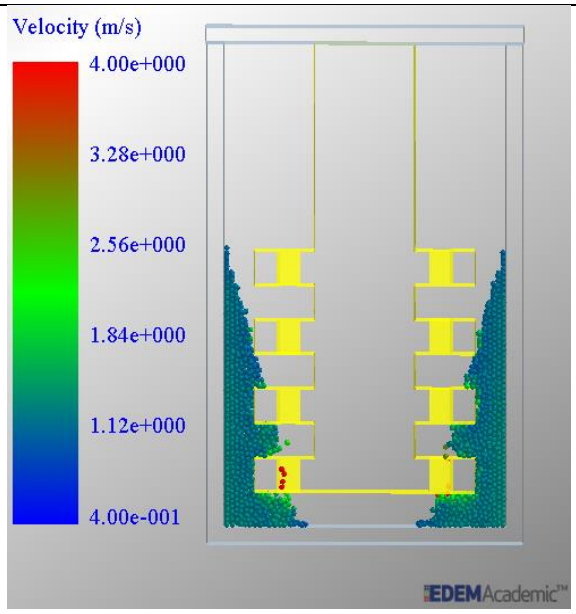

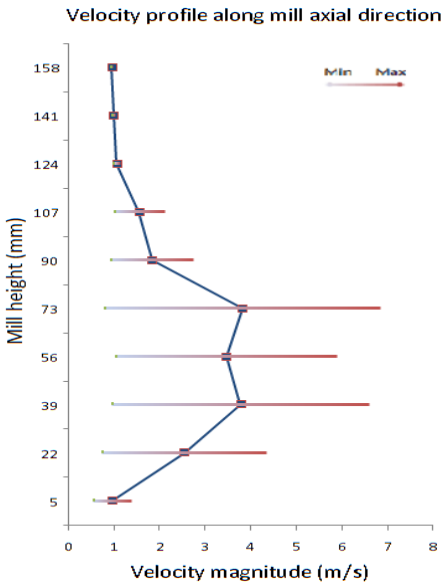

30% v/v at 1100 rpm

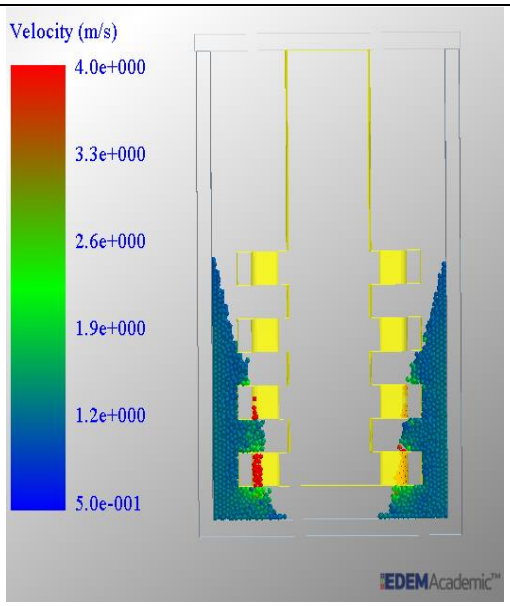

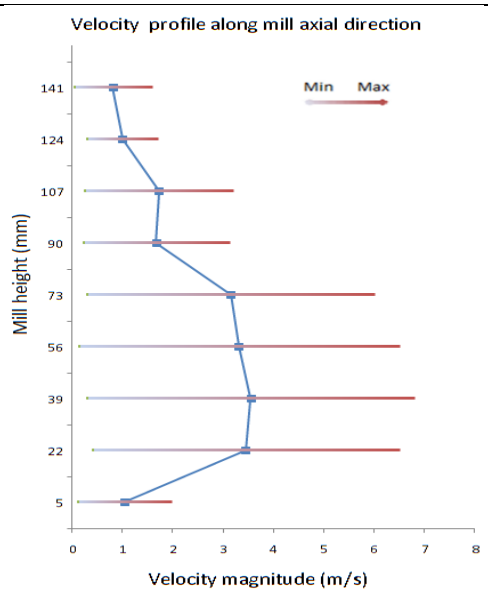

40% v/v at 1100 rpm

Figure 4-19 Cross-sectional view of bead velocity in mill chamber under different slurry solid content

4.3.5 Conclusion

In this section, a thorough study on fluid flow behavior, grinding media motion and velocity distribution in a vertical stirred media mill was carried out.

The snapshots from simulation results showed the characteristics of viscous slurry in a stirred media mill. The centrifugal force generated by stirrers revolving at high speed pushes slurry to the wall and forms an air cone in the center. As the stirrer speed, slurry solid content and viscosity increase, the air column changes its shape from conical to cylindrical, which means the volume of air is expanding while the volume of slurry being processed in the mill is dropping. Meanwhile, the number of air bubbles being trapped in slurry raises due to the increased intensity in mixing. The increases of all the operating parameters could benefit grinding but result in a reduction in effective volume in the mill, which limits the amount of slurry being ground inside the mill. It will cause the throughput of the mill to drop and influence production rate.

The velocity gradients of grinding media from planes along vertical and horizontal direction were plotted and analyzed. Within the same plane, the maximum velocity of grinding media is reached near the disc edges. It then drops along a radial direction and extends parallel to the gap between the disc and the mill wall. It gets to its minimum value near the mill chamber inner wall.

When examining the velocity gradient of a grinding media mill along its axial direction, it is observed that the maximum velocity magnitude is achieved around 2/3 from the top and the minimum velocity always occurs in the top zones. Velocity gradient information on grinding

media could give a good indication on grinding energy distribution in the mill since higher velocity means greater chance of impact and forces.

Grinding media distribution in different sections across the mill was also investigated in this section. Simulation results showed that media in the mill reached an equilibrium state (the number of grinding media across different areas of the mill became unchanged with time) within 0.5 seconds after the stirrer started to rotate. This supports the selection of 2 seconds for the overall simulation time. Subsequently, the operating parameters' influence on grinding media distribution across three zones of the mill was studied. It was found that operating parameters such as stirrer speed and slurry viscosity have an effect on the number of beads distributed in each zone whereas the influence of solid content is minimal. As the stirrer speed increases, the number of grinding media in each zone of the mill tends to be more homogeneous, especially for the top and the middle zone of the mill. As the slurry viscosity increases, grinding media tend to be more dispersed with media number in the top and the middle zone ramping up and bottom zone decreases.

Media movement trajectories from three operating conditions were presented to illustrate media moving traces. Results showed that although there is a velocity component along the mill axial direction, the magnitude of that velocity is minute compared to the radial and tangential velocity in a horizontal plane. The rotational movement within the same height is the dominant movement pattern.

4.4 Effect of Operating Parameters on Inter-particle Forces

4.4.1 Introduction

Massive fracture and attrition are believed to be two major breakage mechanisms in stirred media milling (Hogg, 1999; Yue & Klein, 2004). During the operation of stirred milling, ore particles are exposed to both fracture and attrition. The size reduction process is a combined activity of the two mechanisms. Fracture is caused by the impact and compressive force which results from the normal component of forces applied on ore particles. This can be illustrated in Figure 4-20 A. Attrition breakage is induced by abrasion when two beads are translating or rotating in opposite directions along their contact plane (Figure 4-20 B.). In computer simulations, compressive force can be identified as the normal component of the force, while attrition can be identified as the tangential component of the force (Roufail, 2011). The interaction between two grinding media is defined by Hertz-Mindlin contact force model show in Figure 2-10. From this model, contact force between two colliding DEM particles can be calculated. In this section, the affect of stirrer rotational speed, slurry solid content and slurry viscosity on normal and tangential force distribution are evaluated. For each operating parameter, normal and tangential force between grinding media for each time step was exported from EDEM, and their average were calculated over the total simulation time.

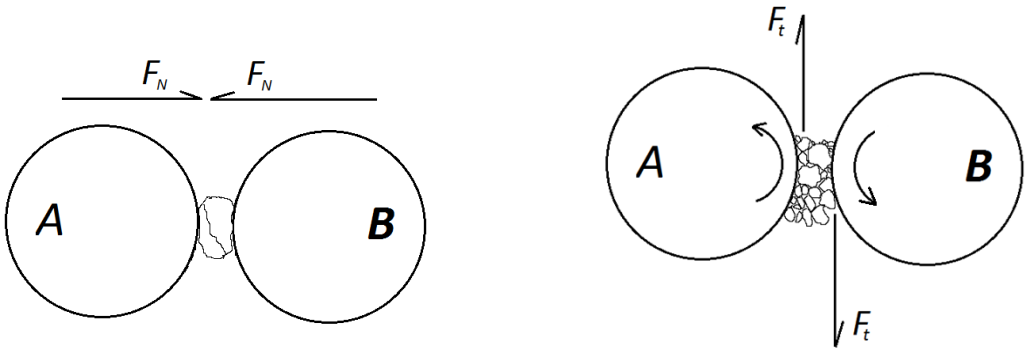

A. Massive fracture **B. Attrition**

Figure 4-20 Illustration of two different breakage kinetics in stirred milling

The grinding test result shown in Figure 4-21 suggests that fracture breakage is the more likely to occur mechanism in a vertical stirred media mill compared to attrition. The particle size distribution curves are chosen from different passes of the same grinding test. The size distribution curves show that although a finer size fraction exists in the product (a rise at the finer end), there is no apparent bimodal distribution indicated in the figure. Instead, it is closer to a normal distribution. By comparing the distribution curves from pass 2, pass 4 and pass 8, it was found that there is an acceleration process in the vanishing of coarse particles as the grinding goes on. At the same time, smaller size particles are being generated causing the curves shift to the left and smaller median value. Nevertheless, the appearance rate of the finer particles is not as high as the disappearance rate of the coarse fraction. When the finer end of those curves is examined, it is seen that they tend to overlap, which means that the amount of fines in each pass remains almost the same. This is due to the particle size reaching the grinding limit, so that the size reduction speed is not as fast as it is in beginning passes. Therefore, throughout the whole

grinding process attrition breakage plays a less important role in the breakage of ore particles in a vertical stirred mill.

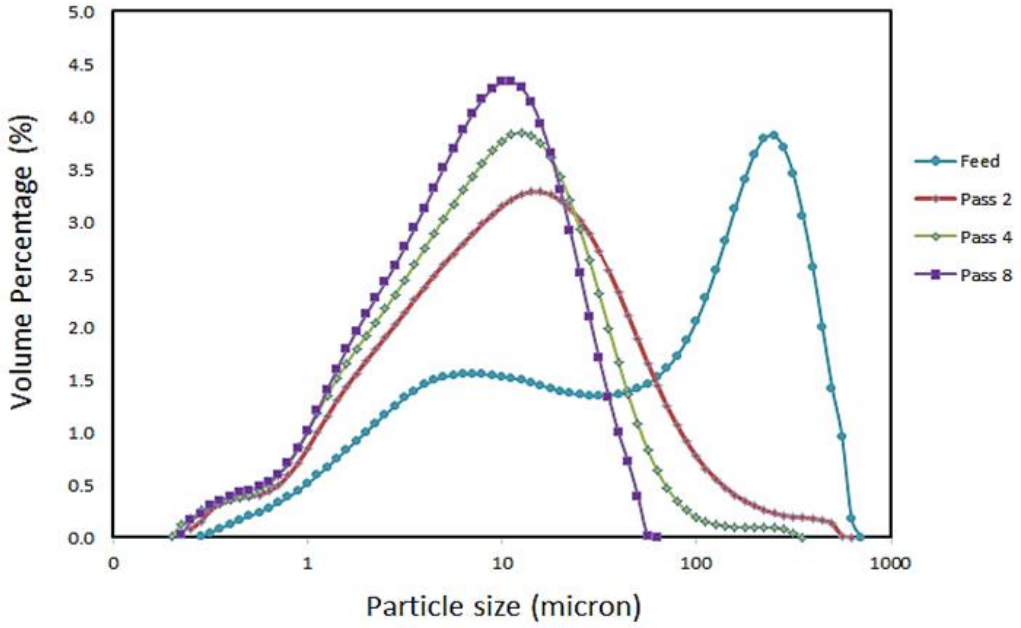

Figure 4-21 Particle size distribution of product of each cycle from grinding tests

4.4.2 Effect of Stirrer Speed

Simulations are run under three different stirrer speeds (test No.2, No.3 and No.4 from Table 3-6) and the force magnitude of each bead is exported and plotted in Figure 4-22. The result suggests that particle-particle force has both normal and tangential components. It implies that both fracture and attrition breakage kinetics exist in a vertical stirred media mill during grinding. The magnitude of the normal force is about three times the tangential force for all speeds tested. Although both force magnitudes increase as the stirrer rotational speed increases, force in the normal direction is always greater than force in tangential direction, which means that compression between two media is more dominant than abrasion. The result also supports the findings in section 4.4.1.

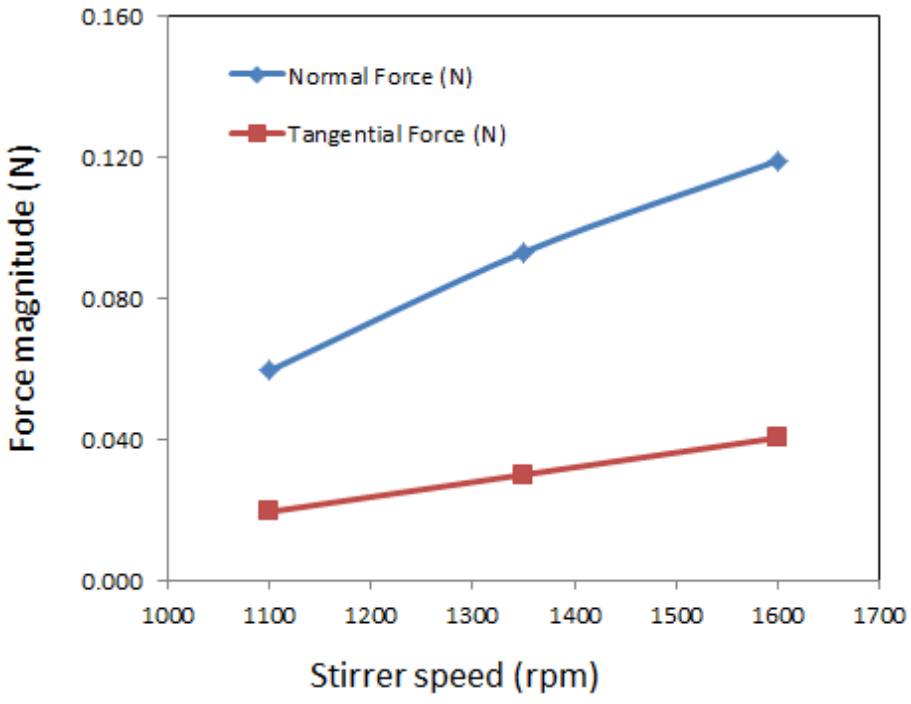

Figure 4-22 Normal and tangential force magnitude under different stirrer speed

According to Hogg (1999), fracture will lead to a fast disappearance rate of coarse particles and result in a shift to finer size fraction in the particle size distribution. Attrition, on the other hand, will result in a finer size fraction and cause a bimodal distribution. Based on this argument, two particle size distributions from two real grinding tests (test No.4 and No.5 in Table 3-2) are plotted in Figure 4-23. The size distribution curves illustrate that when increasing the tip speed from 1100 rpm to 1350 rpm, there is a drop in the number of coarse particles with no emerging finer size fraction. This means that the increase in stirrer speed enhanced the magnitude of the normal force and resulted in a greater fracture rate.

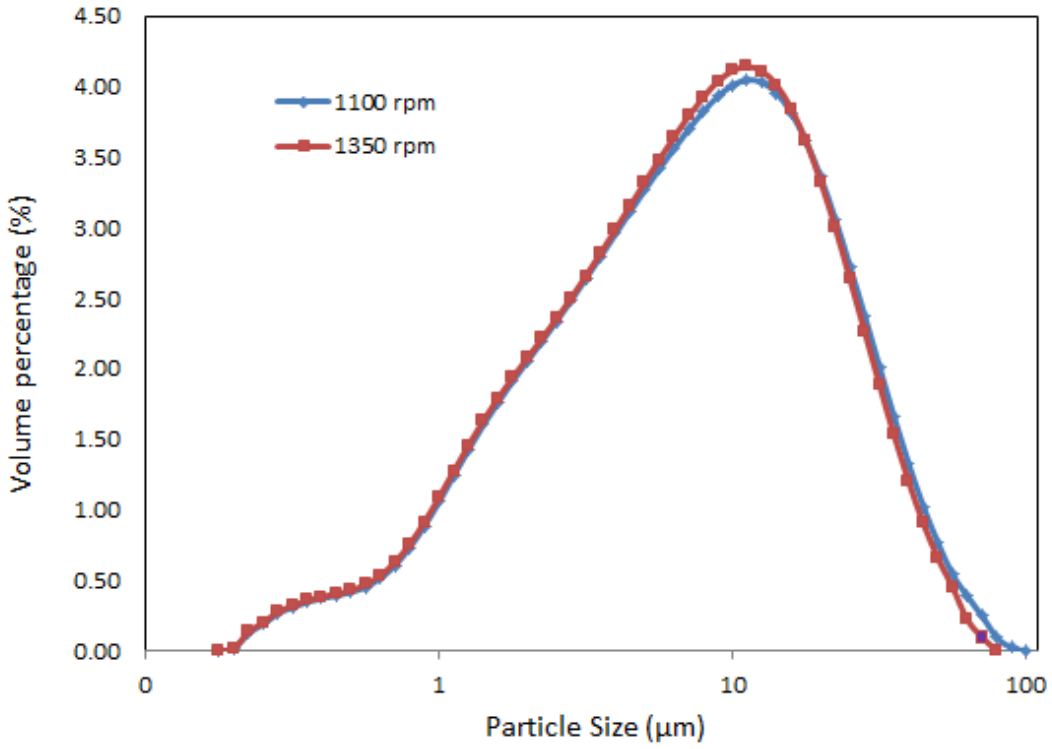

Figure 4-23 Particle size distribution of pass 6 product under two different stirrer speed

Particle size distribution from grinding tests No.2 and No. 5 in Table 3-2 are shown in Figure 4-24. It is observed that when changing the stirrer tip speed from 1350 rpm to 1600 rpm, a diminishing coarse size fraction is observed from the particle size distribution curve. The rate of disappearance is close to that of changing the speed from 1100 rpm to 1350 rpm. At the same time, a small increase in the amount of finer particles is detected because the curve shift slightly to the left suggesting there are some fine particles.

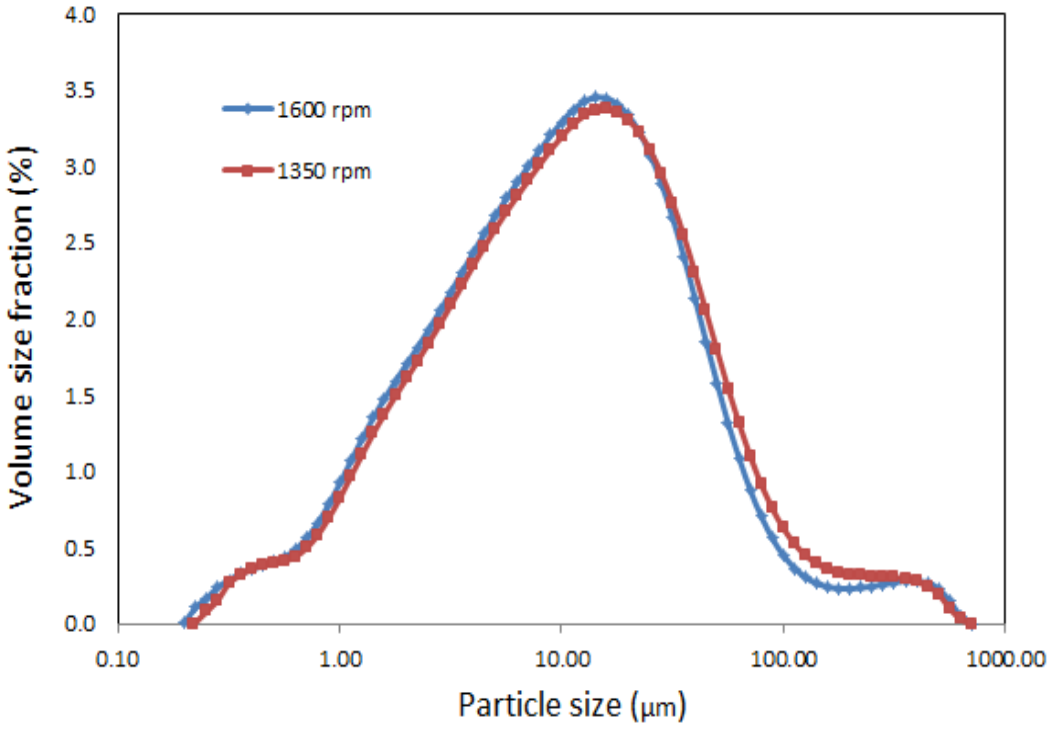

Figure 4-24 Particle size distribution of product at two different stirrer speeds

4.4.3 Effect of Slurry Solid Content

In this part, simulations are run under different slurry solid content (test No.3, No.7 and No.11 from Table 3-6). Normal and tangential force magnitudes are recorded over the simulation time span and their average values are plotted in

Figure **4-25**. It is observed that there is a great difference in force magnitude at low solid content, with a tangential force of 0.03 N and normal force 0.18 N. When the slurry solid content goes up to 30% v/v, the normal force drops while the tangential force increases, the gap between them narrows and the two trend lines tend to converge. When the simulation is run at the highest solid content value of 40% v/v, normal force magnitude continues to drop as expected while tangential force magnitude remains at the same level as 30% v/v solid content. It is important to notice that although the developing trend of normal and tangential force remains the same, their drop and increase rate become smaller. Therefore, it's reasonable to speculate that both normal and tangential component will not change when the solid content reaches a value around 30% v/v.

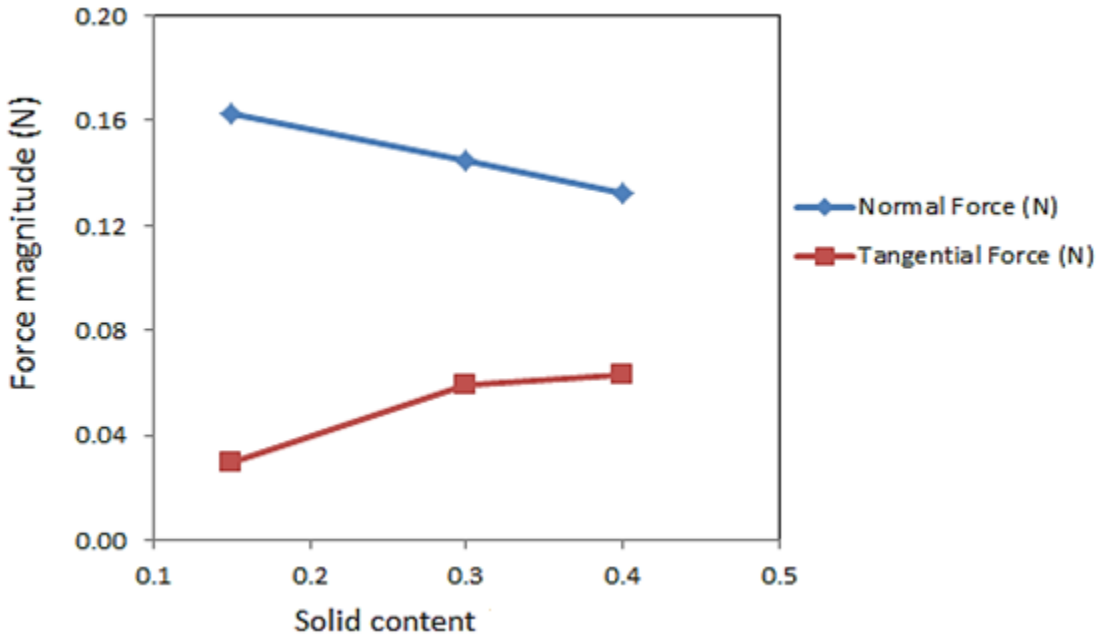

Figure 4-25 Effect of slurry solid content on normal and tangential force magnitudes

Results from the real grinding test are shown in the

Figure 4-25. Particle size distributions of Pass 6 from three different solid contents are chosen and plotted. The tests are No.3 No.7 and No. 11 from Table 3-6. The particle size distribution shows the influence of solid content on the product. By comparing the size distribution curve of 40% v/v and 30% v/v, a distinct drop in coarse end of curve of 30% v/v is observed, which means that the level of fracture at lower solid content is great than fracture at higher solid content. When the solid content reaches 15% v/v, a more aggressive decrease in the number of coarse particles is observed compare to from 40% to 30%. This could be explained by the simulation result on how solid content affects normal and tangential force. As the slurry solid content decreases, the particle size distribution becomes narrower. However, the amount of fine particles generated doesn't change along with the variation in slurry density. The result shows that

fracture breakage mechanism is more important than attrition. Meanwhile, the magnitude of the normal force decreases as the solid content increases, but the decreasing rate drops and trend line becomes almost horizontal. This explains why coarse particles disappear faster when the solid content changes from 30% v/v to 15% v/v than from 40% v/v to 30% v/v. Consequently fracture breakage is more likely to happen over attrition breakage across all the solid content values tested.

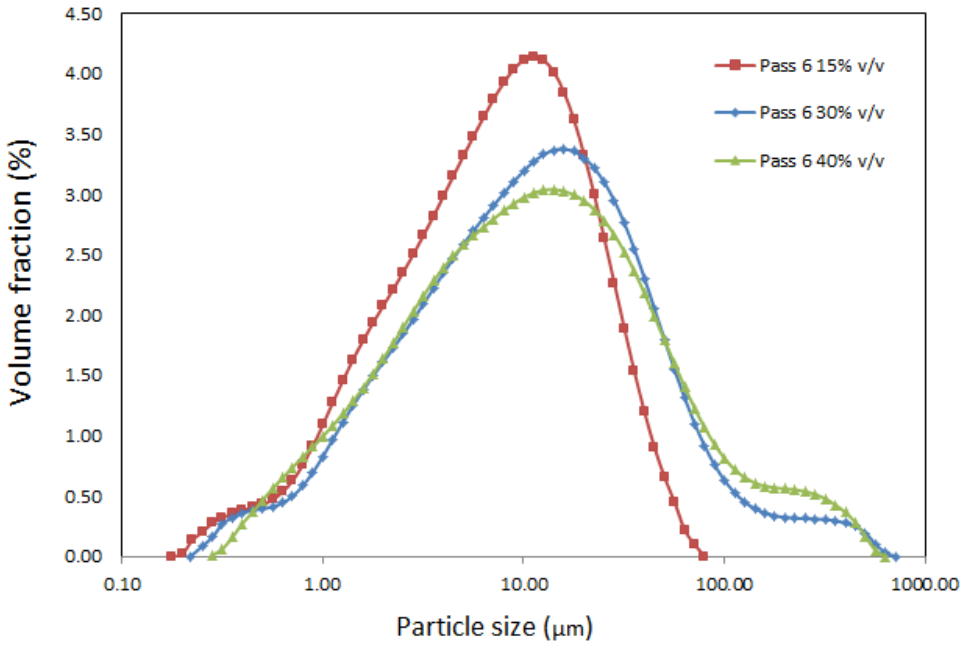

Figure 4-26 Particle size distribution of pass 6 product under different solid contents

4.4.4 Effect of Slurry Viscosity

Figure 4-27 shows how normal and tangential force magnitude changes with the increasing slurry viscosity in a vertical stirred media mill. Simulations are run under three different slurry viscosity values with the same slurry density value. This reflects the grinding process during which slurry viscosity increases as residence time grows.

The curves suggested that both normal and tangential force magnitudes are influenced by slurry viscosity, however since normal force is the dominant force component in grinding, it is more sensitive to the change of slurry viscosity. Both forces increase when the viscosity value is increased from 0.005 Pas to 0.025 Pas and then follow with a significant drop when the viscosity is further increased from 0.025 Pas to 0.125 Pas. The result suggested that a moderate slurry viscosity value will produce a large normal and tangential force which will benefit grinding process. Too high or too low a slurry viscosity will not be so optimal for grinding in terms of force magnitude.

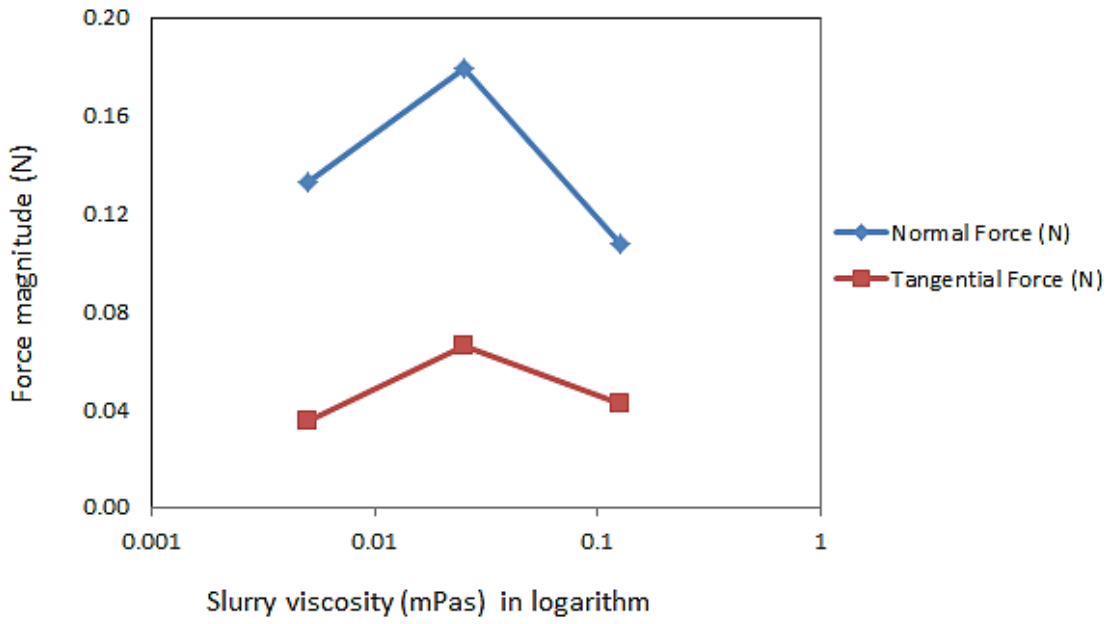

Figure 4-27 Effect of slurry viscosity on normal and tangential force magnitude

4.4.5 Conclusion

In this section, force patterns acting on grinding media and the resulting breakage mechanism were investigated. It was confirmed that both normal and tangential forces exist in grinding

media in a vertical stirred media mill. Normal force was greater than tangential force magnitude among all operating conditions tested which means compression between two grinding media is more likely to occur compared to attrition. Therefore, fracture breakage plays a more important role than attrition in VXPmill.. A Similar result was found by Roufail (2011) from DEM simulation tests on a horizontal stirred mill.

The magnitude of normal and tangential forces of beads changes as operation condition changes. They both increase as the stirrer speed goes up. When slurry solid content increases, the normal force magnitude drops whereas tangential force magnitude increases and the gap between them is narrowed. When looking at the effect of slurry viscosity on forces, they both increase while changing the slurry viscosity from 0.005 Pas to 0.025 Pas, then followed by a significantly drop when the viscosity is further increased to 0.125 Pas.

4.5 Effect of Operating Parameters on Grinding Media Energy

4.5.1 Introduction

Grinding is a process where electrical energy is transformed to mechanical energy from a motor. By coupling the main shaft and motor together, the mechanical power is delivered to grinding media through the stirring motion. The mechanical energy is then converted into kinetic energy of slurry streams around the stirrer and beads driven by the slurry perform breakage on ore particles. The kinetic energy of grinding media is calculated by

$$K_E = \frac{1}{2} M_m {V_m}^2$$ Equation 4-1

and

$$V_m = \sqrt{{V_{mx}}^2 + {V_{my}}^2 + {V_{mz}}^2}$$ Equation 4-2

where K_E is the kinetic energy of grinding media, M_m is the mass of one grinding media and V_m is the velocity magnitude of the grinding media which is calculated by combining velocity component in x, y and z directions represented by V_{mx}, V_{my}, and V_{mz} respectively.

However, during this energy transformation, only a limited amount of energy is utilized in ore grinding activities, as most of it is lost in the form of sound and heat. Assessing the magnitude of bead kinetic energy and bead collision frequency can give a better understanding on energy utilization in grinding.

The stirrer speed is believed to be one of the most crucial influencing parameters in ultrafine grinding (Gao & Forssberg, 1993). To understand the influence of stirrer speed on bead kinetic energy and collision frequency, simulations using three different rotation speeds were carried out. In this part, bead kinetics energy information was exported from the EDEM software. The beads kinetic energy is calculated by averaging the kinetic energy of each bead over the simulation time span. Meanwhile, the collision frequency was defined as the number of contact between any two beads in a simulation time step. Simulation results are exported and analyzed in the following section.

A statistical analysis on grinding media kinetic energy of a test is shown in Figure 4-28. Data from simulation test No. 3 in Table 3-6 are chosen as an example.. The distribution has an

average of 7.9×10^{-5} (J) and a standard deviation of 4.4×10^{-5}. The low standard deviation number suggests that the data points tend to be very close to the average. Therefore, using average beads kinetic energy can reflect the overall kinetic energy level of beads in the mill.

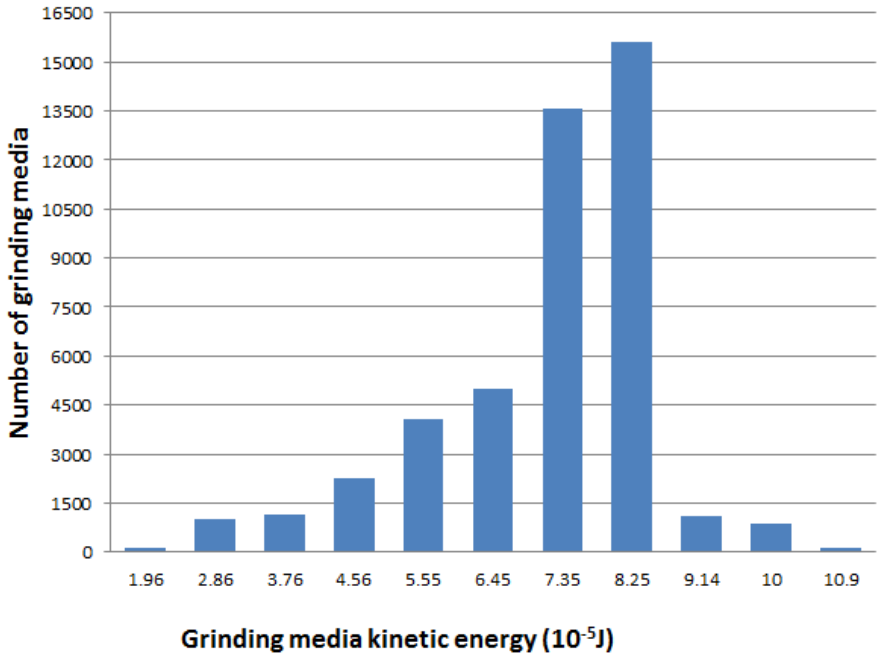

Figure 4-28 Relationship between grinding media kinetic energy and number of media

4.5.2 Effect of Stirrer Speed

Figure 4-29 shows that stirrer speed has an effect on bead kinetic energy. The grinding media kinetic energy is determined by averaging the kinetic energy of each media in the mill. It is expected that high stirrer speed will increase beads kinetic energy. However, it is noteworthy that the boost in kinetic energy from 1350 rpm to 1600 rpm is not as high as from 1100 rpm to 1350 rpm. The low increase in the beads kinetic at higher speed energy can be explained by the fact

that the stirrer is running close to its top speed limit so more energy input will just dissipate in the form of heat and sound rather than being utilized by grinding.

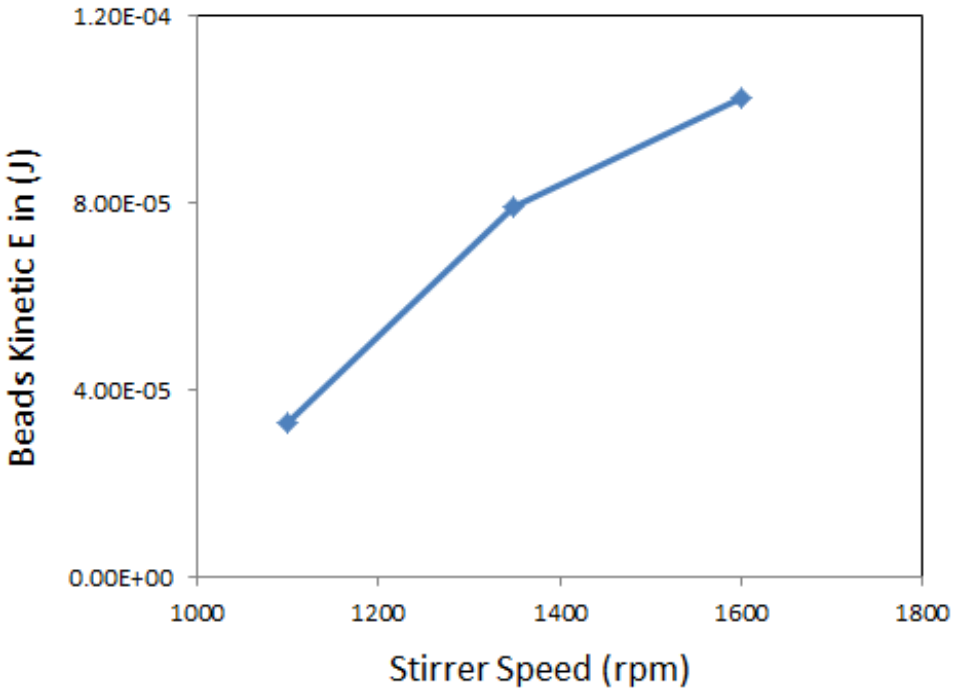

Figure 4-29 Effect of stirrer speed on media kinetic energy

The collision frequency between beads is presented in Figure 4-30. Collision frequency is determined by counting the number of collisions between grinding media in each simulation time step. This is achieved by the EDEM software. This shows that increasing stirrer speed has a positive affect on improving collision frequency between beads. The trend of speed and collision frequency is similar to that of speed and bead kinetic energy.

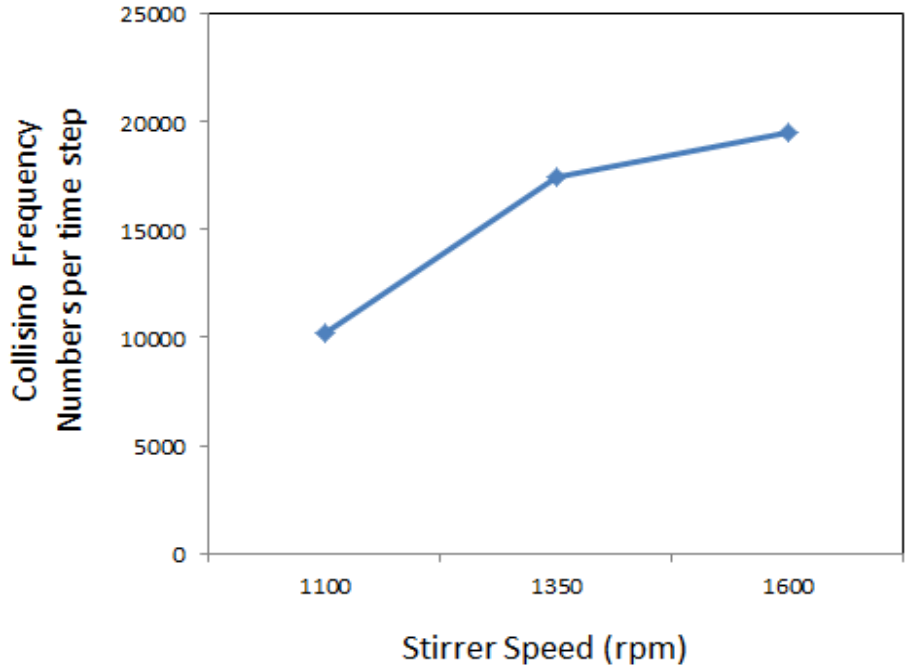

Figure 4-30 Effect of stirrer speed on media collision frequency

In addition to beads kinetic energy of all the beads in the mill chamber, beads kinetic energy in each zone of the mill is also investigated. The three zones are bottom, middle and top zone as shown in Figure 4-2. Stirrer speed's effect on beads average kinetic energy in each zone is simulated and the results are plotted in Figure 4-31. It is seen that higher stirrer speed provides higher velocity to grinding media and result in a higher kinetic energy for media in all three zones of the mill. Among the three zones in the mill, the beads kinetic energy in zone 1 is most sensitive to changes in stirrer speed and beads in that zone have the highest kinetic energy. With the stirrer speed increase from 1100 rpm to 1600 rpm, the beads kinetic energy improved by 3.78 times. Compared with zone 1, beads kinetic energy in zone 2 and zone 3 are less sensitive to change in stirrer disc speed. The beads kinetic energy response to the change of stirrer speed is almost linear in zone 2 and zone 3.

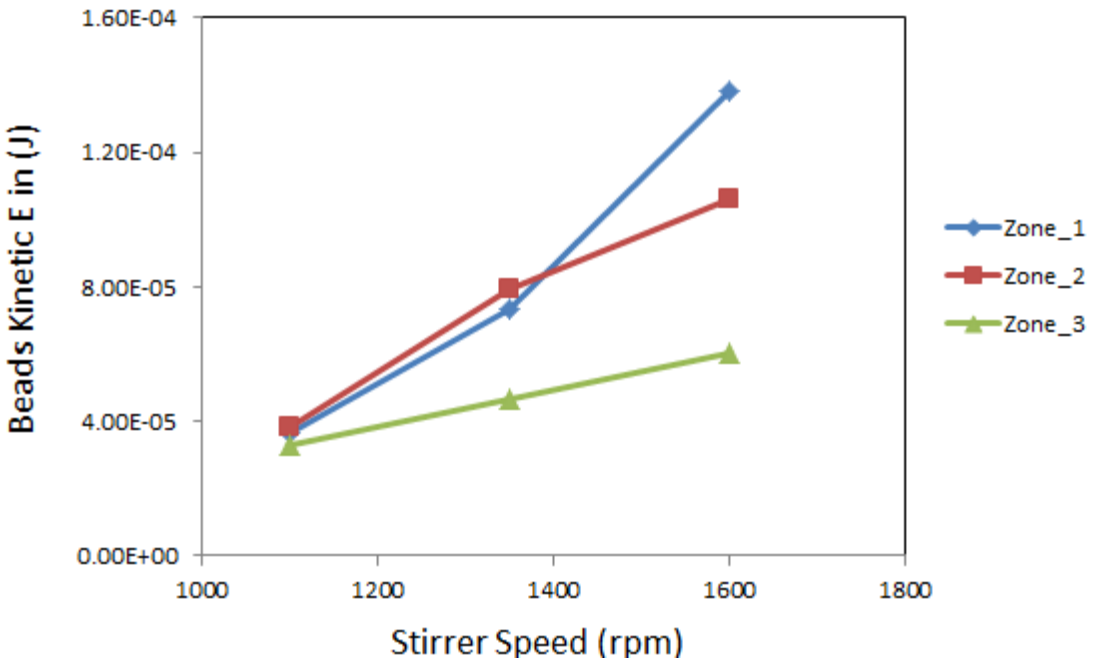

Figure 4-31 Effect of stirrer speed on media kinetic energy in 3 zones

Figure 4-32 shows how different stirrer speed affects the grinding speed in a laboratary test. The relationship curves between product particle size (P_{80}) and grinding pass number (residence time) under different speed level are plotted. It is seen that the higher the stirrer speed is, the faster the size reduction speed will be. However, the improvement in grinding speed is not so significant when the stirrer speed is raised from 1350 rpm to 1600 rpm as from 1100 rpm to 1350 rpm. The overlaped tail between the curve of medium speed and high speed indicates that the size reduction rate is almost the same under two different stirrer speeds. Therefore, increasing the stirrer speed to accelerate the size reduction process when the speed is already high will not be as effective compared to increasing the speed from a lower speed range. This validates the results from the sinulation since the grinding speed is influenced by the combination of stirrer speed and collision frequency. The relationship between beads kinetic energy and stirrer speed, beads

collision frequency and stirrer speed can be used to explain the relationship between grinding speed and stirrer speed.

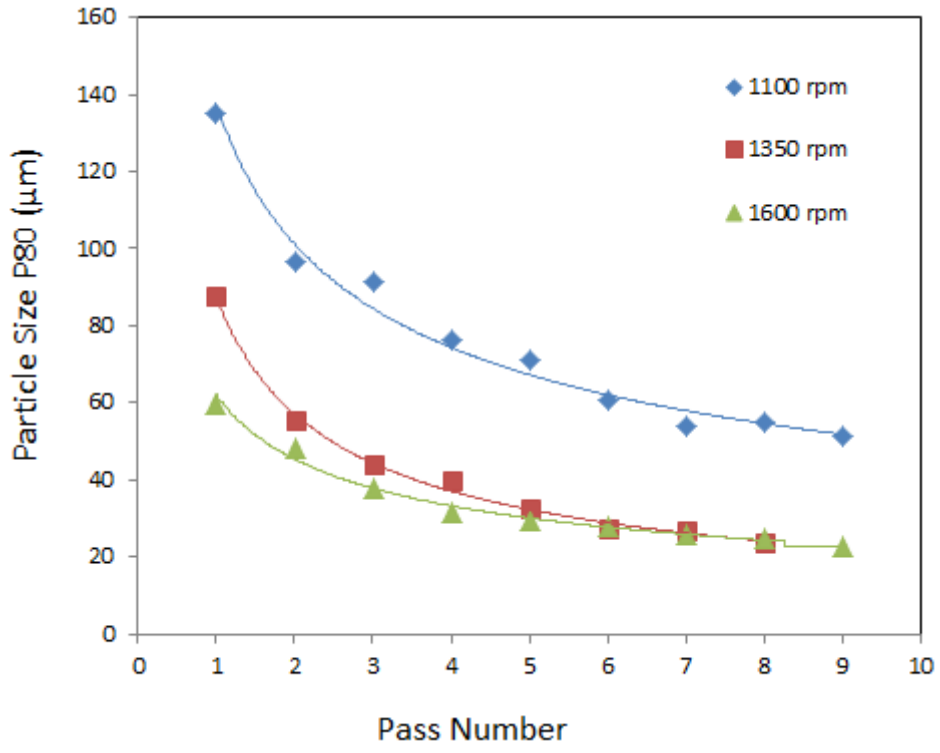

Figure 4-32 Effect of stirrer speed on grinding speed

4.5.3 Effect of Slurry Solid Content

To investigate the effect of slurry solid content on beads kinetic energy in a vertical stirred media mill, three different slurry solid content values are selected (15% v/v, 30% v/v and 40% v/v). The corresponding density values are 1450 kg/m^3, 1630 kg/m^3 and 1720 kg/m^3 respectively. Figure 4-33 shows the relationship between average beads kinetic energy and slurry solid content. It is observed that when the solid content is increased from 15% v/v to 30% v/v, the beads kinetic energy increases dramatically. When increasing the slurry solid content from 30%

v/v to 40% v/v, instead of getting a higher beads kinetic energy value, a slightly drop in kinetic energy value is observed. The relationship between solid content and beads kinetic energy suggests that adding more solids into the slurry at a lower solid content will help increase grinding media kinetic energy and make further improvement on grinding performances. This is because higher slurry density provides a stronger fluid drag force on the beads leading to a higher circulating speed of the grinding media. However, there is an upper limit value of solid content that when the slurry density is beyond that point, the excessive solids in the slurry will hinder the movement of the grinding media. This could be explained by the fact that the increasing slurry density creates a ‘cushioning’ effect on moving particles that prevents them from traveling freely in the grinding fluids. Another reason is that a higher solid content means that the materials be moved by the stirrer is heavier. Since the increase of power draw of the motor is non-linear, it is no longer able to provide the same torque at higher solid content as compared to lower solid content.

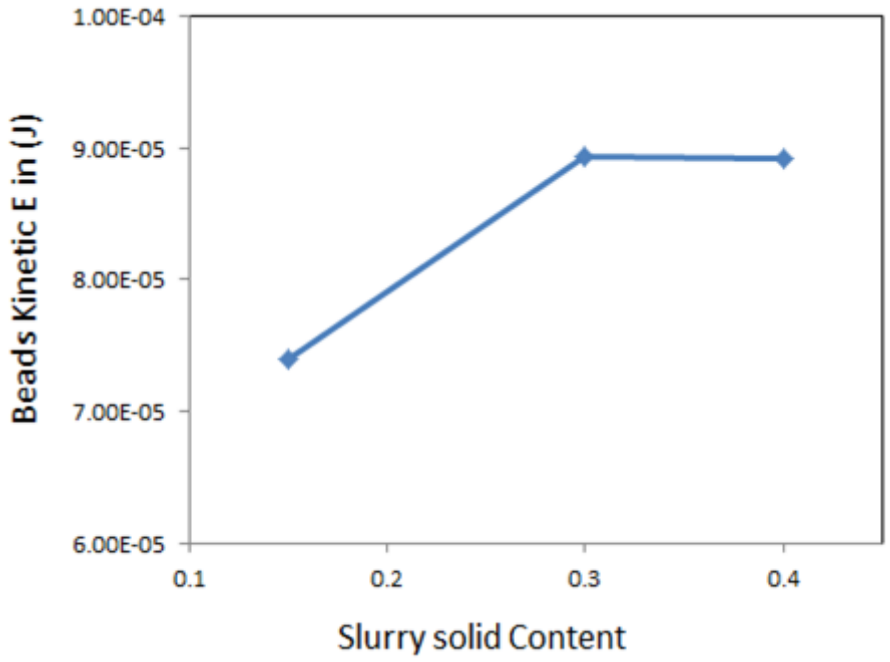

Figure 4-33 Effect of slurry solid content on media kinetic energy

Figure 4-34Figure 4-34 shows the relationship between beads average kinetic energy and slurry solid content in each zone of the mill chamber. The trend of each curve basically follows the relationship between overall bead kinetic energy and solid content. Again the bottom zone (Zone 1) has the highest average beads kinetic energy value compared with Zone 2 and Zone 3.

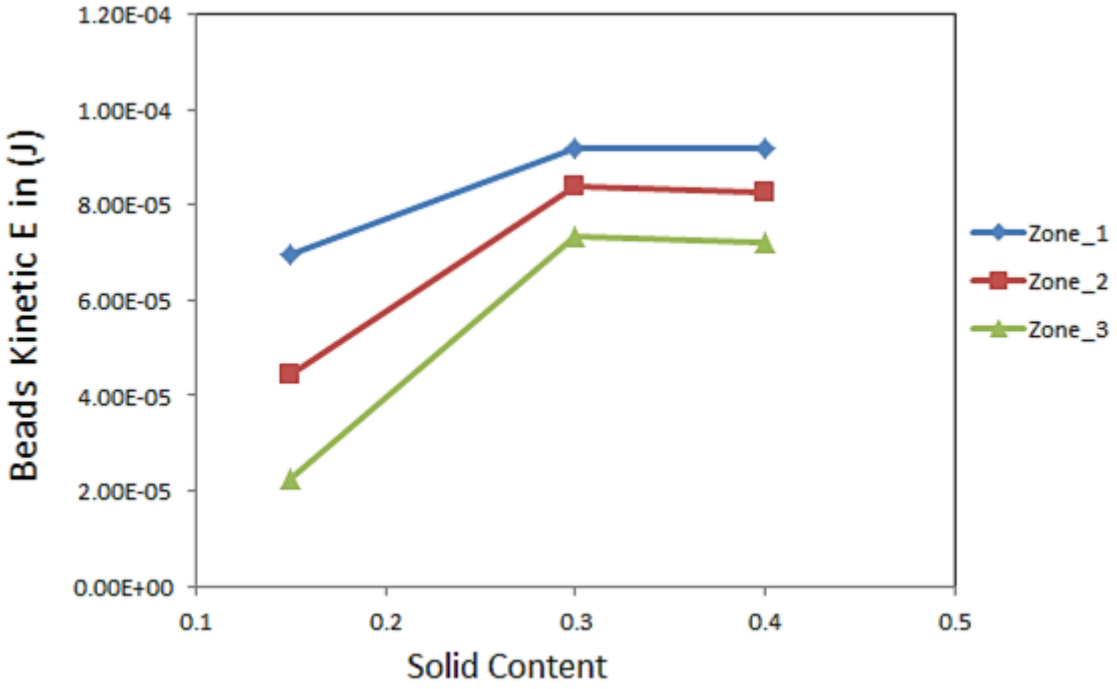

Figure 4-34 Effect of slurry solid content on beads kinetic energy in 3 zones

Figure 4-35 shows the relationship between particle size of each pass and specific energy consumption under three different solid contents. The energy-size relationship from real grinding tests verified the results from modeling. It is shown that specific energy consumption at low solid content is less effective than at medium and high solid content. The improvement of energy efficiency from medium to high solid content is not so significant as compared to from low solid content to medium solid content. The size-energy relationship under various solid contents reveals that increasing slurry solid content between 15% v/v and 30% v/v will help the grinding process in terms of energy consumption. Nevertheless when the solid content goes beyond a peak value (30% v/v in this study), further increase in solid content will not benefit grinding energy efficiency.

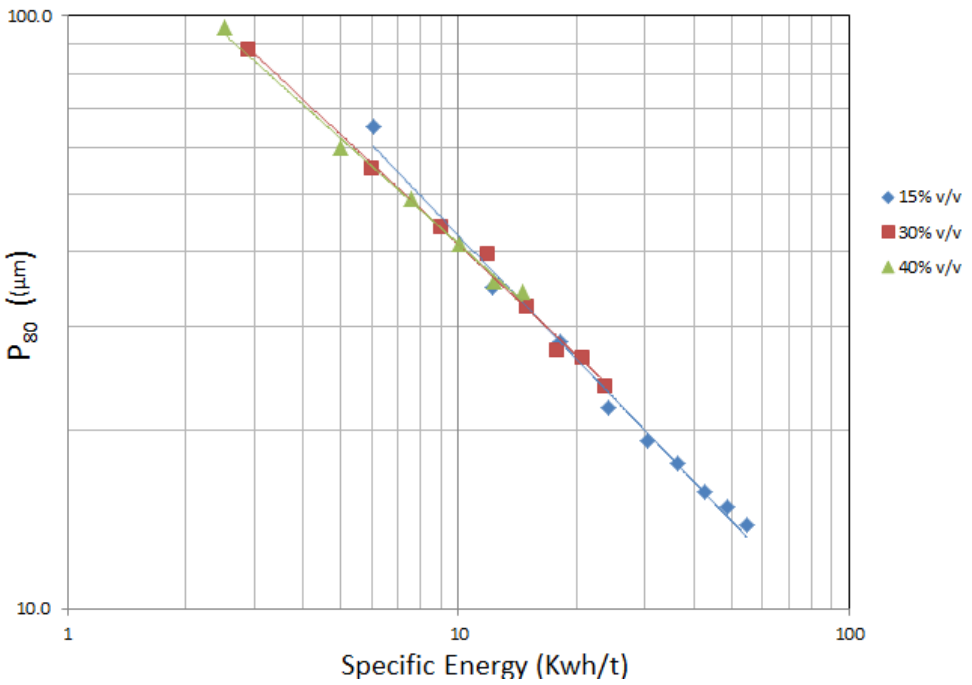

Figure 4-35 Energy-particle size relationship from grinding tests under three different slurry solid content

4.5.4 Effect of Slurry Viscosity

Figure 4-36 shows the influence of slurry viscosity on beads average kinetic energy in the mill. It is seen that when increasing the viscosity of the slurry from 0.005 Pas to 0.025 Pas, there is a slightly increase in beads kinetic energy. It means that the beads are moving faster and are being circulated better in the grinding chamber. The raise in slurry viscosity causes the grinding media to obtain a higher speed. This is because the increase in shear stresses between fluid layers makes the energy transfer more effective. When the viscosity is changed from 0.025 Pas to 0.125 Pas, a dramatic drop in beads kinetic energy is observed. This is due to the increased slurry viscosity preventing beads from being accelerated. As the grinding in the mill goes on, more surface area of ore particles are being created because they are ground finer. The increased shear

stress due to the increased surface tension between particles causes strong resistance and it prevents beads from moving freely in slurry conditions. Due to the "cushioning" effect of viscous slurry, the beads tend to disperse in the mill rather than circulate in the same direction along the annular gap. This effect slows down the speed of grinding media and result in lower bead kinetic energy.

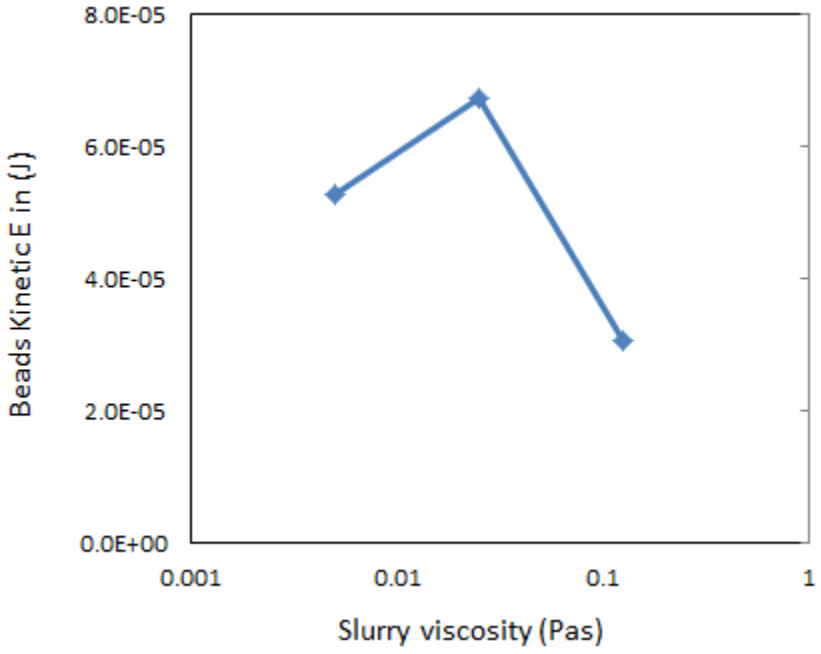

Figure 4-36 Relationship between slurry viscosity and media kinetic energy

The response of beads kinetic energy in three zones to slurry viscosity is also assessed and the result is presented in Figure 4-37. It is obvious that Zone 1 and Zone 2 have similar values and trend and they have a much higher bead average kinetic energy than Zone 3. The kinetic energy increase for all the zones as the viscosity goes from 0.005 Pas to 0.025 Pas then is followed by a large decrease when the viscosity changes from 0.025 Pas to 0.125 Pas. It is noticed that they

almost all fall onto one point when the slurry viscosity is as high as 0.125 Pa s. This may explain the dramatic drop in overall beads kinetic energy when increasing the viscosity from 0.025 to 0.125 Pa s since even beads in Zone 1 and Zone 2 had a major decrease in kinetic energy

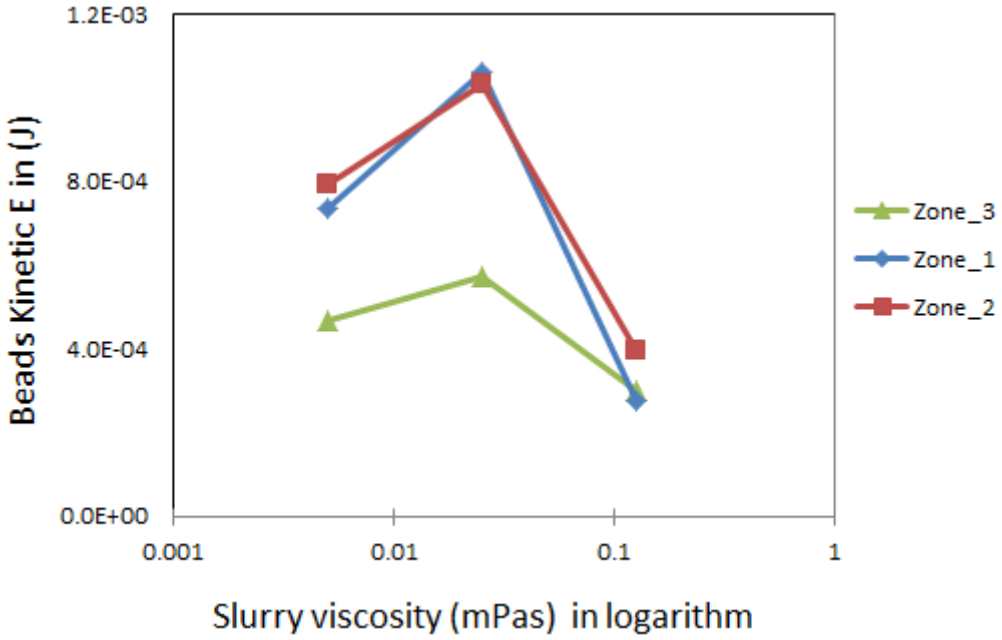

Figure 4-37 Relationship between slurry viscosity and beads kinetic energy in 3 zones

A set of grinding test data is shown to illustrate the effect of slurry viscosity on grinding energy consumption. Figure 4-38 shows the relationship between specific energy and slurry viscosity. It shows that as the slurry viscosity continuously increases, the energy consumption increases dramatically. This could be explained by the increasing slurry viscosity prevented the grinding media from gaining momentum, therefore the lack of kinetic energy resulted in less collision energy and causing more energy being used.

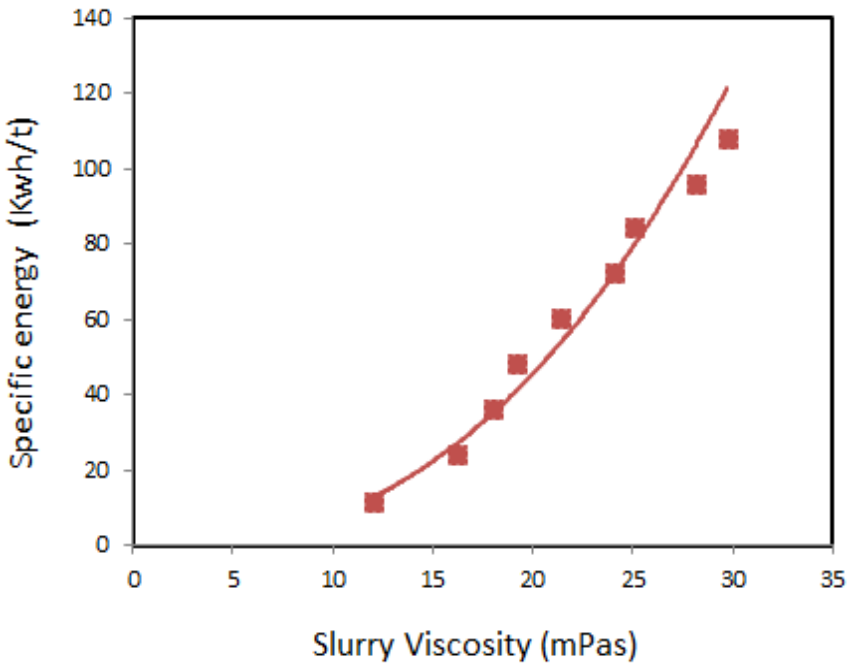

Figure 4-38 Relationship between slurry viscosity and grinding energy

4.5.5 Effect of Mill Stress Intensity

Becker et al. (2001) stated that comminution is a combined effect of a stress event and the collision energy of each event. A Stress event in is referred to as the number of collisions between two grinding media in a unit time (Kwade & Schwedes, 2002). Stress energy is usually described as stress intensity of grinding media and it is defined in Equation 2-7. The stress intensity of grinding beads SI_m is a function of grinding media diameter D_m, grinding media density ρ_m, slurry density ρ and stirrer tip speedv_t. It is a combined effect of the four operating parameters and once the geometry of a mill is given, the stress intensity will only be influenced by those parameters. Therefore, the influence of stress intensity on grinding performance of vertical stirred media mill is an integrated effect of various operating parameters.

For a given material type, feed size and targeted product particle size, there is an optimum stress intensity range where the mill should be operated. In this range, the maximum grinding efficiency is achieved. The stress intensity is useful in mill selection, operation optimization and mill scale-up.

In this study, multiple simulations are done using varying combinations of operating parameters to get a number of stress intensity values. The influence of stress intensity on beads kinetic energy and collision frequency is analyzed.

Figure 4-39 illustrates the relationship between stress intensity and grinding media kinetic energy in wet comminution in a vertical stirred mill. It is clear that the kinetic energy of beads increases with the increase of stress intensity. The effect is evident when the stress intensity is below 0.2 Nm×0.001. When the stress intensity increases beyond 0.3 Nm×0.001, the kinetic energy of the grinding media has almost reached their limit so that further increasing the stress intensity will not help grinding. From Equation 2-7, the stress intensity is proportional to media diameter and density as well as stirrer speed. However, the media diameter and media density together defines the mass of grinding media. The speed of grinding media is directly related to the speed of the stirrer. Therefore, it is almost certain that high stress intensity will lead to high bead kinetic energy during the process of grinding. High stress intensity is favored for increasing bead kinetic energy and further improving grinding performance.

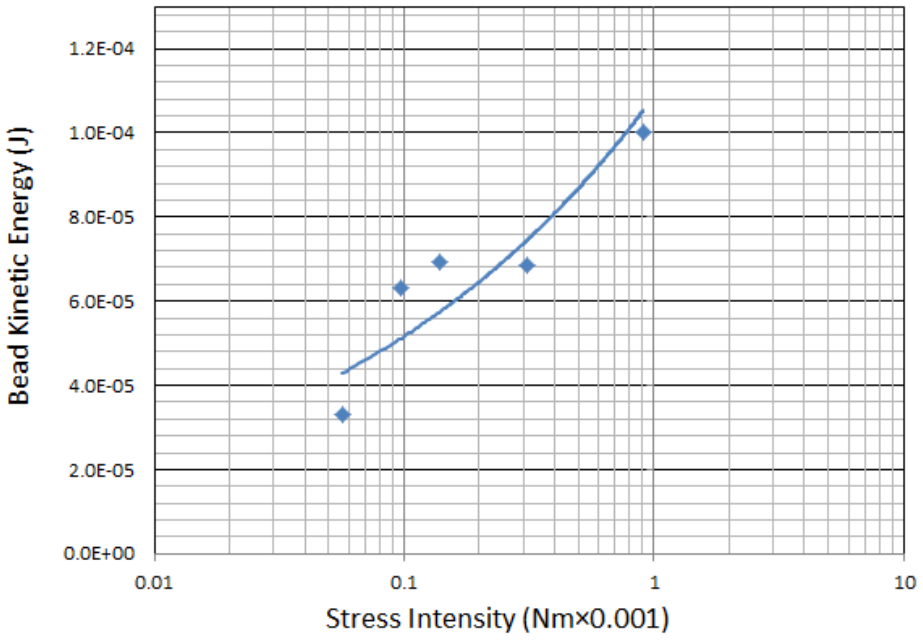

Figure 4-39 Influence of stress intensity's on media kinetic energy

The relationship between grinding media stress intensity and media collision frequency is studied and it is plotted in the Figure 4-40. The trend is similar to that of stress intensity versus beads kinetic energy. The collision frequency here is defined as the average number of collisions between grinding media that were detected in each simulation time step, namely 0.002 s. It is seen that the collision frequency goes up when the stress intensity increases. When the SI is less than 0.2 Nm×0.001 the collision frequency value increases a lot with the change in SI. However, when the SI goes above 0.2 Nm×0.001, the increasing rate of collision frequency slows down. The result suggested that the optimum SI value in terms of collision frequency in around 0.2.

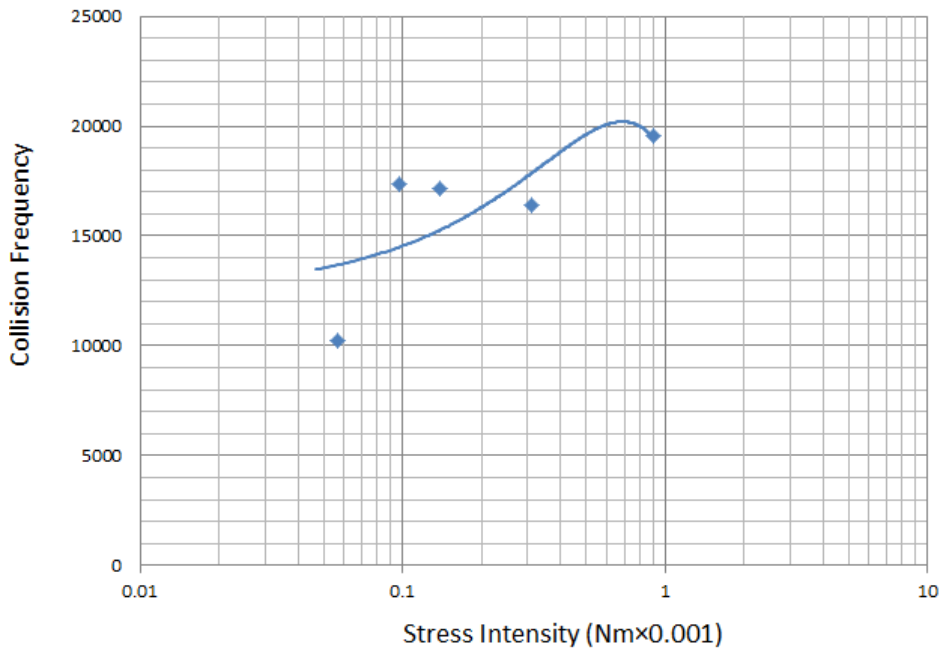

Figure 4-40 Stress intensity's influence on media collision frequency

4.5.6 Conclusion

The effect of operating parameters on grinding media kinetic energy and collision frequency were studied in this section. There is a positive correlation between stirrer speed and media kinetic energy/ media collision frequency. Increasing the stirrer speed may speed up grinding media and improve the number of collisions over time. However, it is more effective when increasing the speed from a small number to a medium number than from a medium number to a high number which indicates there is probably an optimal operating range. The same thing was observed when examining the influence of slurry solid content on grinding media kinetic energy and collision frequency. Results showed that increasing the slurry solid content within 30% v/v would improve energy utilization and above this value, further increasing solid content would have no affect on grinding media kinetic energy. Slurry viscosity influences the two parameters

in a way that beads kinetic energy and collision frequency increase slightly when the viscosity is increased from 0.005 Pas to 0.025 Pas. As well, there is a large drop when continuing to increasing the slurry viscosity from 0.025 Pas to 0.125 Pas which means slurry that a high viscosity will have a negative effect on grinding media kinetic energy.

4.6 Effect of Mill Geometry on Grinding Performance

4.6.1 Introduction

There are a number of design parameters that affects stirred media mill operating performance such as stirrer type, disc thickness and diameter, number of discs, disc alignment, mill chamber geometry and ratio of mill width to height etc. (Kwade, 1999). It is difficult to examine every single parameter's influence, because it is difficult to change only one parameter at a time while keep others fixed. Radziszewski (2013) pointed out that even though a great number of geometry factors could affect mill performance; the driving force behind those parameters is the shear volume of a mill. It is defined in Equation 2-16.

For the purpose of simplicity, the performance of mill will be examined under different shear volumes. Three different mill configurations were used to examine the affect of shear volume to mill performance and their schematics are given in Figure 4-41. Figure 4-41(b) is the original design used in this test work. By adding or removing one disc from the shaft based on (b), mill geometry (a) and (c) are given. Some detailed parameters of the mills are listed in Table 4-1.

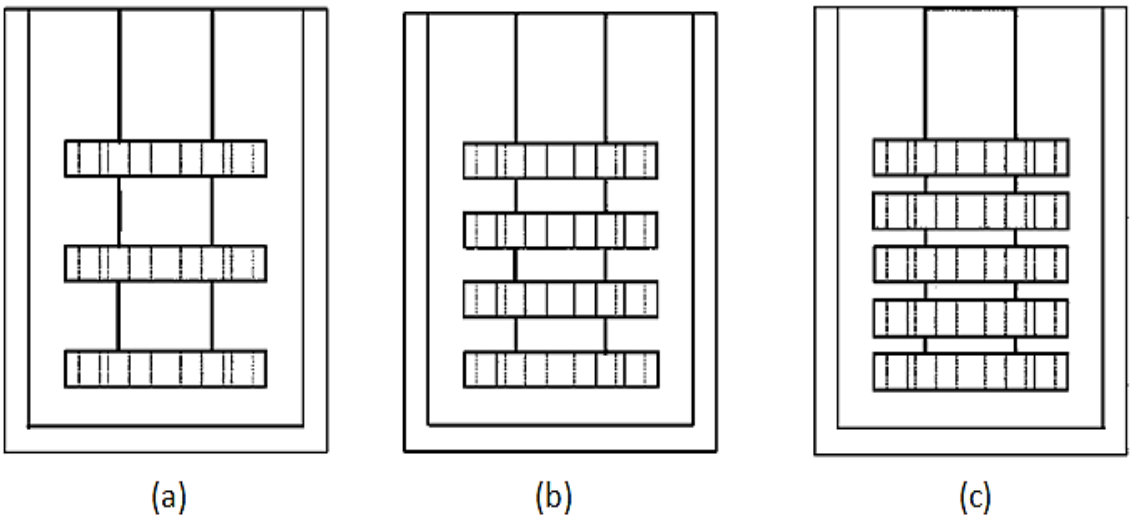

Figure 4-41 Mill geometry with different shear volume

Table 4-1 Geometry parameters of simulation models

	Shear Volume	Number of Discs	Disc Gap	Disc Thickness
(a)	0.03	3	0.04	0.02
(b)	0.037	4	0.02	0.02
(c)	0.044	5	0.01	0.02

4.6.2 Effect of Shear Volume on Grinding Performance

The effect of shear volume on grinding media kinetic energy and collision frequency were examined and their results are shown in Figure 4-42. Simulations were run at the same operating conditions (1100 rpm, 15%v/v, 0.005 Pas) but with different shear volumes. It was found that there was almost no difference in beads kinetic energy between 0.03 m^3 and 0.044 m^3. When the

shear volume value was increased to 0.044 m^3, a 10% increase in beads kinetic energy was observed.

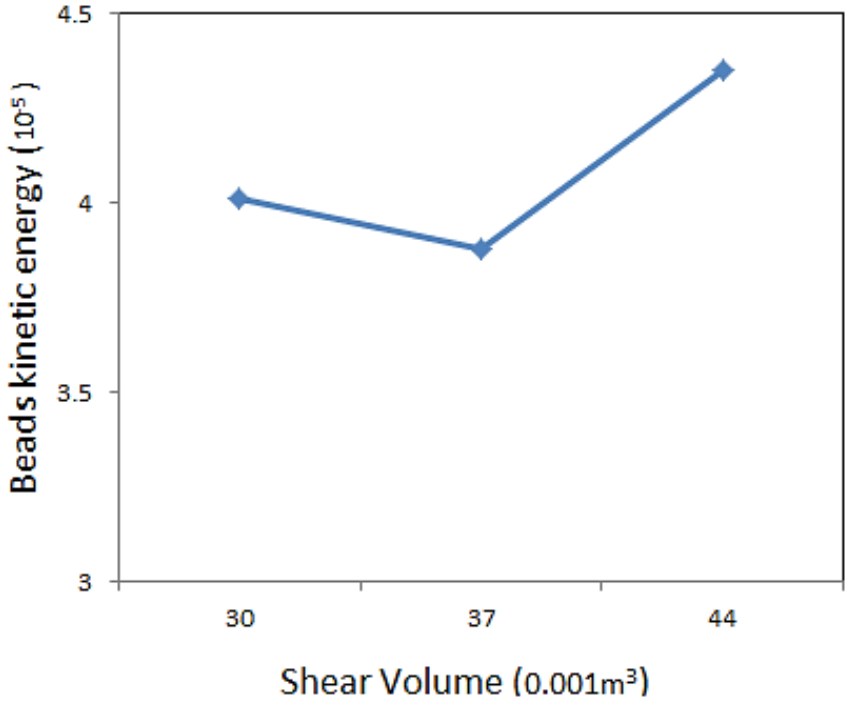

Figure 4-42 Effect of shear volume on media kinetic energy

As to grinding media collision frequency, the maximum value was observed at the middle shear volume level (Figure 4-43), approximately 15,000 collisions per simulation time step. Both 0.03 m^3 and 0.044 m^3 got lower collision frequency than at 0.037 m^3.

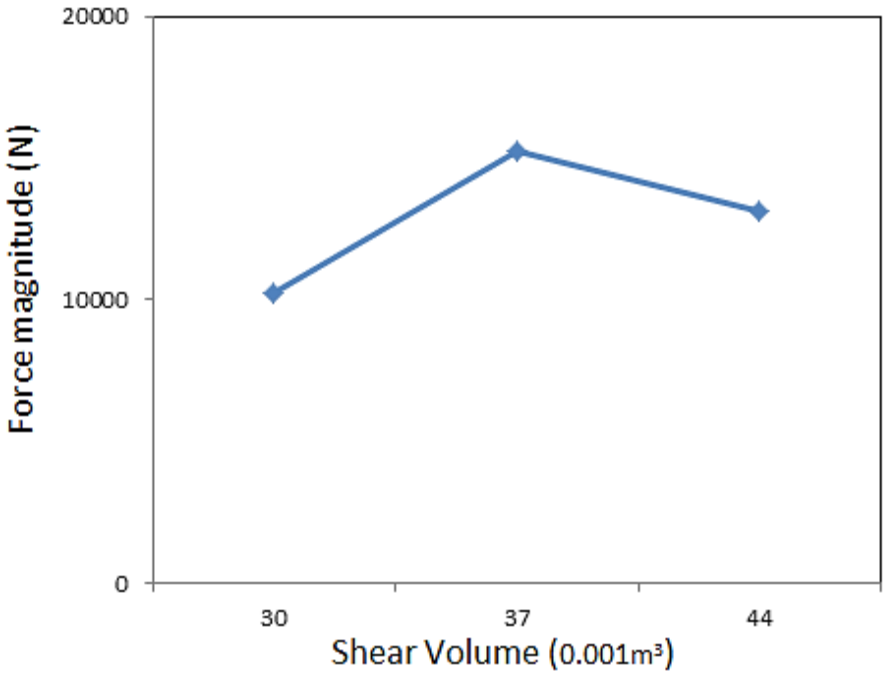

Figure 4-43 Effect of shear volume on media collision frequency

It is expected that mill geometry with higher shear volume could lead to greater bead kinetic energy because the surface area contacting with slurry and beads is larger at higher shear volume. Thus, the shear stress magnitude that the stirrer disc is able to provide is greater than at smaller shear volume. However, the same argument does not apply to the affect on collision frequency since the number of collisions is decided not only by the intensity of the grinding media movement, but is influenced by the space where they are moving as well. Although greater shear volume could provide higher shear forces, there is less space between discs as well as disc and walls for grinding media to move freely. Therefore, a decrease in collision frequency is observed at the highest shear volume.

Normal and tangential force magnitude were also investigated as part of the effect of geometry. Result below shown in Figure 4-44 demonstrates that normal and tangential force magnitude both increase when the shear volume was increased from 0.03 m^3 to 0.37 m^3. When increasing shear volume, a slight drop in both normal and tangential force magnitude was observed.

The result also shows that during grinding in the mills with high shear volume, a larger amount of coarse size fraction particles could be expected since the gap between normal and tangential force is widened. It indicates that massive fracture breakage outweighs attrition breakage mechanism in this scenario. The result also suggested that there is little difference in changing force magnitude for a shear volume number over 0.037 m^3.

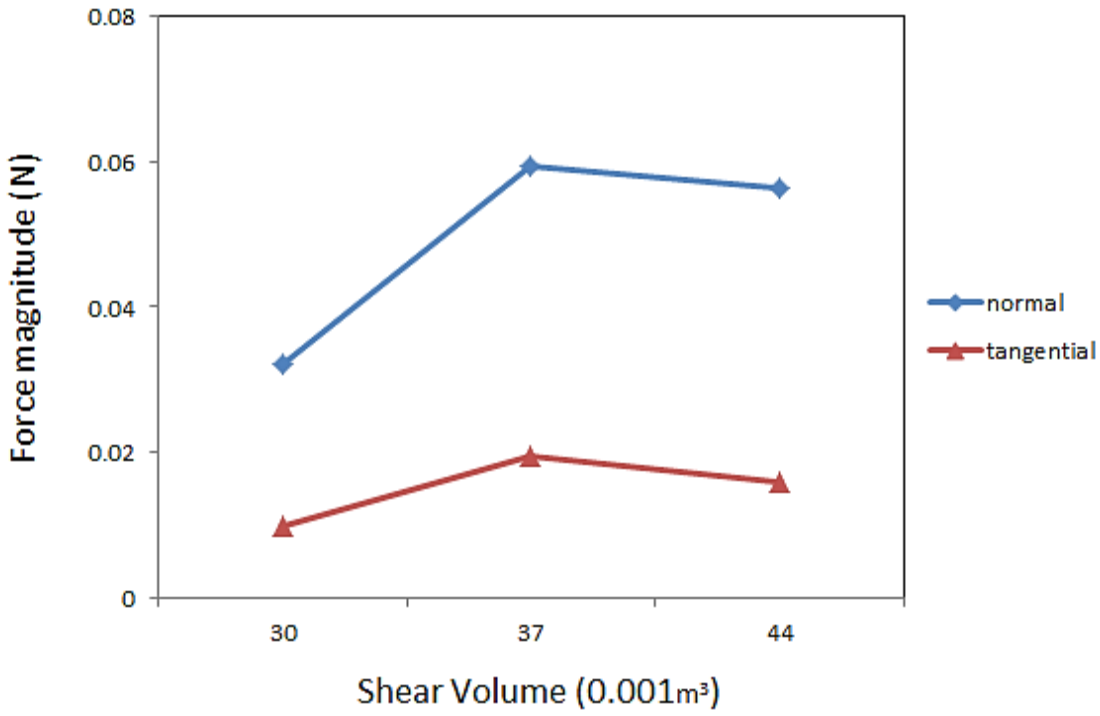

Figure 4-44 Effect of shear volume on normal and tangential force magnitude

4.6.3 Conclusion

In this part, the mill performance is examined with respect to mill geometry configuration, specifically shear volume. Three mill configurations with different shear volume numbers are evaluated.

It was found that shear volume could influence the average kinetic energy, collision frequency and force magnitude of grinding media. A shear volume value that is greater than 0.037 m^3 can effectively improve kinetic energy of the grinding media while no difference in kinetic energy was observed between 0.03 m^3 and 0.037 m^3. The highest collision frequency is observed in the mill with 0.037 m3 shear volume, neither higher nor smaller shear volume result in a higher collision frequency.

Different mill configurations also change the force magnitude level and the percentage of fracture and attrition breakage mechanism during ore breakage. Force magnitude increases when the shear volume is increased from 0.03m3 to 0.037m3 then followed by a mild decrease when it is further increased to 0.044m3. Results showed that a medium shear volume level is favored since it is possible to provide the best grinding performance.

Chapter 5: Conclusions and Recommendations

5.1 Conclusions

The primary objective of this research project was to investigate the effect of operating parameters as well as geometry configurations on the mill performance of a vertical stirred media mill-VXPmill. In order to achieve this aim, computer modeling techniques were utilized and the results were supported by experimental data obtained from real grinding tests performed on a 10 L pilot scale VXPmill. The conclusions of this research work can be summarized as follows:

- The discrete element method is a powerful tool in simulating systems consisting of particles. By employing EDEM software for modeling a grinding process in vertical stirred media mill, it is possible to get detailed information such as particle velocity, forces, collisions and movement trajectory.
- An air column exists in the center of the mill chamber when the shaft is rotating where there is no grinding activity. The volume of the air column expands when stirrer speed and slurry viscosity increases and diminishes when the slurry density increases. Additionally, the outline of the slurry body changes with the altering of operating parameters. Air bubbles trapped in the body of fluid were observed and the number of them increases with the rise in mixing speed. It is also found that increasing the stirrer speed, slurry density and slurry viscosity diminish the effective grinding space of a vertical stirred mill. It will affect the throughput of the equipment during production.
- Velocity gradients of grinding media exist in horizontal and vertical sections in vertical a stirred mill. Grinding, media velocity increases along disc radial direction and reach a maximum near the stirrer tip. It then decreases across the gap between the disc edge and

the mill inner wall and get to its minimum at the wall surface. In the vertical plane, the highest average media velocity is observed at 1/3 of mill height from bottom, where the first two discs are located. Then media velocity continues to drop with height. The velocity gradients indicated that there are zones with different energy intensity existing in the mill.

- Grinding media distribution in the mill chamber is heavily influenced by stirrer speed and slurry viscosity. Higher stirrer rotational speed results in media distributed more homogenously across the chamber while higher slurry viscosity makes media more dispersed. Slurry solid content does not have much influence on the media distribution in the mill.
- Grinding media trajectory revealed that media movement is less influenced by slurry buoyant forces in the mill axial direction. Instead, their movement is mostly trapped within the same height.
- Fracture breakage plays a more important role than attrition breakage in a VXPmill because it is found that the normal force magnitude is greater than the tangential force. Both forces increase as the stirrer speeds up and decrease as the slurry solid content increases. The change in breakage mechanism will cause a difference in the percentage of coarse and fines in product particles.
- The breakage of ore particles is a combined effect of grinding media kinetic energy and numbers of collisions happening in a given time. Both grinding media kinetic energy and collision frequency are influenced by mill operating parameters. Increasing stirrer speed and slurry solid content up to a point will help increase media kinetic energy and the number of collisions between media, therefore improve grinding performance and energy

utilization. Beyond a certain value, increasing theses parameters will reduce the improvement in kinetic energy and collision frequency. The same result is observed with the effect of slurry viscosity. However, the drag effect of excessive viscosity is more significant than that of stirrer speed and solid content. Hence there is an optimal point of stirrer speed, solid content and slurry viscosity for the mill to operate at.

- Shear volume can be used as a criterion to assess the geometry effect on mill performance. Within the shear volume values tested, the higher the shear volume number is, the higher grinding media kinetic energy will be observed. The highest grinding media collision frequency was observed at a medium shear volume level which means that there is an optimal mill design which could provide the most space for the beads to move freely. A higher shear volume number can provide higher normal and tangential force magnitude, but the ratio of normal force to tangential force increases with shear volume. The mill design with higher shear volume will lead to more massive fracture breakage than attrition. As a result, more coarse particles are expected.

5.2 Recommendations

The research was completed by using computer modeling technology and verified by grinding trials data. Although computer simulations could provide an insight and understanding as well as a good approximation to real conditions, some inaccuracies and deviations from real data exist. To better duplicate real operation conditions, efforts could be spent on seeking physical models that can describe the comminution process more precisely. Meanwhile, to develop a more

accurate model it is suggested to use, more powerful computers. With higher computing abilities, it is possible to achieve the objective of simulating more sophisticated models.

The characteristics of slurry flow as well as grinding media movement were demonstrated. Results showed that areas with the highest energy intensity are in the vicinity of the stirrer discs in the bottom part of the mill. The breakage of ore particles is mostly achieved in this area. As the grinding media distribution result suggested, most media reside in the bottom part of the mill chamber. Therefore discs and liners in that area may suffer the heaviest wear. Further investigations need to be done to confirm the velocity gradient achieved by computer simulations. Techniques such as particle tracing could be applied to better visualize the behavior of solids and fluids in the mill chamber.

The current research results confirmed that both fracture and attrition exist in the grinding process of a vertical stirred milling and fracture is the dominant breakage mechanism rather than attrition. It suggests that a fast disappearance rate of coarse particles could be expected, compared to the generating rate of finer particles. It is suggested that more grinding tests under different operating conditions should be done and more particle size analysis should be performed on ground samples to confirm this result.

Mills need to be operated at a relatively high speed to achieve higher energy intensity, collision frequency and greater force magnitude on beads. Operating the mill with the slurry solid content controlled within a certain range could help the grinding process. In this case, no more than 30% v/v slurry solid content value is recommended. It is also suggested that the slurry viscosity should be, no higher than 0.125 Pas in this case, since high shear induced by excessively viscous

slurry could reduce grinding media kinetic energy, collision frequency and result in a reduced energy efficiency

Improvement in mill design could be focused on increasing the shear volume in the mill such as adding discs within a fixed distance, increasing disc thickness or expanding disc surface area. However, enough empty space must be provided for grinding media to move freely. The effect of shear volume in the mill on grinding performance is given, but further study should be carried out on trial grinding test to confirm simulation results.

References

Bannikov, V. V., Shein, I. R., & Ivanovskii, A. L. (2012). Mechanical properties and electronic structure of zircon: Ab inito FLAPW-GGA calculations. Inorganic Materials: Applied Research, 3(1), 7-10.

Barley, R. W., Conway-Baker, J., Pascoe, R. D., Kostuch, J., McLoughlin, B., & Parker, D. J. (2004). Measurement of the motion of grinding media in a vertically stirred mill using positron emission particle tracking (PEPT) Part II. Minerals engineering, 17(11), 1179-1187

Blecher, L., Kwade, A., & Schwedes, J. (1996). Motion and stress intensity of grinding beads in a stirred media mill. Part 1: energy density distribution and motion of single grinding beads. *Powder Technology*, 86(1), 59-68.

Chen, H., Ding, Y., & Tan, C. (2007). Rheological behaviour of nanofluids. New Journal of Physics, 9(10), 367.

Cleary, P. W. (1998). Predicting charge motion, power draw, segregation and wear in ball mills using discrete element methods. Minerals Engineering, 11 (11), 1061-1080.

Cundall, P. A., & Strack, O. D. (1979). A discrete numerical model for granular assemblies. Geotechnique, 29(1), 47-65.

Deen, N. G., Van Sint Annaland, M., Van der Hoef, M. A., & Kuipers, J. A. M. (2007). Review of discrete particle modeling of fluidized beds. Chemical Engineering Science, 62(1), 28-44.

EDEM (2012). EDEM User's Guide. DEM solutions, Edinburgh, UK.

FLSmidth Knelson (2012). *Stirrer Mill user manual*, Model VSM10. A Division of FLSmidth ltd, Langley, British Columbia, Canada, pp64

Gao, M. W., & Forssberg, E. (1993). A study on the effect of parameters in stirred ball milling. International journal of mineral processing, 37 (1), 45-59.

Gao, M. W., Forssberg, K. S. E., & Weller, K. R. (1996). Power predictions for a pilot scale stirred ball mill. International Journal of Mineral Processing, 44, 641-652.

Gers, R., Climent, E., Legendre, D., Anne-Archard, D., & Frances, C. (2010). Numerical modelling of grinding in a stirred media mill: Hydrodynamics and collision characteristics. Chemical Engineering Science, 65(6), 2052-2064.

He, M., & Forssberg, E. (2007). Influence of slurry rheology on stirred media milling of quartzite. International Journal of Mineral Processing, 84(1), 240-251.

He, M., Wang, Y., & Forssberg, E. (2006). Parameter effects on wet ultrafine grinding of limestone through slurry rheology in a stirred media mill. Powder technology, 161(1), 10-21.

He, M., Wang, Y., & Forssberg, E. (2004). Slurry rheology in wet ultrafine grinding of industrial minerals: a review. Powder Technology, 147(1), 94-112.

Hertz, H. (1882). Über die Berührung fester elastischer Körper. Journal für die reine und angewandte Mathematik, 92, 156-171

Hukki, R. T. (1961). Proposal for a solomonic settlement between the theories of von Rittinger, Kick, and Bond. Trans. AIME, 220, 403-408.

Klein, B. (1992). Rheology and stability of magnetite dense media (Doctoral dissertation, University of British Columbia).

Kwade, A., Blecher, L., & Schwedes, J. (1996). Motion and stress intensity of grinding beads in a stirred media mill. Part 2: Stress intensity and its effect on comminution. Powder Technology, 86(1), 69-76.

Kwade, A. (1999). Wet comminution in stirred media mills—research and its practical application. Powder Technology, 105(1), 14-20.

Kwade, A., & Schwedes, J. (2002). Breaking characteristics of different materials and their effect on stress intensity and stress number in stirred media mills. Powder Technology, 122(2), 109-121.

Langley, B. C., & Consulting, (2011) K. W. M. Knelson-Deswik Milling Technology: Bridging the Gap between Low and High Speed Stirred Mills.

Lichter, J. K., & Davey, G. (2006). Selection and sizing of ultrafine and stirred grinding mills. Advances in comminution, 69.

Mannheim, V. (2011). Empirical and scale-up modeling in stirred ball mills.Chemical Engineering Research and Design, 89(4), 405-409.

Mankosa, M. J., Adel, G. T., & Yoon, R. H. (1986). Effect of media size in stirred ball mill grinding of coal. Powder technology, 49(1), 75-82.

Mankosa, M. J., Adel, G. T., & Yoon, R. H. (1989). Effect of operating parameters in stirred ball mill grinding of coal. Powder technology, 59(4), 255-260.

Metso (2014). Stirred Milling – VERTIMILL Grinding Mills & Stirred Media Detritor. Metso Minerals Industries, Inc. York, PA.

Mio, H., Kano, J., & Saito, F. (2004). Scale-up method of planetary ball mill.Chemical engineering science, 59 (24), 5909-5916.

Mishra, B. K., & Rajamani, R. K. (1994). Simulation of charge motion in ball mills. Part 1: experimental verifications. International Journal of Mineral Processing, 40(3), 171-186.

Morrison, R. D., & Cleary, P. W. (2004). Using DEM to model ore breakage within a pilot scale SAG mill. Minerals Engineering, 17 (11), 1117-1124.

Munson, B. R., Young, D. F., & Okiishi, T. H. (1990). Fundamentals of fluid mechanics (pp. 105-120). New York.

Muster, T. H., & Prestidge, C. (1995). Rheological investigations of sulphide mineral slurries. Minerals Engineering, 8 (12), 1541-1555.

Jankovic, A. (2001). Media stress intensity analysis for vertical stirred mills. Minerals Engineering, 14(10), 1177-1186.

Jankovic, A. (2003). Variables affecting the fine grinding of minerals using stirred mills. Minerals Engineering, 16 (4), 337-345.

Jankovic, A., Valery, W., & La Rosa, D. (2008). Fine Grinding in the Australian Mining Industry.

Jankovic, A., & Sinclair, S. (2006). The shape of product size distributions in stirred mills. Minerals engineering, 19 (15), 1528-1536.

Jayasundara, C. T., Yang, R. Y., Guo, B. Y., Yu, A. B., & Rubenstein, J. (2009). Effect of slurry properties on particle motion in IsaMills. Minerals Engineering, 22(11), 886-892.

Jayasundara, C. T., Yang, R. Y., Guo, B. Y., Yu, A. B., Govender, I., Mainza, A., ... & Rubenstein, J. (2011). CFD–DEM modelling of particle flow in IsaMills–Comparison between simulations and PEPT measurements. Minerals Engineering, 24 (3), 181-187.

Jayasundara, C. T., Yang, R. Y., & Yu, A. B. (2012). Effect of the size of media on grinding performance in stirred mills. Minerals Engineering, 33, 66-71.

Outotec (2013). Outotec HIGmills Manual. Outotec, Finland.

Powell, M. S., & Morrison, R. D. (2007). The future of comminution modelling.International Journal of Mineral Processing, 84(1), 228-239.

Radziszewski, P. (2013). Assessing the stirred mill design space. Minerals Engineering, 41, 9-16.

Rahal, D., Roberts, K., & Rivett, T. (2011) Knelson-Deswik Mill: Evaluation of Operating Variables.

Reem, A. R. (2011). The effect of stirred mill operation on particles breakage mechanism and their morphological features (Doctoral dissertation, University of British Columbia).

Rule, C., & De Waal, H. (2011). IsaMill™ Design Improvements and Operational Performance at Anglo Platinum.

Santos-Moreau, V., Brunet-Errard, L., & Rolland, M. (2012). Numerical CFD simulation of a batch stirred tank reactor with stationary catalytic basket.Chemical Engineering Journal, 207, 596-606.

Shi, F., Morrison, R., Cervellin, A., Burns, F., & Musa, F. (2009). Comparison of energy efficiency between ball mills and stirred mills in coarse grinding.Minerals Engineering, 22(7), 673-680.

Sinnott, M., Cleary, P. W., & Morrison, R. D. (2011). Slurry flow in a tower mill.Minerals Engineering, 24(2), 152-159.

Sinnott, M. D., Cleary, P. W., & Morrison, R. D. (2011). Is media shape important for grinding performance in stirred mills?. Minerals Engineering, 24(2), 138-151.

Stein, E., de Borst, R., & Hughes, T. J. (2004). Encyclopedia of computational mechanics. Wiley.

Theuerkauf, J., & Schwedes, J. (1999). Theoretical and experimental investigation on particle and fluid motion in stirred media mills. Powder Technology, 105(1), 406-412.

Toraman, O. Y., & Katırcıoglu, D. (2011). A study on the effect of process parameters in stirred ball mill. Advanced Powder Technology, 22(1), 26-30.

Weller, K. R., Spencer, S. J., Gao, M., & Liu, Y. (2000). Tracer studies and breakage testing in pilot-scale stirred mills. Minerals engineering, 13(4), 429-458.

Wang, Y., & Forssberg, E. (2007). Enhancement of energy efficiency for mechanical production of fine and ultra-fine particles in comminution. China Particuology, 5(3), 193-201.

Xstrata (2014). IsaMill-Breaking the boundaries, brochure.

Yamada, Y., & Sakai, M. (2013). Lagrangian–Lagrangian simulations of solid–liquid flows in a bead mill. Powder Technology, 239, 105-114.

Yang, R. Y., Jayasundara, C. T., Yu, A. B., & Curry, D. (2006). DEM simulation of the flow of grinding media in IsaMill. Minerals engineering, 19(10), 984-994.

Yoon, S. H. (1994). Scale-up method for a horizontal-type jet mill. Advanced Powder Technology, 5(1), 53-59.

Yuan, J., & Murray, H. H. (1997). The importance of crystal morphology on the viscosity of concentrated suspensions of kaolins. Applied clay science, 12(3), 209-219.

Yue, J., & Klein, B. (2004). Influence of rheology on the performance of horizontal stirred mills. Minerals engineering, 17(11), 1169-1177.J.

Yue, J., and B. Klein. "Particle breakage kinetics in horizontal stirred mills.“Minerals engineering 18.3 (2005): 325-331.

Yue, J., & Klein, B. (2006). Effects of bead size on ultrafine grinding in a stirred bead mill. Advances in comminution, 87.

Zhu, H. P., Zhou, Z. Y., Yang, R. Y., & Yu, A. B. (2008). Discrete particle simulation of particulate systems: A review of major applications and findings. Chemical Engineering Science, 63(23), 5728-5770.

Appendices

Appendix A Supplementary data for section 4.3.1

A.1 Grinding media distribution in 3 zones over time (test No. 2 in Table 3-6)

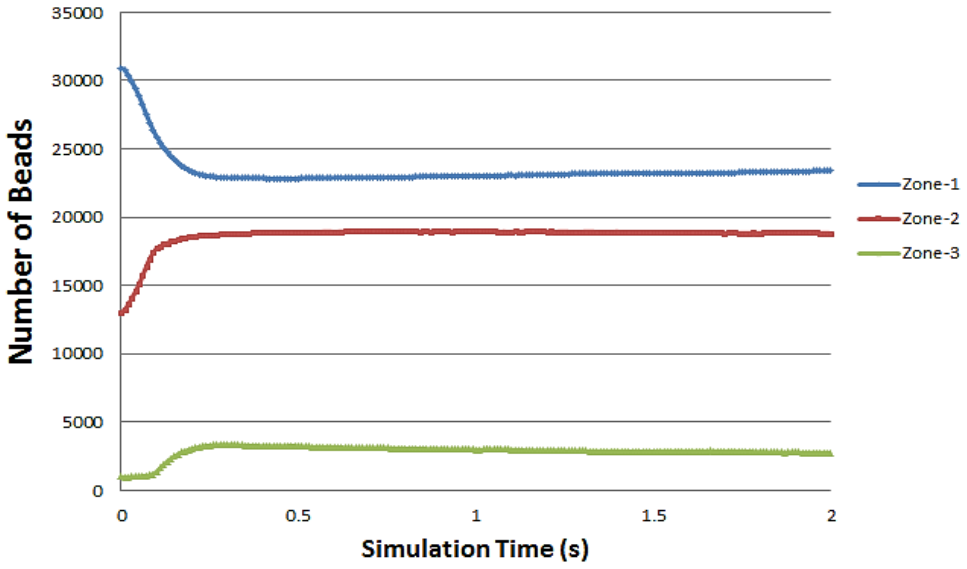

A.2 Grinding media distribution in 3 zones over time (test No. 10 in Table 3-6)

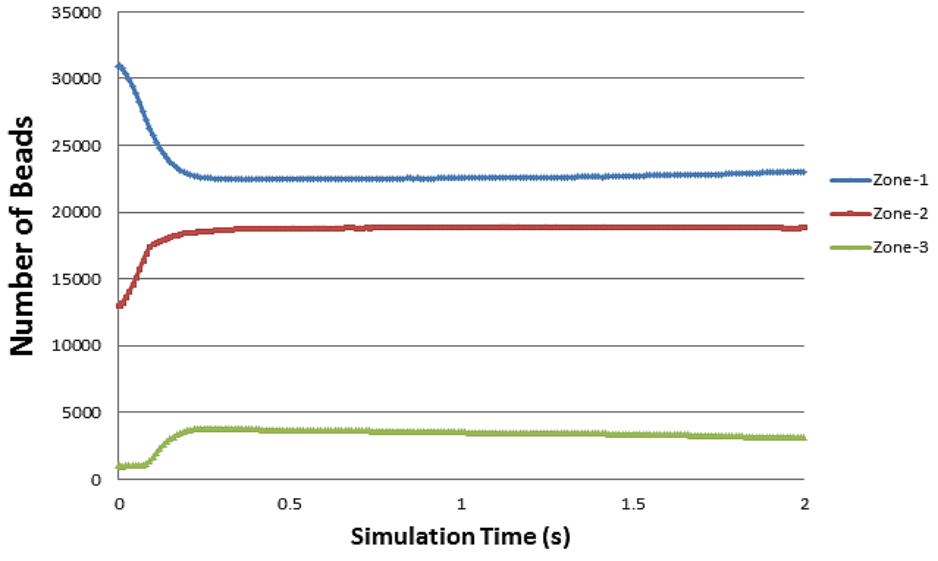

Appendix B Appendix B Experiment data for grinding tests

B.1 Grinding Test 1 Results

Test work 1 (1100 rpm, 15% v/v)				
Pass #	Yield stress	Apparent viscosity at 100 (1/s)	P_{80}	Specific energy
	Pa	mPas	µm	kWh/t
Feed			200	
Pass 1	0.3501	11.4	65	6.04
Pass 2	0.4909	11.7	34.94	12.17
Pass 3	0.6605	13.6	28.19	18.19
Pass 4	0.8559	16.17	21.83	24.16
Pass 5	1.054	17.21	19.18	30.35
Pass 6	1.11	18.25	17.6	36.35
Pass 7	1.081	18.77	15.8	42.47
Pass 8	1.3	21.38	14.87	48.5
Pass 9	1.389	21.84	13.88	54.57

B.2 Grinding Test 2 Results

Test work 2 (1350 rpm, 15% v/v)				
Pass #	Yield stress	Apparent viscosity at 100 (1/s)	P_{80}	Specific energy
	mPas	mPas	µm	kWh/t
Feed			200	
Pass 1	0.3233	10.95	61.52	9.12
Pass 2	0.8882	16.12	33.65	18.62
Pass 3	0.9196	16.8	26.78	27.96
Pass 4	1.12	18.25	21.97	37.95
Pass 5	1.253	19.3	19.4	47.41
Pass 6	1.355	20.9	16.81	57.05
Pass 7	1.495	24.4	15.45	67.39
Pass 8	1.654	25.3	14.6	76.2
Pass 9	1.675	26	13.9	85.52

B.3 Grinding test 3 results

Test work 3 (1600 rpm, 15% v/v)				
Pass #	Yield stress	Apparent viscosity at 100 (1/s)	P_{80}	Specific energy
	Pa	mPas	µm	kWh/t
Feed			200	
Pass 1	0.405	11.96	51.9	11.83
Pass 2	0.823	16.17	32.0	24.24
Pass 3	0.970	17.95	25.3	36.3
Pass 4	1.070	19.14	20.6	48.72
Pass 5	1.303	21.38	18.7	60.51
Pass 6	1.564	24	16.2	72.73
Pass 7	1.644	25	15.4	84.58
Pass 8	2.000	28.1	14.0	96.41
Pass 9	1.976	29.7	13.5	108.05

B.4 Grinding test 4 results

Test work 4 (1100 rpm,30% v/v)					
Pass #	Yield stress	Apparent viscosity at 100 (1/s)	P_{80}	Specific energy	Apparent viscosity at 100 (1/s)
	Pa	mPas	µm	kWh/t	mPas
Feed			200		
Pass 1	4.327	67.20	88.0	2.882	67.20
Pass 2	4.112	62.6	55.5	5.955	62.6
Pass 3	5.233	72.5	44.2	8.965	72.5
Pass 4	5.541	77	39.9	11.765	77
Pass 5	7.577	97.5	32.5	14.858	97.5
Pass 6	6.518	86.05	27.5	17.748	86.05
Pass 7	9.281	129.4	26.7	20.619	129.4
Pass 8	9.872	131.4	23.9	23.598	131.4

B.5 Grinding test 5 results

Test work 5 (1350 rpm, 30% v/v)				
Pass #	Yield stress	Apparent viscosity at 100 (1/s)	P_{80}	Specific energy
	Pa	mPas	µm	kWh/t
Feed			200	
Pass 1	5.463	80.8	75.0	5.06
Pass 2	5.373	79.3	52.2	10.06
Pass 3	6.450	99.1	43.2	14.8
Pass 4	8.346	113.3	37.0	19.44
Pass 5	10.420	134.6	34.1	24.75
Pass 6	10.990	142.4	31.3	29.22
Pass 7	12.460	157.6	27.4	33.92
Pass 8	12.040	159.1	24.5	38.42
Pass 9	11.900	152.2	24.7	42.97

B.6 Grinding test 6 results

Test work 6 (1600 rpm, 30% v/v)				
Pass #	Yield stress	Apparent viscosity 1t 100 (1/s)	P_{80}	Specific energy
	Pa	mPas	µm	kWh/t
Feed			200	
Pass 1	6.7	97	59.9	6.470
Pass 2	6.8	89	48.0	12.780
Pass 3	9.5	116.8	38.1	19.170
Pass 4	9.6	119.9	31.8	25.570
Pass 5	12.7	153.4	29.4	31.990
Pass 6	13.1	154.3	27.7	38.350
Pass 7	13.8	164	25.7	44.840
Pass 8	14.9	174.7	24.8	51.240
Pass 9	15.2	200.30	22.6	57.850

B.7 Grinding test 7 results

Test work 7 (1100rpm, 40% v/v)				
Pass #	Yield stress	Apparent viscosity at 100 (1/s)	P_{80}	Specific energy
	Pa	mPas	µm	kWh/t
Feed			200	
Pass 1	23.3	322.6	95.6	2.5
Pass 2	25.8	351.3	59.9	5.0
Pass 3	35.0	472.0	49.3	7.6
Pass 4	37.7	469.3	41.2	10.0
Pass 5	33.9	432.9	35.6	12.3
Pass 6	44.5	609.5	34.2	14.5

B.8 Grinding test 8 results

Test work 10 (1350 rpm, 40%)				
Pass #	Yield stress	Apparent viscosity at 100 (1/s)	p80	Specific energy
	Pa	mPas	microns	kWh/t
Feed			200	
Pass 1	10.05	139.98	90	4.22
Pass 2	11.32	162.93	72.1	8.24
Pass 3	13.70	193.33	50.3	12.66
Pass 4	17.28	224.16	47.0	16.50
Pass 5	19.60	245.94	40.8	20.45
Pass 6	22.11	276.49	38.9	24.57
Pass 7	26.29	337.16	32.0	32.37
Pass 8	28.09	343.49	31.6	36.09

B.9 Grinding test 9 results

Test work 8 (1600 rpm, 40% v/v)				
Pass #	Yield stress	Apparent viscosity at 100 (1/s)	P_{80}	Specific energy
	mPas	mPas	µm	kWh/t
Feed			200	
Pass 1	22.09	294.2	98.6	3.426
Pass 2	29.41	339.5	72.0	6.740
Pass 3	27.96	366.1	59.0	10.000
Pass 4	31.96	390.6	50.0	13.400
Pass 5	41.37	503.8	43.2	16.900
Pass 6	45.61	577.3	39.7	20.400

B.10 Grinding test 10 results

Test work 9 (600 rpm, 30% v/v)				
Pass #	Yield stress	Apparent viscosity at 100 (1/s)	P_{80}	Specific energy
	Pa	mPas	µm	kWh/t
Feed			200	
Pass 1	3.25	46.27	135	0.711
Pass 2	3.67	51.62	96.5	1.490
Pass 3	3.75	55.33	91.6	2.330
Pass 4	3.84	62.37	76.6	3.130
Pass 5	3.98	63.15	71	3.890
Pass 6	4.14	65.27	61	4.690
Pass 7	4.35	69.34	53.9	5.41
Pass 8	4.47	71.19	55.3	6.16
Pass 9	4.50	74.06	51.2	6.91

Appendix C : Input parameters to ANSYS-FLUENT (example: 15% v/v, 5 mPas, 600rpm)

C.1 General input parameters

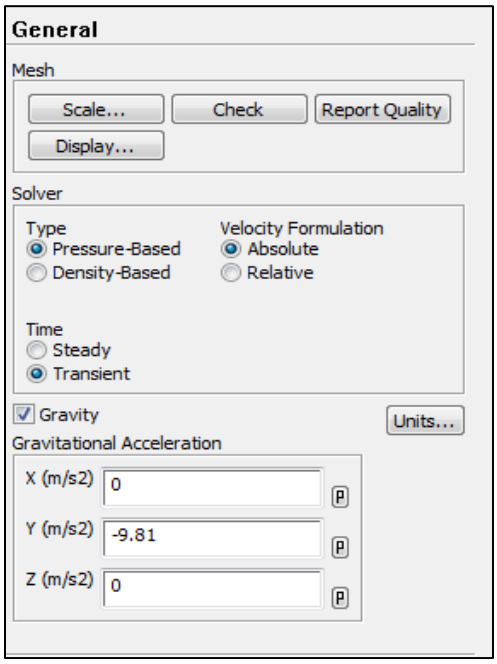

C.2 Model-multiphase model parameters

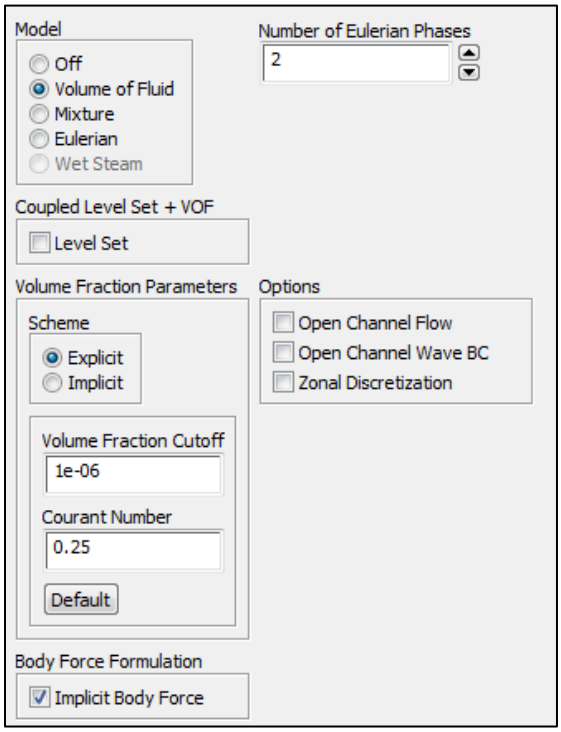

C.3 Model-viscous model parameters

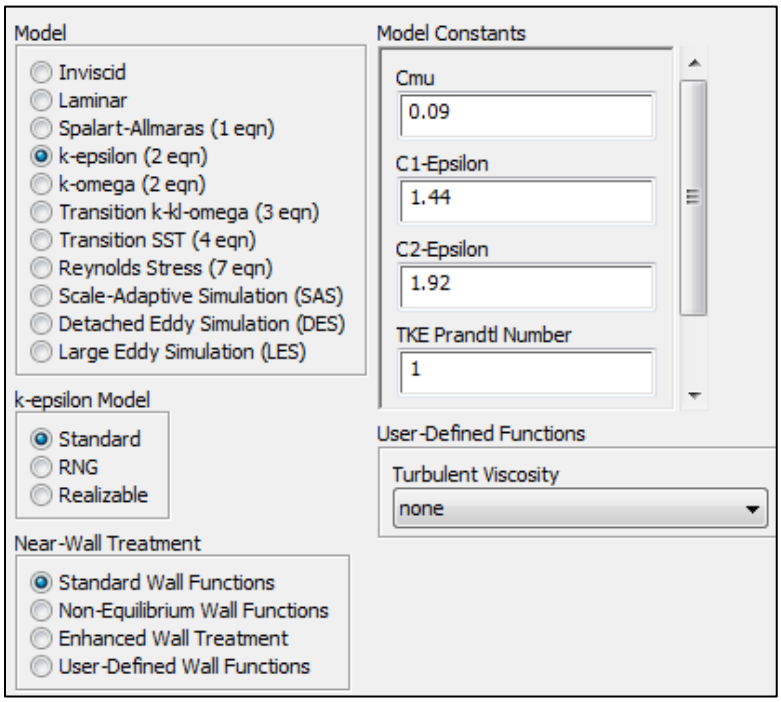

C.4 Material-air property input parameters

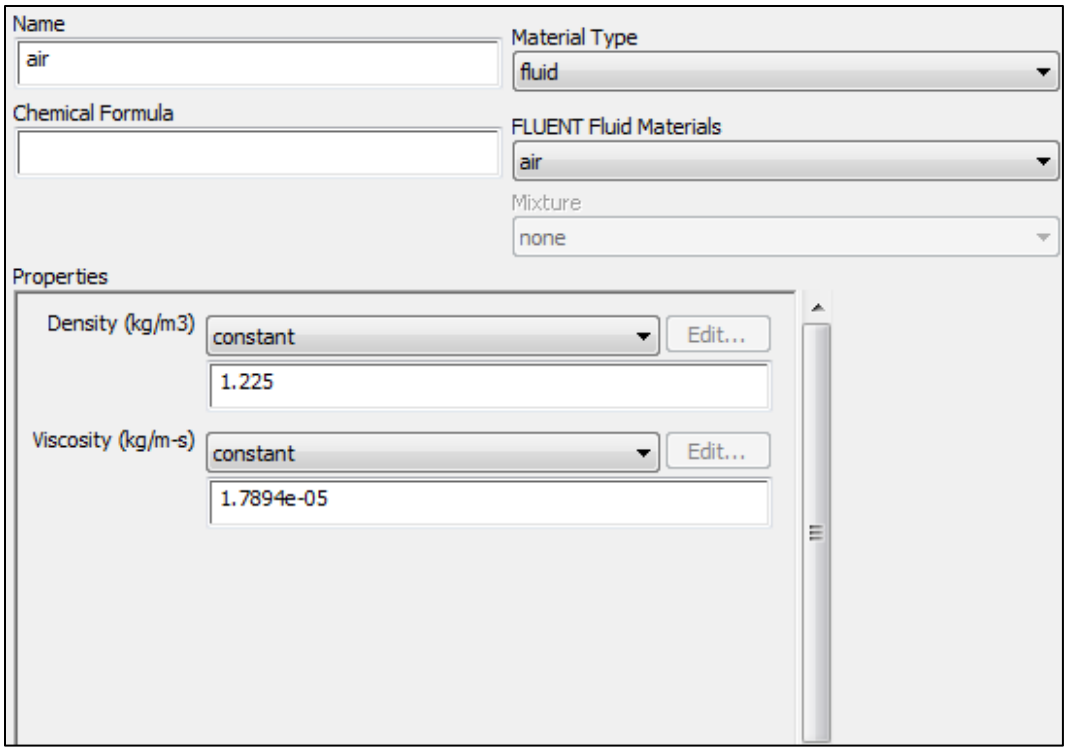

C.5 Material-slurry property input parameters

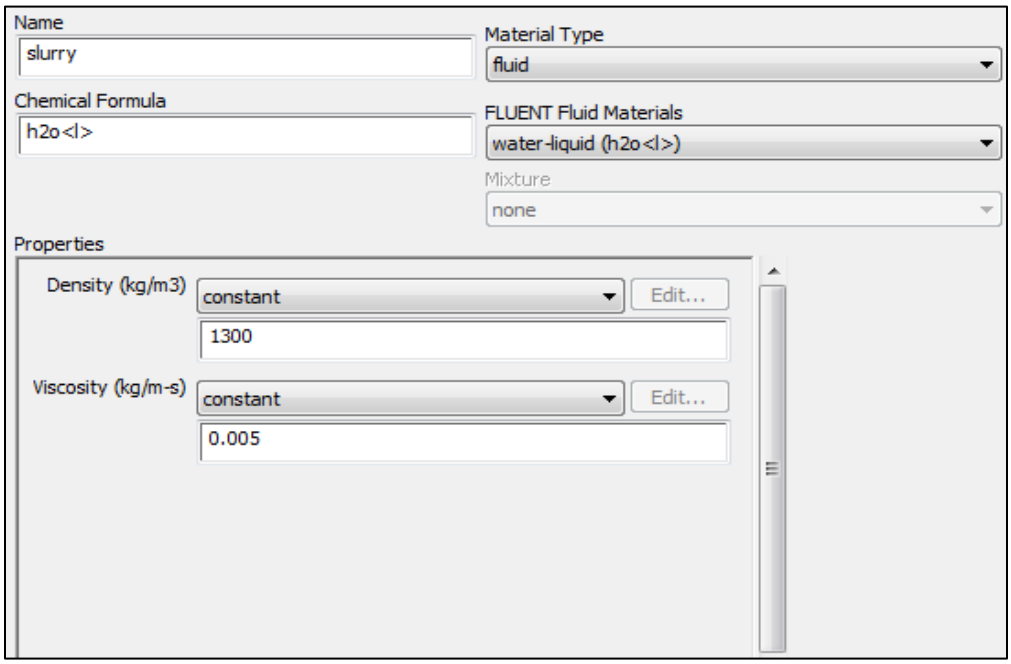

C.6 Rotating domain parameters

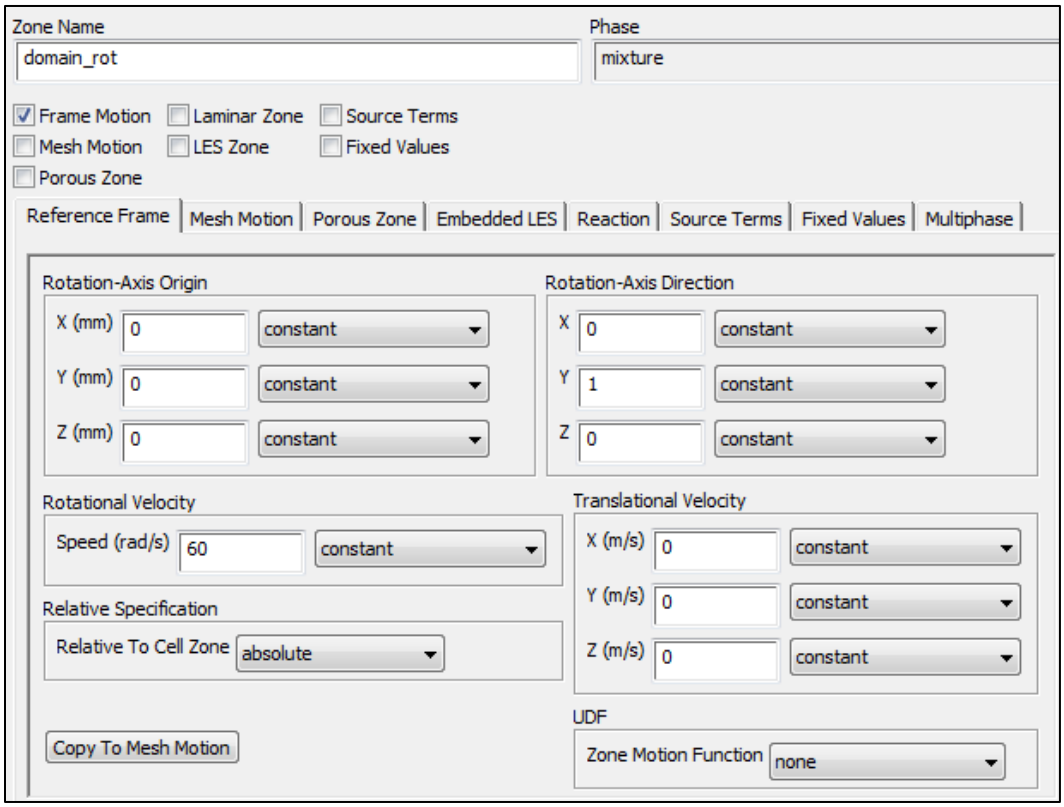

C.7 Solution method selection

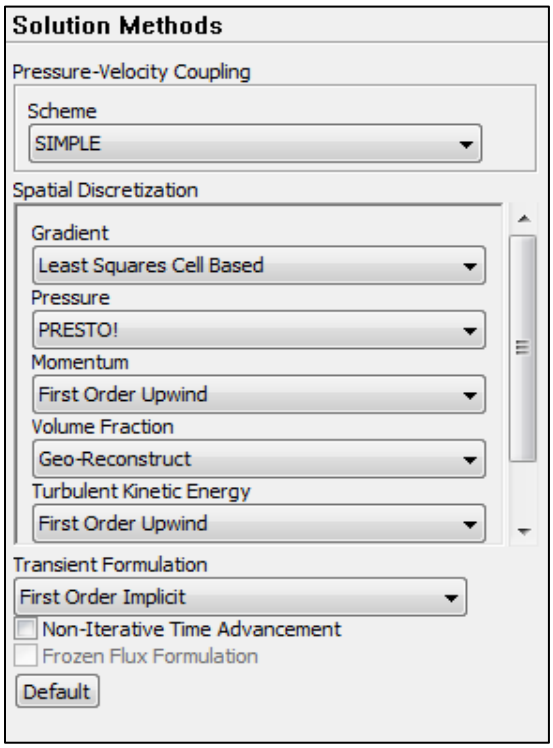

C.8 Solution control parameters

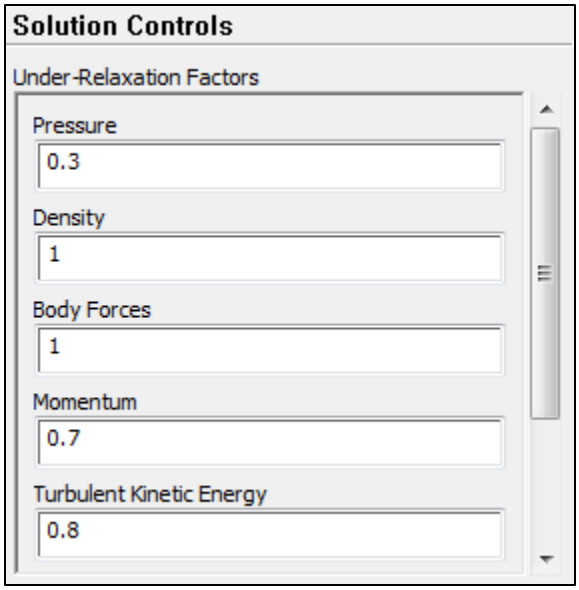

C.9 Time step and step number input parameters